Parsimonious Biosonar-inspired Sensing for Navigation Near Natural Surfaces

Haosen Wang

Thesis submitted to the Faculty of the
Virginia Polytechnic Institute and State University
in partial fulfillment of the requirements for the degree of

Master of Science
in
Mechanical Engineering

Rolf Müller, Chair
Alexander Leonessa
Nicole T. Abaid

February 21, 2019
Blacksburg, Virginia

Keywords: Sonar, acoustic sensors, time-of-flight, echo energy, echo duration

Parsimonious Biosonar-inspired Sensing for Navigation Near Natural Surfaces

Haosen Wang

(ABSTRACT)

Achieving autonomous in complex natural environments has the potential to transform society by bringing the benefits of automation from the confines of the factory floor to the outdoors. There, it could benefit areas such as environmental monitoring and clean-up, precision agriculture, delivery of goods. A fundamental requirement for achieving these goals are sensors that can provide reliable support for navigation, e.g., a drone, in natural environments. In this thesis, sonar-based navigation has been investigated as an approach to parsimonious autonomous sensing for drones. Bats living in dense vegetation have demonstrated that autonomous navigation in a complex, natural environment based on two one-dimensional ultrasonic echo streams is feasible. Here, a biomimetic sonar head has been used to collect echo data from recreations of natural foliage in the lab under controlled conditions. This data was used to address the research question whether the grazing angle at which the sonar is looking at a surface can be estimated from the echoes – despite the random three-dimensional nature of the scatter from the foliage. To investigate this, the echoes have been subjected to statistical analysis such as spectral coherence and cross correlation. Most importantly, the foliage data was compared against predictions made by the Endura method (energy, duration, and range method) that has been devices for two-dimension random scatterers. The results of this analysis shows that – despite their profoundly random nature – echoes can be used to estimate the sonar grazing angle directly, i.e., without the need to resort to reconstructions of the foliage geometry. This opens the possibility of developing simple devices for navigation control in natural environments that can control the direction of motion at a very little computational cost.

Parsimonious Biosonar-inspired Sensing for Navigation Near Natural Surfaces

Haosen Wang

(GENERAL AUDIENCE ABSTRACT)

Autonomously flying drones is a potential technology that could bring benefits to the society and improve the quality of life for humans[22]. Therefore, a study of autonomously flying in a natural environment is necessary, and this thesis will focus on drone that could recognize objects with different grazing angle and acoustic signal by collecting data from near foliage surface. For example, when a bush wall is in front of the drone, a on board computer could inform drone whether the drone airline will collide with the bush wall or the bush wall is safely out of drone's path[5]. If on board computer reads that there will be a collision with bush wall, then drone needs to make decision (change direction or stop immediately) to avoid crush on to bush wall. A sonar based navigation system has been investigated as an approach to achieve autonomous sensing for drones, which is inspired by bats. Bats use their natural sonar system to navigate in cave or forest, hence, it is hardly to see bats slam into any obstacles while flying. Bats navigation behaviours could be reconstructed as a sonar based autonomy. Hence, this thesis is inspired by bats to determine if there is a computational way to illustrate that sonar based sensor could be a solution to achieve reactive autonomy by using different grazing angle of the surface's acoustic signals.

Dedication

To My Parents: Linjie Wang and Yumei Ni

To My Wife: Xiaolan Zou

Acknowledgments

I want to thanks my academic advisor Dr. Rolf Müller for his knowledge, counseling, and support through my undergraduate and graduate school life. Dr. Müller is my academic guiding star. Without his leading, my academic knowledge is in a chaos. His preciseness and wisdom encourage me to be a professional engineer. I would also appreciate all my committees' help for putting their effort and support on my thesis. It is my great honor to work with all committees for such profound knowledge.

Contents

List of Figures

List of Abbreviations

σ_P is a measure of the duration

r_{00} is the distance to the surface along the line of sight of the sensor;

c is the speed of sound in air;

$t_0$is the delayer from the start of the pulse to its center;

σ_T is a measure of the Gaussian beam profile of the transducer;

Chapter 1

Introduction

1.1 Background

Achieving autonomy in a complex natural environments has the potential to transform society by bringing the benefits of automation from the confines of the factory floor to the outdoors. There, it could benefit areas such as environmental monitoring and clean-up, precision agriculture, delivery of goods. Currently, there are three different levels of autonomy: Sensory-motor autonomy, Reactive autonomy, Cognitive autonomy[22].

The sensory-motor autonomy could reach a given altitude, perform circular trajectory, move to global positioning system (GPS) coordinates or maintain position. This level is the most common way in the consumer market, which allow autonomously flying drone with less computational approach, but requires human supervision.

The Reactive autonomy could set the drone to maintain current position, avoid obstacles and maintain a safe or predefined distance from the ground. This level of autonomy requires less human supervision but larger computational approach.

The Cognitive autonomy could perform simultaneous localization and mapping, resolve conflicting information and self learning. This level of autonomy requires zero human supervision but full of computational approach, which is the final goal of drone autonomy.

This thesis is using a sonar based sensor to achieve reactive autonomy, but could be the

beginning of the cognitive autonomy. An artificial sonar uses multiple sonar detectors[43], but for a bat, it only has one speaker (vocal), and two receivers (ears)[40]. This design by mother of nature has incomparable advantage on saving processing time and reducing overall information processing[10]. It also gives a bat ability to distinguish objects and picks the optimistic direction to fly in a timely fashion. Recently, autonomous driving has become one of the most popular topics, and attracted more attention due to the convenience and potential[37]. If artificial autonomous driving drone could navigate as accurate as bats do, there would be a great benefit for the drone to do a much better job in navigation. Hence, it is necessary to study and control the autonomous flying method, which bats have for advanced autonomous control by knowing their signal process method and simulating their signal process progress. For this thesis, there are two approaches to get a sonar based reactive autonomy. One approach is using traditional statistical method to discover the similarity and difference of different acoustic echo signal. Second approach is using the "Endura" method to find the 3-D version of energy duration changing by changing the angle[11]. By improving the autonomy of a drone, it can allow more practical usage of a drone in civilian, commercial and military fields. For instance, geographers can improve the clarity of a map when using a drone as a field mapping tool. Or like the workers in the big warehouse can use drones to collect information about their products.

1.2 Literature Review

Currently, autonomous drones can be distinguished into three levels[22] : Sensory motor autonomy[23], Reactive autonomy and Cognitive autonomy. Researches related to reactive autonomy drones have been identified by many researchers and facilities. Most of autonomy researches are using Lidar (Light Detection and Ranging) equipment[26] as a detection

method. Lidar detection provides drones a high speed object obstacle detection ability [38]. However, Lidar based autonomy in a forest environment can be expensive and needs a great amount of calculation process [17][42]compare to the sonar based reactive autonomy[29]. In addition, Lidar can only accurately detected 73 percent of the trees that are greater than 20cm width within 3m flight path. For the small leaf and bush wall, Lidar would not work effectively[15].

Bats navigation behaviours has a lower computational cost and faster processing time. This behaviours navigates through natural environment by using its sonar system to act like a flying drone with reactive autonomy[36]. There are three reasons why bats navigation behaviours can classify as reactive autonomy:

- First, bats use many ultrasonic ranging skills that are more complex than simple time-of flight sensing approach, include frequency modulation, Doppler shrift[29].
- Secondly, bats use echolocation to determine different objects' location and their current location in order to sense surrounding environment[44].
- Thirdly, bats can navigate in a dense vegetation environment[33], and the same echo from a foliage is never seen twice. This theory of assumption provide a more in-depth statistical analysis of the possibility for coherence and correlation analysis.

There are multiple biomimetic researches have been developed based on bats' navigation behaviours. A biomimetic echolocation had been used as a method of autonomous navigation. "Echoic flow(EF) field" and scene perception are the keys to help bats have autonomous navigate skill[3]. A bat is like a developed sonar system that used acoustic obstacles[4], but the sonar system is still using 2-D flat surface as detected object, and localized using time-of flight (TOF) measurement. For the different surface sonar detection analysis, an analysis method called the Endura method is used for the 2-D surface[11]. This method has different

situations on a smooth surface, rough surface or moderate rough surface. For different surface, the echo energy and echo duration have different relation with different grazing angle of surface.

However, since bats not only can do obstacle in a 2-D surface, but also could adapt to the environment with a 3-D obstacle[24]. Therefore, an artificial sonar based autonomy is desired to be developed that can do what bats can do[16].

Huzefa Akbarally had developed a novel sonar, which can localise and classify 3D target [2]; however, this system was using three transmitters and three receivers, and the idea of this design is based on three dimensional docking acoustic sensor[27]. Hence, the design of three dimensional ultrasonic sensor is not as good as a two dimensional sensor, which requires the object to be larger than a beamwidth, otherwise the detected object would only shows a result of larger deform[1]. In addition, multiple transducers are not recommend as a drone on board sensor especially for marketing purpose. Furthermore, ultrasonic sensors have many shortcomings, such as poor direction, specular reflections when angle between wave front and normal to surface is too large[8]. Therefore, a 3-D bat-like ultrasonic sensor is less desirable to be built due to many uncertainties.

Then Dr. Chen M. came up with using sonar as a detective method to detect foliage, which also shows different foliage types in different echo shapes[31]. Biosonar potentially works for 3-D foliage bush wall because different vegetation has different shapes, and all vegetation are 3-D object. And a computational model for biosonar echoes from foliage also support the relation between foliage properties and echo parameters[30].

The sonar based reactive autonomy near a 3-D natural bush wall by using different grazing angle is still an unknown area, it is more important to understand that Cognition requires stimulation by sensors that can be originally obtained by sensory input. Further research

by this thesis should focus on exploring sonar based reactive autonomy near a 3-D natural environment by referring current 2-D sonar based reactive autonomy result.

1.3 Outline of this Thesis

This thesis documents the experimental results and analysis from Bio-inspired sonar head collected data, which illustrate that sonar based sensor could be a solution to help autonomous drone to achieve reactive autonomy. The first chapter gives basic introduction of this thesis, including background, outline and literature review. The second chapter introduces experimental setup, experimental method and analysis methods, which are coherence method and Endura method("energy - duration - range"). Third chapter shows results of experimental data, which include the result of raw echo, coherence method and Endura method. A Monte-Carlo simulation based on Endura method's result is also included in the chapter. The fourth chapter are the conclusion and summary which conclude this thesis and provides a future work plan. The last chapter is summary of achievements.

Chapter 2

Methods

With background motivation and previous work's experience, this thesis is trying to find the possible solution for autonomous drone obstacle avoidance in the natural environment by using acoustic signal from different grazing angle from the bush wall surface. In this chapter, experiment method and two analysis methods are introduced. The experiment method is collecting data for analysis by using a mechanical bio-inspired sonar system, which contains a signal emitter, analog/digital (A/D) converter, and signal receiver. Statistics analysis method and Endura method are used for the experiment. The statistics method would focus on the relation between each echo signal's original information. The Endura method would focus on the echo's energy, duration, and range.

2.1 Experimental Setup

In order to collect data based on an acoustic signal: a sonar based experiment setup and experiment method have been developed. An artificial bush wall is used as target object, as (Figure 2.1) and (Figure 2.2) shown below. This bush wall has three layers, and different number of layers work as different experimental objects. As (Figure 2.3) shown, the sonar head is placed in front of the object with different range and rotation degree from 50 ° to 130 ° with 5 ° increment for each trial. Therefore, there are 17 positions fixed on the ground, and each position is measured by an angle gauge and a fixed distance ruler. A calibration

system has a laser point projected to a drawn center point on the bush wall. This laser point is from a laser pointer, which is fixed next to the microphone.

Figure 2.1: Front View of three layers of bush wall

Figure 2.2: Side View of three layers of bush wall

Figure 2.3: Sonar head in front of the one layer bush wall

2.1.1 Data Acquisition Software setting

At first, a series of software setting is required for the experiment. This section describes the detailed setting for the software. The system is assigned with different parameters for different purpose. In doing so, the following steps are described in detail about the system setting below:

- First, the sample frequency is set as 500k Hz, which means the computer would read 500 thousand times record in one second.

- Second, the number of replicates is set as 100, which means for one trial of experiment, system would collect 100 times of experiment result.

- Third, acquisition time is set as 15 millisecond, which means each single time of experiment would take 15 milliseconds.

- Fourth, rotation degree is set from 50 ° to 130 °, and it will be increased by 5 ° for each trial, which means for each single trial, the sonar head would be place by 17 different positions.

- Fifth, the distance is set as 0.5 meter, 0.8 meter and 1.2 meters, which provides more comparisons of the experiment.

- Sixth, a chirp signal is used as an emitted signal that has 20kHz as the lower boundary acoustic signal and the 105kHz as upper boundary acoustic signal.

- Seventh, a Hamming Window is applied into the system to smooth the chirp signal.

2.1.2 Data Acquisition Hardware system

Next, a data acquisition hardware system is interpreted in this section. As for data acquisition hardware system, similar to the bat's sonar system, this mechanical sonar system comes with a vocal (loud-speaker), a paired of ears(microphones), a smart brain(on board computer). However, artificial sonar system also needs an Analog/Digital (A/D) converter to transfer analog signal into digital signal. Therefore, the whole system comes with high frequency range loud speaker, high frequency range ultrasound microphone, a faster A/D converter and a mother board. For this sonar system, ultrasonic sensor (Model 600, Senscomp, Livonia, MI, USA) is used as loud speaker, which is shown below in (Figure 2.4). Capacitive MEMS microphone (monomic, Dodotronic, Rome, Italy) is used as microphone, which is shown below in (Figure 2.6). The microphone outputs are converted to a digital signal representation (PXI 6351, National Instruments, Dallas, Texas, USA, Figure 2.7). An embedded PC (Model 3,Raspberry PI , London,UK) is used as on board mother board, which is shown below in (Figure 2.5). The laboratory version is using NI 6351 as A/D converter, PC as mother board. For the on board version, the NI Pixel 6351 is the A/D converter, Raspberry pi is mother board, and APEX 91 is the power amplifier. The finish Sonar head is shown as (Figure 2.8), and (Figure 2.9) is the Sonar head on a DJI S900 drone.

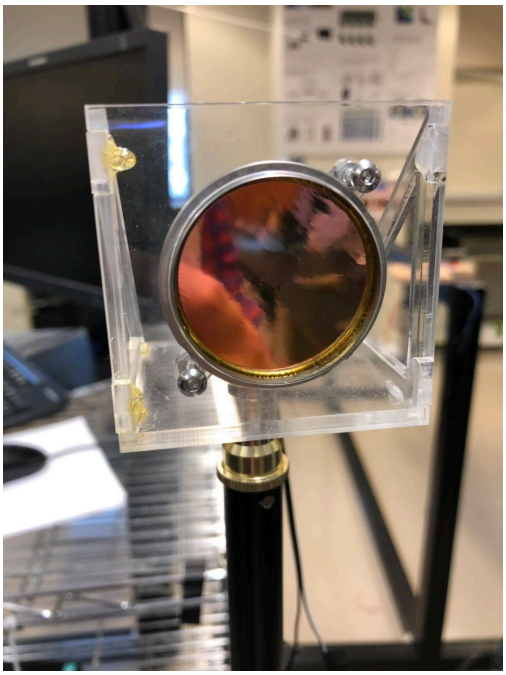

Figure 2.4: High Frequency Ultrasonic Loud Speaker (Model 600, Senscomp, Livonia, MI, USA)

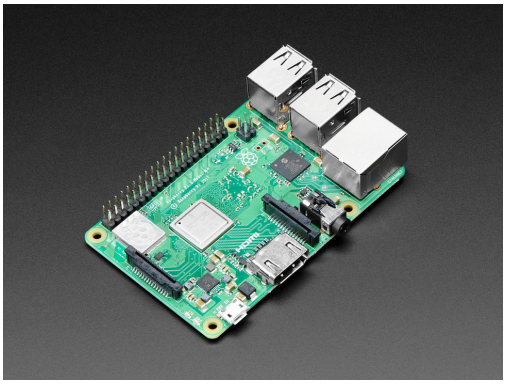

Figure 2.5: On Board Controller Computer(Model 3,Raspberry PI , London,UK)

Figure 2.6: Analog Ultrasonic Microphone(monomic, Dodotronic, Rome, Italy)

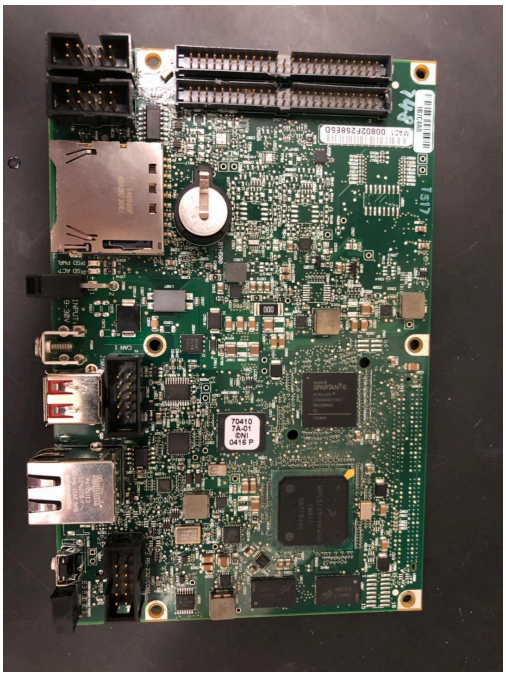

Figure 2.7: National Instrument Pixel 6351 Multifunction Input and Output Device (PXI 6351, National Instruments, Dallas, Texas, USA

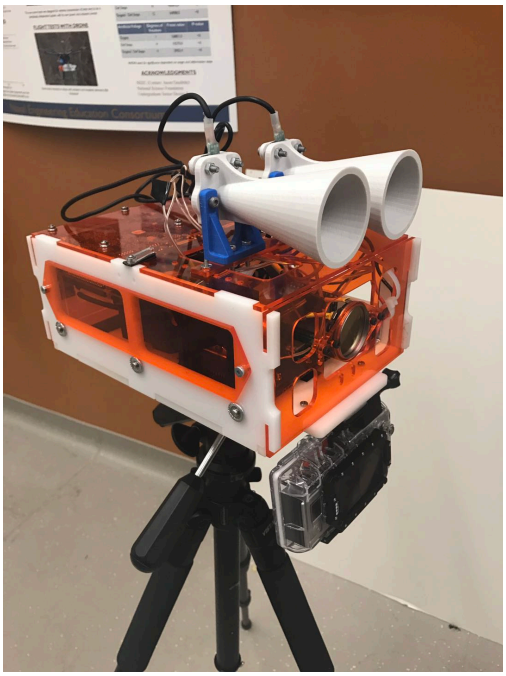

Figure 2.8: Sonar Head with High Frequency Ultrasonic Loud Speaker, A Pair of Analog Ultrasonic Microphone, Multifunction Input and Output Device and On Board computer

Figure 2.9: Sonar Head on a DJI S900 Drone (S900, DJI, Shenzhen, Guangdong, China)

2.1.3 Loud speaker circuit Design

This system's loud speaker is desired to be a high frequency and high amplitude speaker. The loud speaker requires a high voltage power to operate functionally, which means an operational amplifiers is necessary in the system. Since this system is designed to work on a drone, in the other words, the battery has to be a regular 22 V lithium battery. Therefore, a shrink size of high voltage power operational amplifiers is desired in this system. After researched and compared, the best choice is APEX PA91, which is a high voltage and low quiescent current MOSFET operational amplifier in (Figure 2.10). This amplifier uses low power and piezoelectric positioning method to operate the loud speaker. The schematic for operating the amplifier is shown below in (Figure 2.11). The print circuit is shown as (Figure 2.13), and the power distribution print circuit board is shown as (Figure 2.12) If the power source comes from a 3.3V power supply, for example a USB power bank, then it needs to connect to pin 1 low voltage input, pin 1 op-amplifier has a gain value equal to 6, which increase voltage to 20V . If the power supply comes from a 22V lithium ion battery, then it needs to connect to pin 2 direct input. Pin 3 has an op-amplifier gain value equal to 20, which deliver a final voltage that is greater than 400 Voltage(+200V and -200V). The pin 4 is the output of this print circuit board with a safety resistor(R8), the output voltage is between +225V and -225V.

Figure 2.10: Operational Amplifier Chip (PA91, APEX,Tucson, AZ, USA)

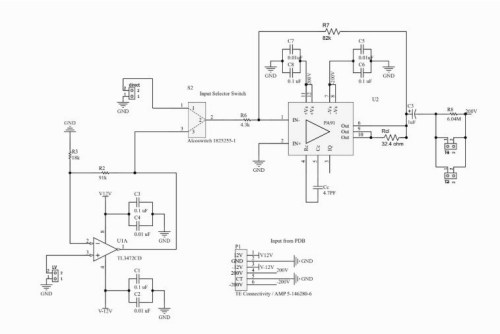

Figure 2.11: Operational Amplifier Schematic

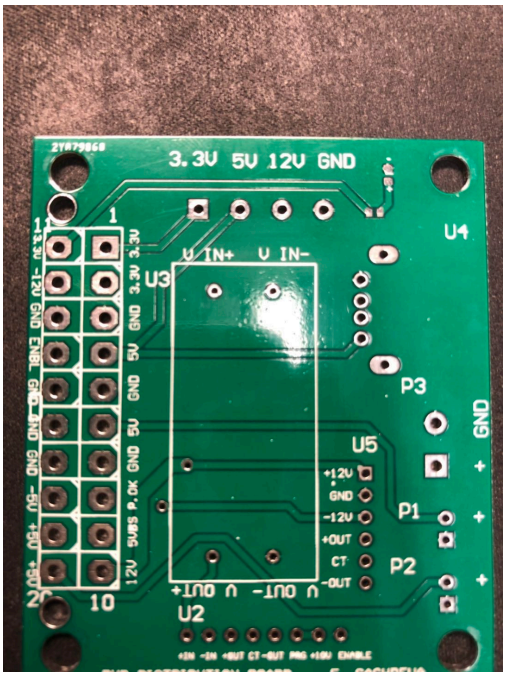

Figure 2.12: Power distribution print circuit board with input 22V output 3.3V,5V,12V

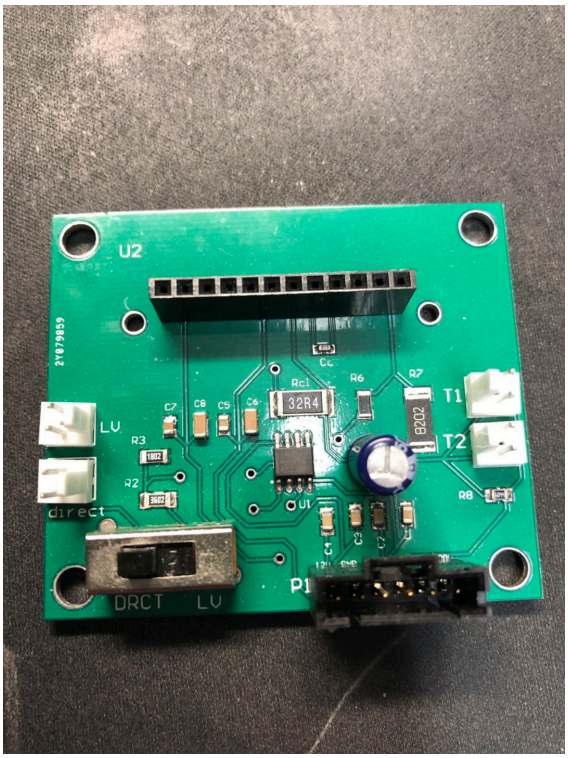

Figure 2.13: Printed circuit board for operational amplifier schematic in 2.11

2.2 Statistical Analysis

Statistics analysis describes the relative relation or the relation between two different data group. The auto-correlation, cross correlation and coherence are the most common analysis methods for doing statistics analysis. However, coherence shows the relation of the data in frequency domain[34]. Once the result is in frequency domain, it would be more easier to extract the test chirp range (20kHz to 105kHz).

$$C_(xy)(f) = \frac{G_(xy)(f)^2}{G_(xx)(f) * G_(yy)(f)} \tag{2.1}$$

Where,

$G_(xy)(f)$ is the cross-spectral density between data set x and data set y, and $G_(xx)(f)$ and $G_(yy)(f)$ the autospectral density of x and y respectively

For the coherence analysis, it is easy and clear to have a result, when we know a given position's data. For example, with a given grazing angle of 90 °, which means the sonar head facing the bush wall, the closer the angle between the second test with the 90 ° grazing angle test, the higher coherence amplitude between these two test would be. However, in the actual experiment case, the on board computer has no idea which data set from which angle. Hence, the on board computer could not use 90 ° test result as a reference. Therefore, the coherence with same angle is chosen as the best way to analyze data. With many times of experiment observations, when the sonar directly faces the bush wall, the coherence between N time and the N+1 times (N start from 1) are very close. However, when sonar head faces bush wall with an angle, the higher angle is, the lower coherence amplitude between N time and N+1 times. Therefore, different angles might have different coherence amplitude. As the data collection procedure explained above, for each angle experiment, the system would have 100 trials. Also the experiment has repeatedly tested ten times. The experiment

collected data from 50 ° to 130 ° (90 ° happened when sonar head directly faced the bush wall). Totally, there were 1000 experiment results for a fixed angle. After collecting data, the N+1 times (N start from 1) would be used to run a coherence with N time data set. This method was more focused on the echo instead of using the whole data set, therefore, a threshold is applied into data set. In addition, a Hilbert transform[6] would also apply into echo, in order to get an envelop of the echo signal. The reason why an envelop is desired is echo envelop has more characteristic than a normal echo [19]. Same analysis method that has described above will also applied to echo envelop, in order to get a envelop coherence result. After getting those coherence from each position, a summary of coherence will be generated based on the total value of coherence amplitude. In the theoretical case, the summary of coherence will increase as grazing angle increase.

2.3 Endura Method Apply in 3-D Bush

The Endura method stands for Energy, Duration and Range method, which is a physical model-based on Kirchhoff approximation method[41]. Other methods are focus on the homogeneous environments, certain rough scatterers [9][18][21] or specular scatterers[12][28][14]. However, in the practical world, most of surface can not set with a certain value or can be considered as moderately rough. This method could interpret sensor data in heterogeneous environments, and this method is also based on scattering from surface with varying degrees of different situation surface. The method for analyzing the reflected echo from randomly rough surfaces is based on the Kirchhoff approximation method(KAM)[20]. The forward model describe echo characteristic, which combine physical reflection model with sonar model. The result of model are represented as: intensity, energy and duration. The

echo energy describes the energy content of the echo can be represented below:

$$P = \int s^2(t)dt \tag{2.2}$$

where,

$s^2(t)$ is the echo intensity.

The echo duration is defined from the second moment of echo can be represented below:

$$D = (\frac{\int (t-\mu)^2 s^2(t)dt}{\int s^2(t)dt})^{\frac{1}{2}} \tag{2.3}$$

where,

$$\mu = \frac{\int t s^2(t)dt}{\int s^2(t)dt}$$

and the integration is taken over the time interval in which s(t)>0.

For this method, there are three different models, which base on smooth surface, moderately rough surface and rough surfaces. With different situation, the sonar map vary from each other's[45]. Endura method is a forward model of reflection from surface with varying degree of roughness, this method is based on the Kirchhoff approximation method. Although a single slide of foliage has a smooth surface but since the bush wall comes with thousands of foliage, therefore, the bush wall would have moderately rough surface. According to the Endura method model, a Gaussian distribution rough surface and standard deviation σ_S is used to define smooth surface, moderately rough surface or rough surface. If the standard deviation of the surface heights is far less than wavelength of ultrasonic transducers, then it would be a smooth surface. If the standard deviation is far greater than the wavelength, then it would be a rough surface. As for this research, the rough surface would be more suitable over the other two cases. The echo intensity is the essential factor for echo energy

and echo duration, the echo intensity's equation can be represented below.

$$s^2(t) = \frac{R^2\sigma_T^2}{128r_{00}^2 cos^5\theta\sigma_P}\frac{T_S^2}{\sigma_S^2}\frac{1}{c}e^{\frac{-T_S^2}{\sigma_S^2}\frac{tan^2\theta}{4}}e^{-\frac{t-t_0-\frac{2r_{00}^2}{c}}{4c^2}^2} \tag{2.4}$$

Where,

R is the reflection coefficient,which would be 0.7 in our case [];

T_S is the correlation length, which describe the distribution of valleys and hills on the surface;

σ_S is surface height standard deviation;

r_{00} is the distance to the surface along the line of sight of the sensor;

c is the speed of sound in air;

σ_P is a measure of the duration;

$t_0$is the delayer from the start of the pulse to its center;

σ_T is a measure of the Gaussian beam profile of the transducer;

For the echo energy, equation below is defined as echo energy:

$$P = \frac{R^2\theta_o^2\sqrt{\pi}}{256r_{00}^2 cos^5\theta\sigma_P}\frac{T_S^2}{\sigma_S^2}e^{\frac{-T_S^2}{\sigma_S^2}\frac{tan^2\theta}{4}} \tag{2.5}$$

The echo duration is represented as equation below, which is defined from the second moment of the echo.

$$D = \sqrt{4\sigma_S^2\frac{cos^2\theta}{c^2} + \theta_o^2 r_{00}^2\frac{tan^2\theta}{4c^2} + \frac{\sigma_P^2}{2}} \tag{2.6}$$

The Endura method is a science base to find relation between varying degrees and foliage surface. However, current Endura method is based on a 2-D surface. The result for a

3-D surface might vary from the original Endura method. In the ideal case, after knowing surface height by Gaussian distribution[13], the result based on energy and duration equation will compare with experimental data. If Endura method works well with 3-D surface, the experimental result should be similar to the equation generate result. For the experimental result, energy can be described as probability density function[35], which is used to describe the statistical distribution of the height data. And the duration could be described as RMS, which is the standard deviation of this model. In the end, Monte carlo simulations[7] are run for the prediction of angle recognition. With the error bar and fit in equation from the result, a Monte carlo simulation has been created to evaluate the system's accuracy. Since the result on theory are symmetric, therefore, when one duration value input into the Monte carlo simulation, two potential angle would come up.

Chapter 3

Results

This chapter presents the results of the experiment and analysis method that are described in the methods section. The first section represents the raw and processed echo results with different range and foliage layers in detail. The second section demonstrates the results of the coherence with the same data group by using different distance and calculated summary of coherence. The third section represents the results of Endura method approach, Gaussian fit and Monte Carlo Simulation result.

3.1 Echo shape results

For this section, there are three different subsections, which are named using different distance. There are only 5 representative results shown in each subsection, the rest of position results can be found in Appendix II. These five grazing angles are : 50 °, 75 °, 90°, 105 ° and 130 °. When sonar head face to bush wall, 50° and 130° grazing angle are the first and final position from the left hand side. 90° grazing angle is the middle position from the left had side. 75° is between first and middle position, while 105° is between middle and final position. For each angle's result, the top side would be the raw data results, which contain all collected information, and the first 2 millisecond is a direct receive from the speaker. This direct receive is a testing for chirp signal generation. The bottom side would be the cutting echo result, which is the reflection from bush wall.

3.1.1 0.5 meter echo results

In this subsection, there are two groups being represented. The first one is the 0.5 meter with one layer bush wall, and the second group is 0.5 meter with three layers of bush wall. These two results have exactly same distance from the sonar, but with different layers of bush wall. The reason for comparing these two results is to know the echo difference between 2-D foliage surface and 3-D bush wall. The depth factor of the bush wall generates more echoes than a flat 2-D bush surface. For each grazing angle position, one layer of bush wall echo is placed on the left hand side, and three layers of bush wall is on the right hand side. Echo length is based on power spectral densities of the emited chirp, the echo section is Figure 3.1 yellow highlight part.

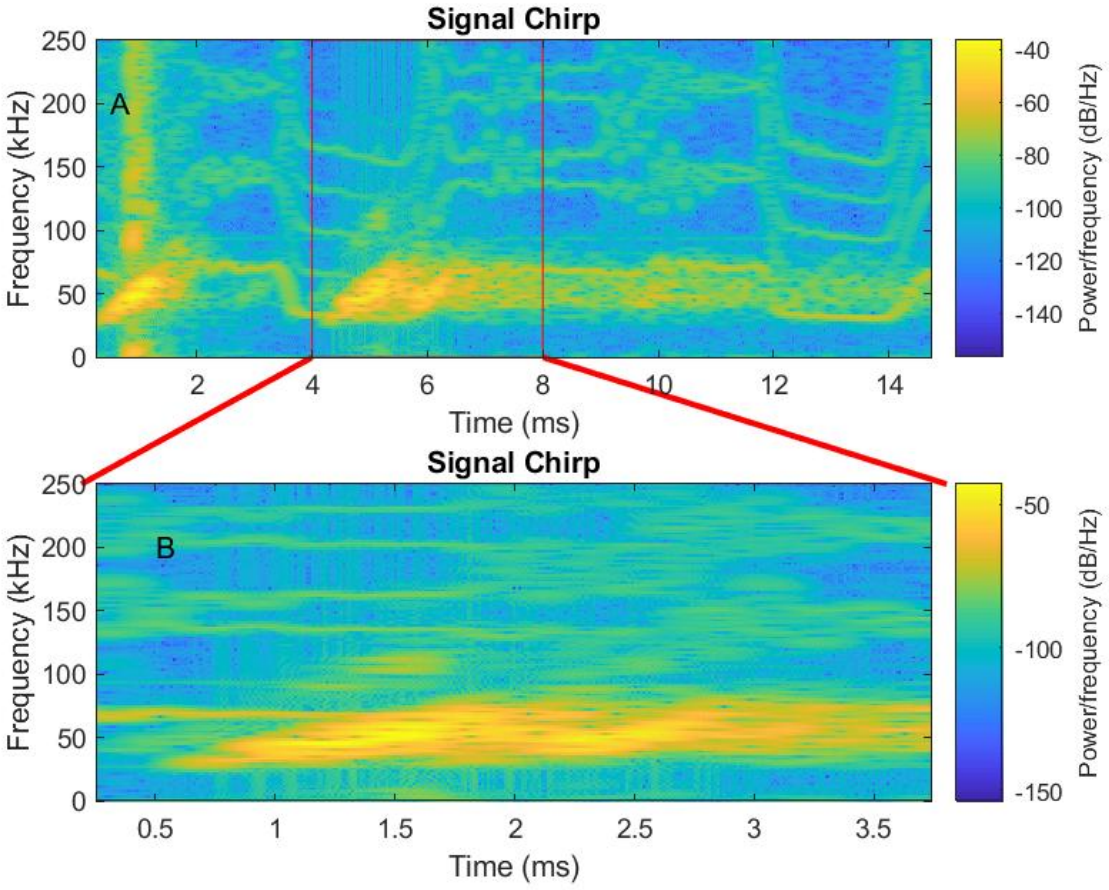

Figure 3.1: Spectrogram for three layers bush wall surface with grazing angle 90°, 0.5 meter from bush wall at position 9.a) Entire Spectrogram.b) Zoom in view of marked rectangular section as echo spectrogram

For one layer of bush wall with a sonar head placed at a 50° grazing angle from bush wall surface that is 0.5 meter away Figure 3.2, echo happen very early and echo shape is more dispersed than echo from a 75° grazing angle Figure 3.4 or a 90° grazing angle Figure 3.6. In addition, there is a slight difference between 75° and 90°'s resulting echo when the bush wall is only one layer. The echo becomes more and more dispersed as the angle continuous to be greater than 90°. On the other hind, three layers of bush wall has a stronger amplitude and intensity than one layer of bush wall. However, there are some results that remain the same as the result from one layer of bush wall, like the face that the echo from three layers bush

wall has most concentrated shape at 90° grazing angle Figure 3.7, and the most dispersed shape at 50° grazing angle Figure 3.3 or 130 ° grazing angle Figure 3.11. 75° grazing angle result shows an increment of concentrated shape from 50° to 90° Figure 3.5 and 105°grazing angle result shows an increment of dispersed shape from 90° to 130° Figure 3.9. For the aspect of spectrum, the chirp energy increase from 50 ° to 90 ° and decrease from 90 ° to 130 °

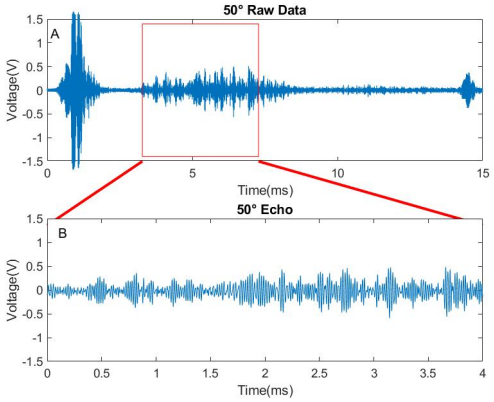

Figure 3.2: Reflected signal from one layer bush wall surface with grazing angle 50°,0.5 meter from bush wall at position 1.a) Entire reflected signal.b)Zoom in view of marked rectangular section

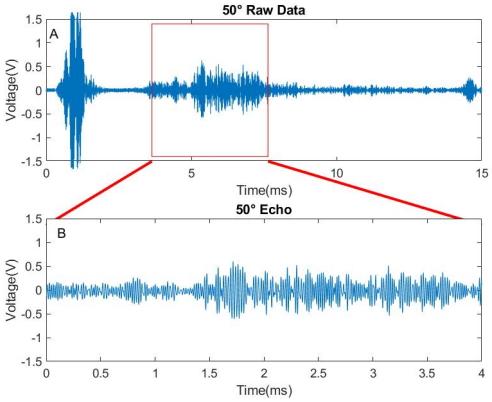

Figure 3.3: Reflected signal from three layers bush wall surface with grazing angle 50°,0.5 meter from bush wall at position 1.a) Entire reflected signal.b)Zoom in view of marked rectangular section

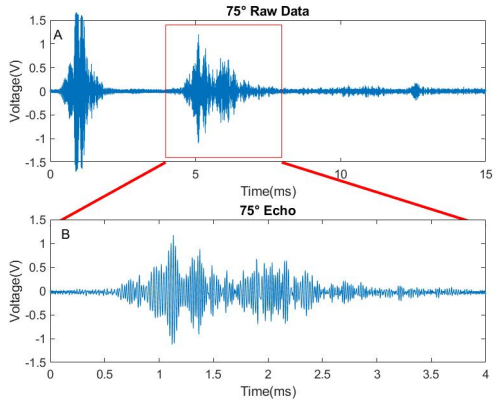

Figure 3.4: Reflected signal from one layer bush wall surface with grazing angle 75°,0.5 meter from bush wall at position 6.a) Entire reflected signal.b)Zoom in view of marked rectangular section

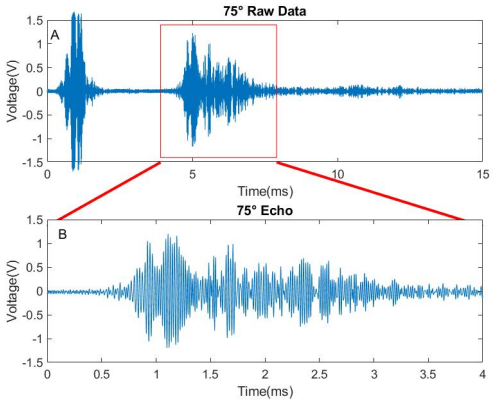

Figure 3.5: Reflected signal from three layers bush wall surface with grazing angle 75°,0.5 meter from bush wall at position 6.a) Entire reflected signal.b)Zoom in view of marked rectangular section

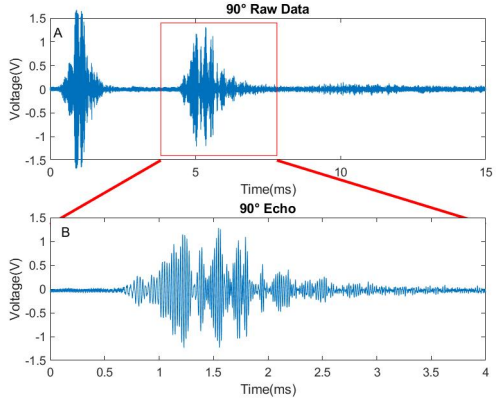

Figure 3.6: Reflected signal from one layer bush wall surface with grazing angle 90°,0.5 meter from bush wall at position 9.a) Entire reflected signal.b)Zoom in view of marked rectangular section

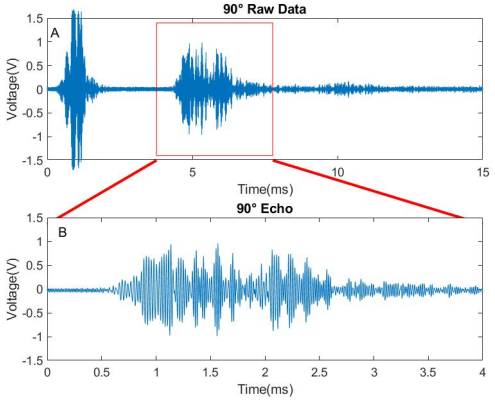

Figure 3.7: Reflected signal from three layers bush wall surface with grazing angle 90°,0.5 meter from bush wall at position 9.a) Entire reflected signal.b)Zoom in view of marked rectangular section

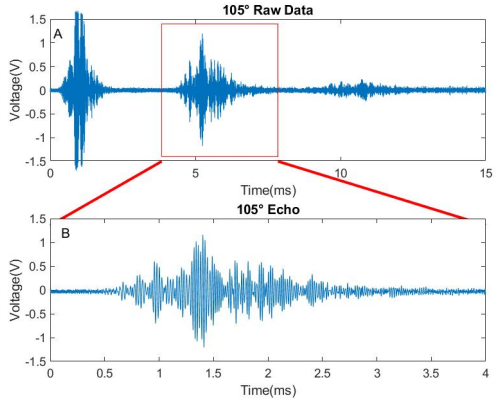

Figure 3.8: Reflected signal from one layer bush wall surface with grazing angle 105°,0.5 meter from bush wall at position 12.a) Entire reflected signal.b)Zoom in view of marked rectangular section

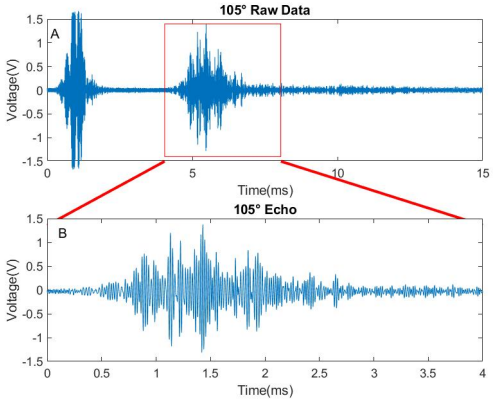

Figure 3.9: Reflected signal from three layers bush wall surface with grazing angle 105°,0.5 meter from bush wall at position 12.a) Entire reflected signal.b)Zoom in view of marked rectangular section

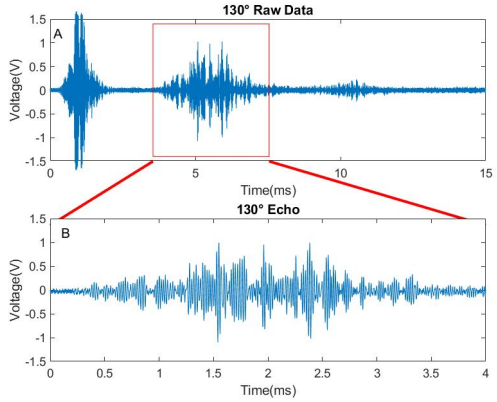

Figure 3.10: Reflected signal from one layer bush wall surface with grazing angle 130°,0.5 meter from bush wall at position 17.a) Entire reflected signal.b)Zoom in view of marked rectangular section

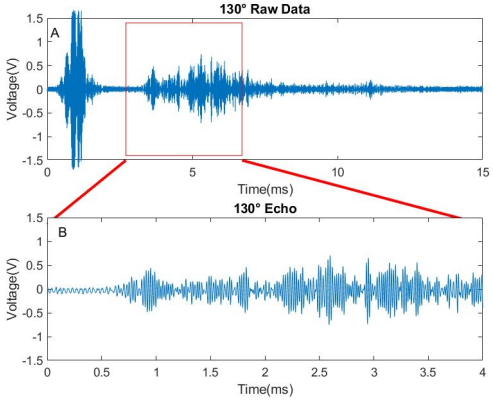

Figure 3.11: Reflected signal from three layers bush wall surface with grazing angle 130°, that is 0.5 meter from bush wall at position 17.a) Entire reflected signal.b)Zoom in view of marked rectangular section

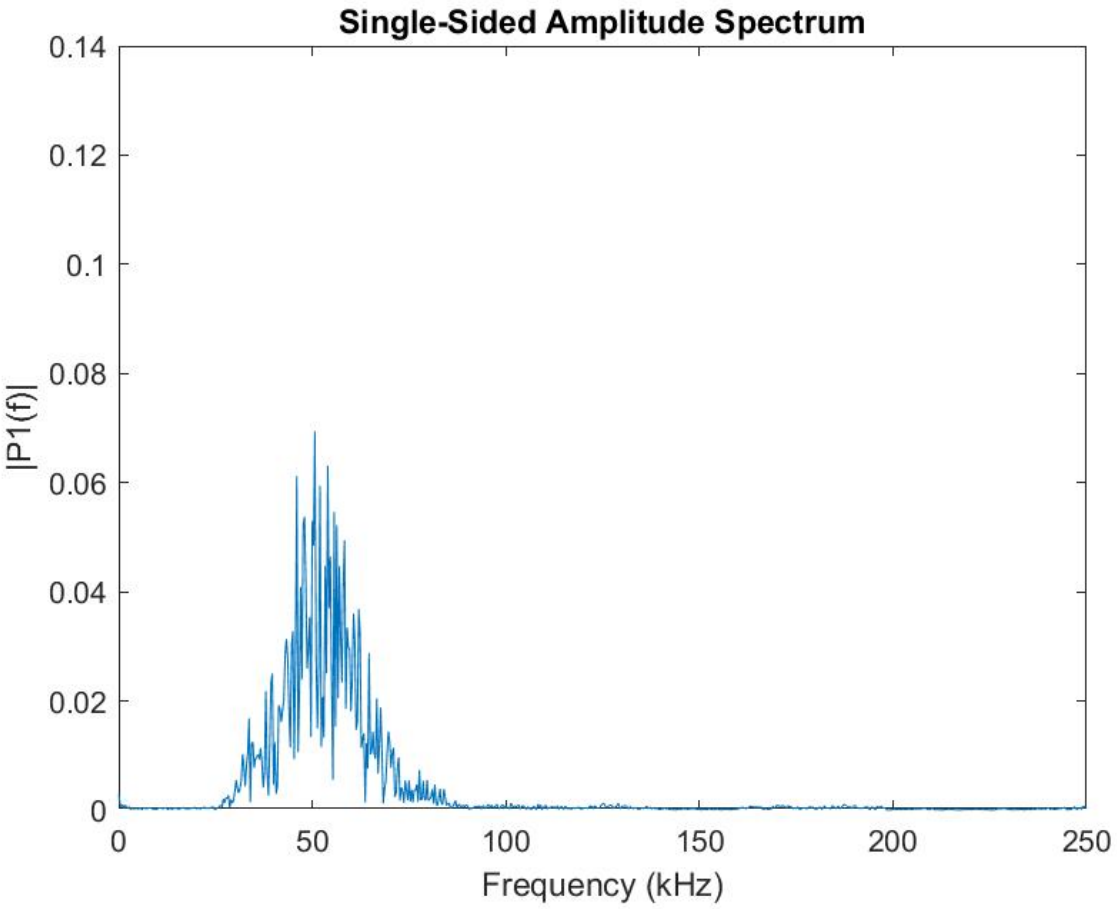

Figure 3.12: Spectrum for three layers bush wall surface with grazing angle 50 °,0.5 meter from bush wall at position 1.

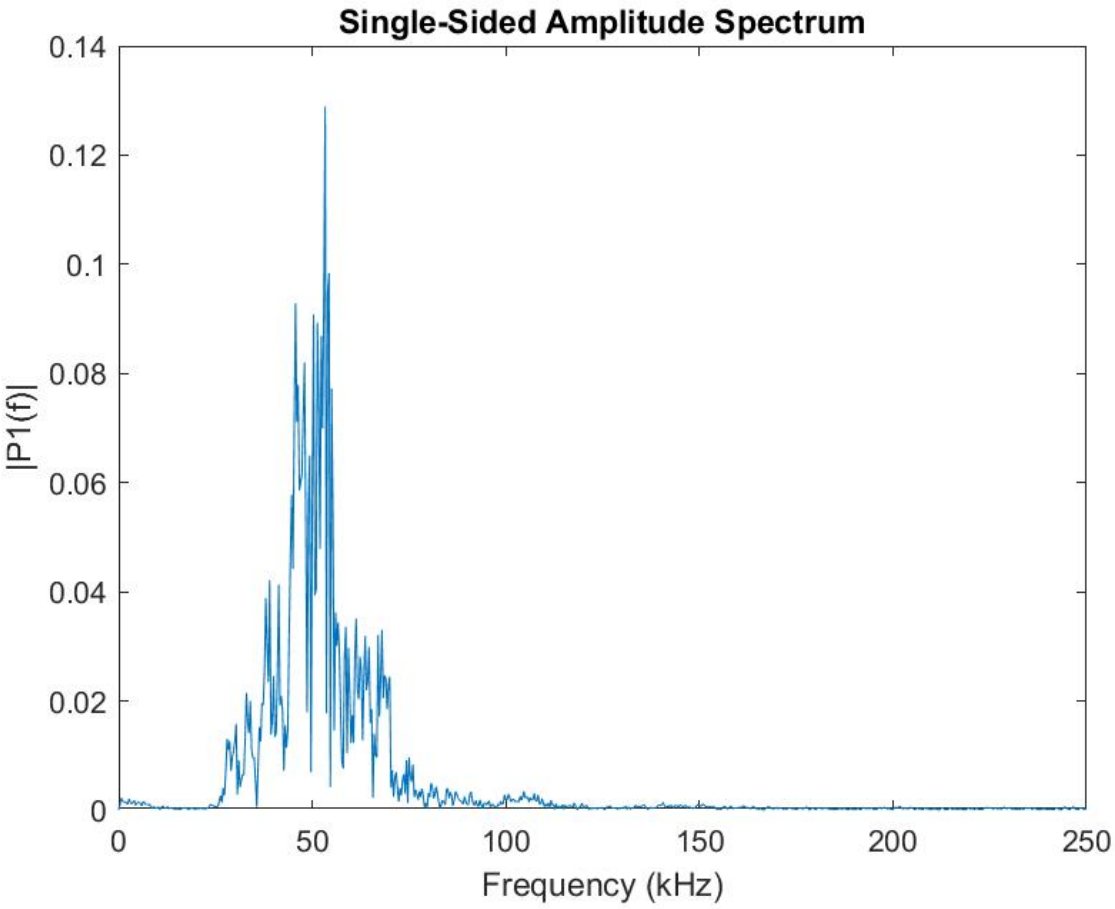

Figure 3.13: Spectrum for three layers bush wall surface with grazing angle 90°,0.5 meter from bush wall at position 9

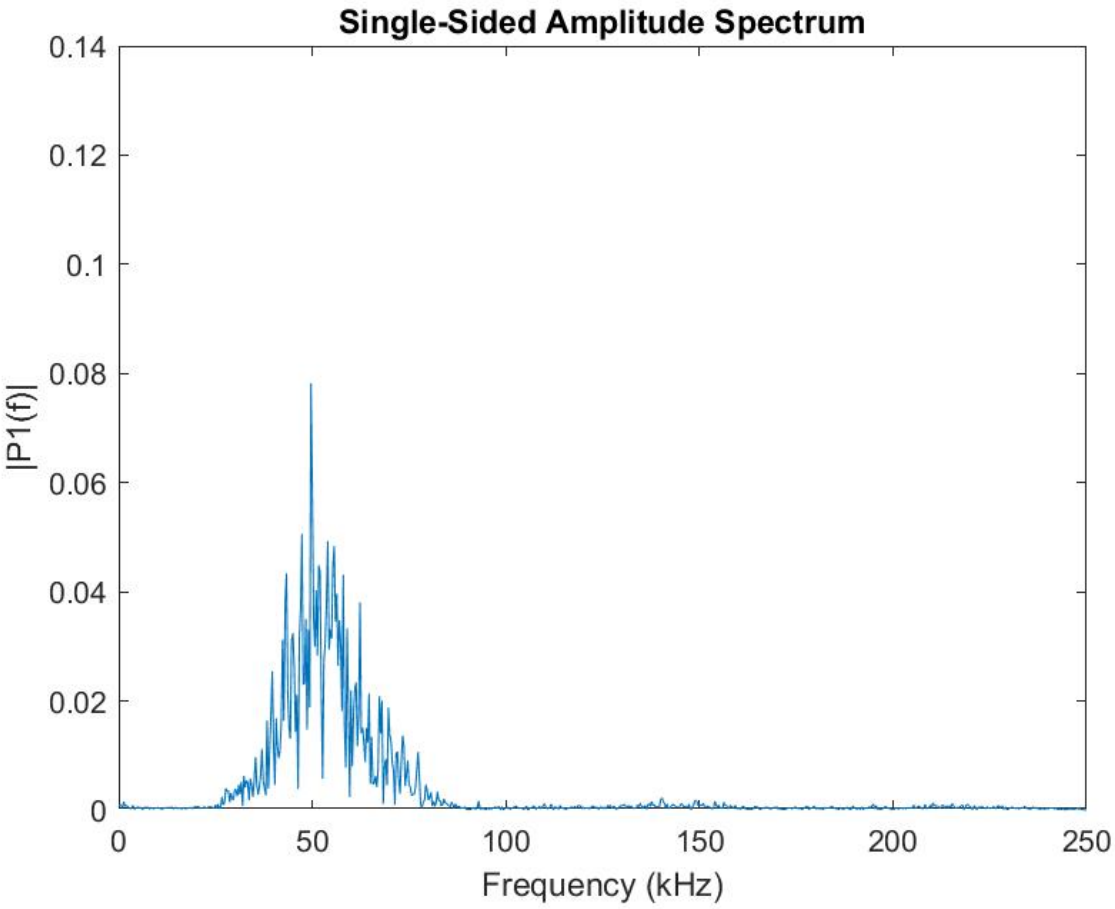

Figure 3.14: Spectrum for three layers bush wall surface with grazing angle 130°,0.5 meter from bush wall at position 17.

3.1.2 0.8 meter echo results

When sonar head placed 0.8 meter away from the bush wall, the amplitude and intensity is less stronger than the 0.5 meter result. However, according to the result of echo, these data set are still very appropriate data set. Since the echo is always received after 5 milliseconds, therefore, echo is more accuracy.

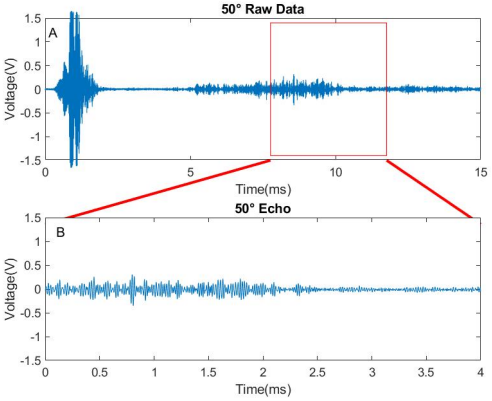

Figure 3.15: Reflected signal from one layer bush wall surface with grazing angle 50°,0.8 meter from bush wall at position 1.a) Entire reflected signal.b)Zoom in view of marked rectangular section

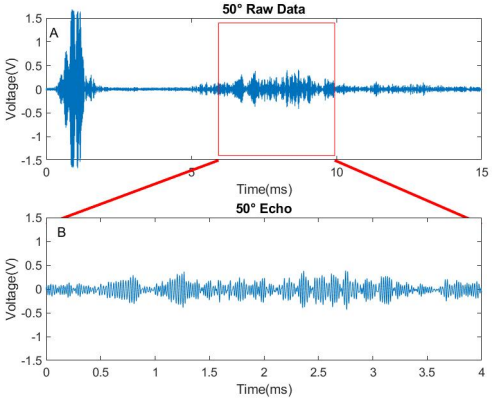

Figure 3.16: Reflected signal from three layers bush wall surface with grazing angle 50°,0.8 meter from bush wall at position 1.a) Entire reflected signal.b)Zoom in view of marked rectangular section

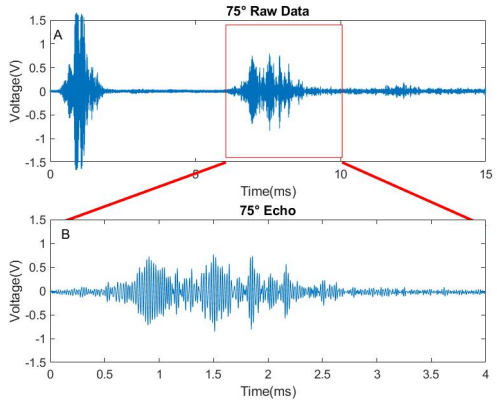

Figure 3.17: Reflected signal from one layer bush wall surface with grazing angle 75°,0.8 meter from bush wall at position 6.a) Entire reflected signal.b)Zoom in view of marked rectangular section

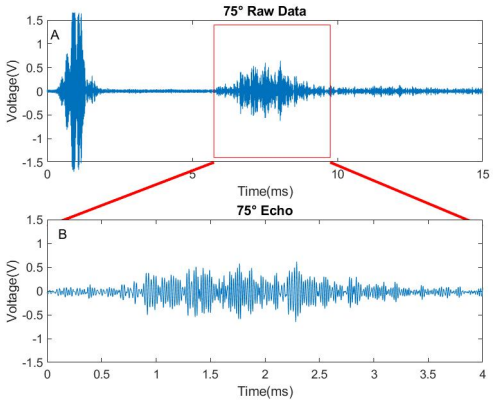

Figure 3.18: Reflected signal from three layers bush wall surface with grazing angle 75°,0.8 meter from bush wall at position 6.a) Entire reflected signal.b)Zoom in view of marked rectangular section

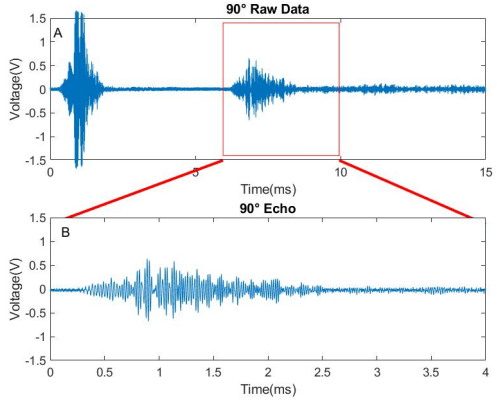

Figure 3.19: Reflected signal from one layer bush wall surface with grazing angle 90°,0.8 meter from bush wall at position 9.a) Entire reflected signal.b)Zoom in view of marked rectangular section

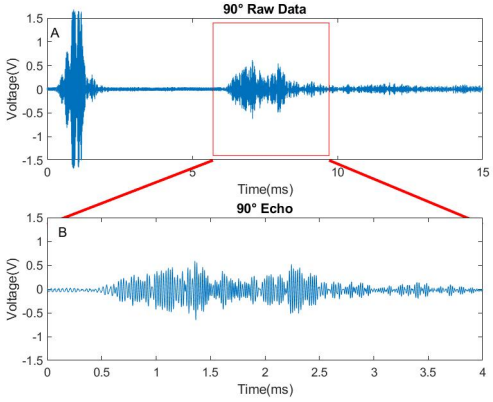

Figure 3.20: Reflected signal from three layers bush wall surface with grazing angle 90°,0.8 meter from bush wall at position 9.a) Entire reflected signal.b)Zoom in view of marked rectangular section

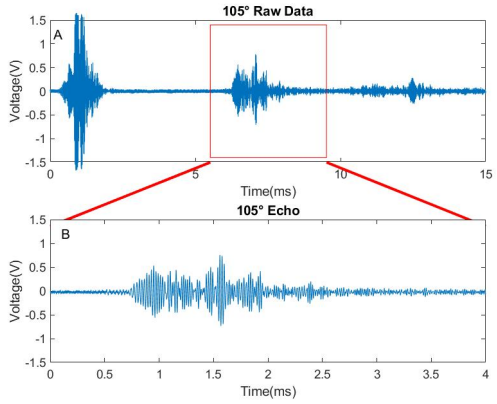

Figure 3.21: Reflected signal from one layer bush wall surface with grazing angle 105°,0.8 meter from bush wall at position 12.a) Entire reflected signal.b)Zoom in view of marked rectangular section

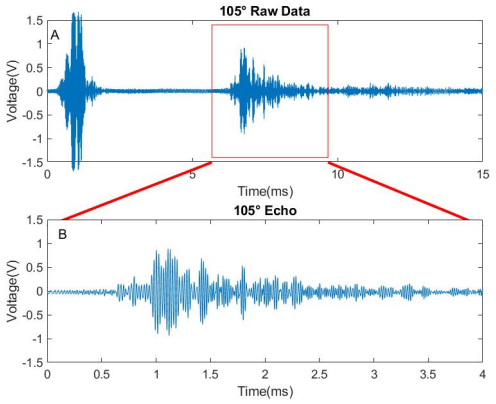

Figure 3.22: Reflected signal from three layers bush wall surface with grazing angle 105°,0.8 meter from bush wall at position 12.a) Entire reflected signal.b)Zoom in view of marked rectangular section

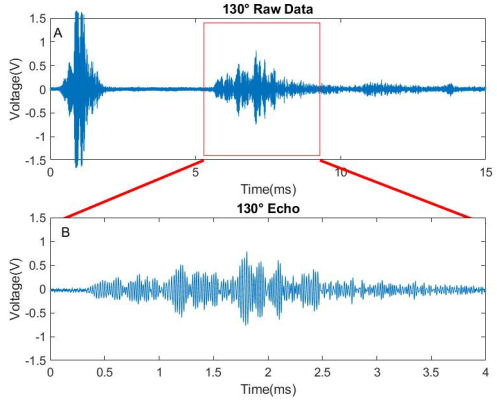

Figure 3.23: Reflected signal from one layer bush wall surface with grazing angle 130°,0.8 meter from bush wall at position 17.a) Entire reflected signal.b)Zoom in view of marked rectangular section

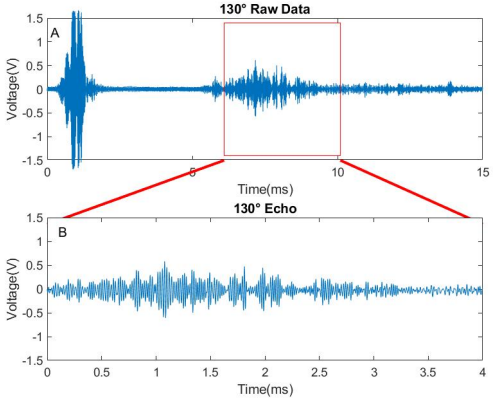

Figure 3.24: Reflected signal from three layers bush wall surface with grazing angle 130°,0.8 meter from bush wall at position 17.a) Entire reflected signal.b)Zoom in view of marked rectangular section

3.2 Same data group coherence results

For this section, there are three different subsections listed as follow :

1. The envelop result, which is echo has been processed by Hilbert transform. Only top

side of envelop would be represented

2. Coherence result at 0.5 meter with 50 °,75 °, 90 °, 105 ° and 130 °grazing angle. On the left hand, the result is the original whole echo's coherence result. On the right hand, the result is the top edge of echo envelope's coherence result. In the end, a summary of coherence range by different grazing angle is also being demonstrated.

3. Summary of Coherence result at 0.8 meter with variety of grazing angle

3.2.1 Coherence results with Hilbert transform

The following results are the top edge of echo envelop from 50 ° (Figure 3.25),75 °(Figure 3.26), 90 °(Figure 3.27), 105 °(Figure 3.28) and 130 °grazing angle (Figure 3.29). On the top side is the original echo, and on the bottom side is the top edge of echo envelop.

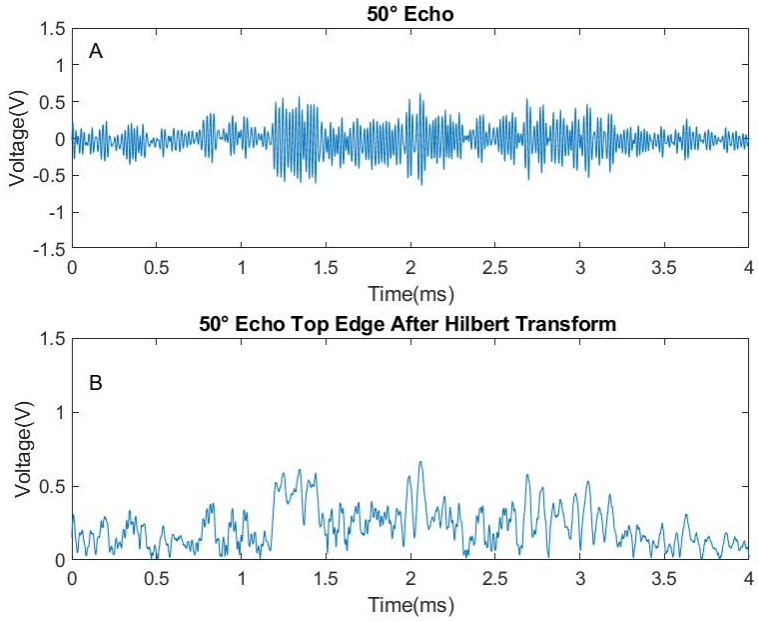

Figure 3.25: Reflected signal echo from three layers bush wall surface with grazing angle 50°,0.5 meter from bush wall at position 1.a) Entire reflected echo signal.b)Top edge of envelop from Echo by using Hilbert Transform

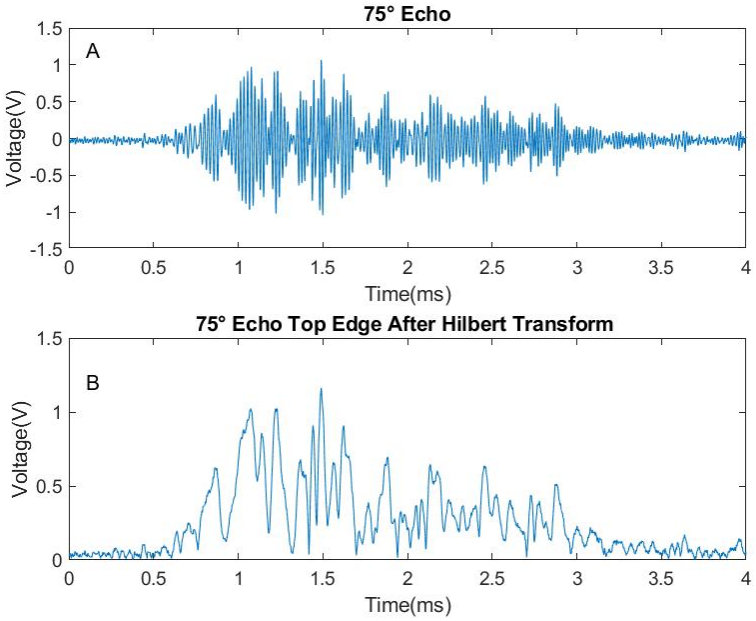

Figure 3.26: Reflected signal echo from three layers bush wall surface with grazing angle 75°,0.5 meter from bush wall at position 6.a) Entire reflected echo signal.b)Top edge of envelop from Echo by using Hilbert Transform

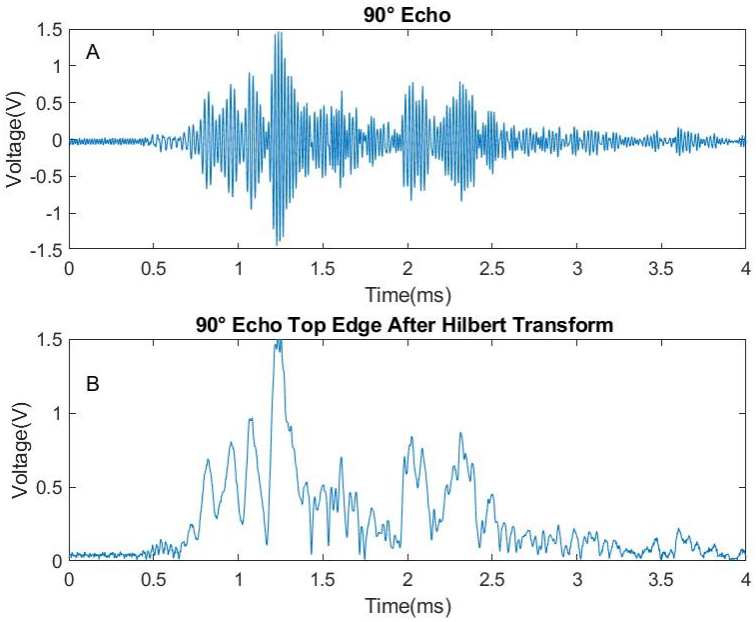

Figure 3.27: Reflected signal echo from three layers bush wall surface with grazing angle 90°,0.5 meter from bush wall at position 9.a) Entire reflected echo signal.b)Top edge of envelop from Echo by using Hilbert Transform

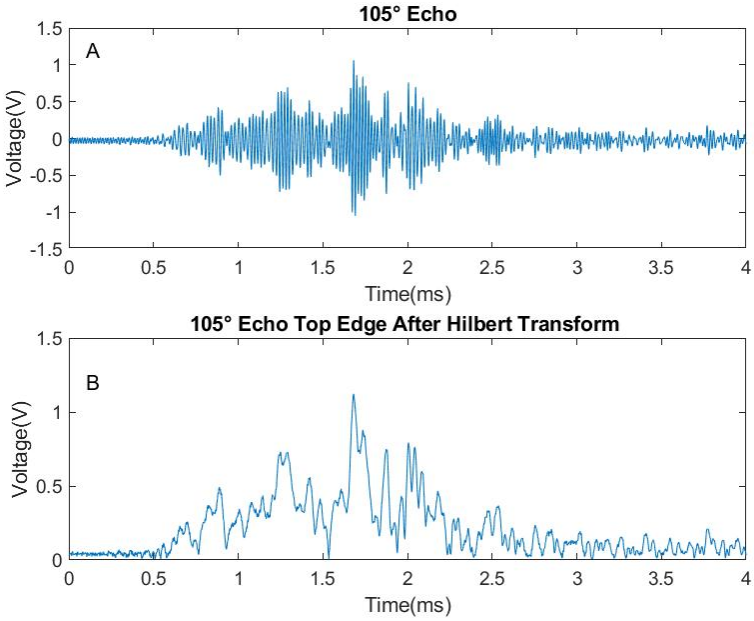

Figure 3.28: Reflected signal echo from three layers bush wall surface with grazing angle 105°,0.5 meter from bush wall at position 12.a) Entire reflected echo signal.b)Top edge of envelop from Echo by using Hilbert Transform

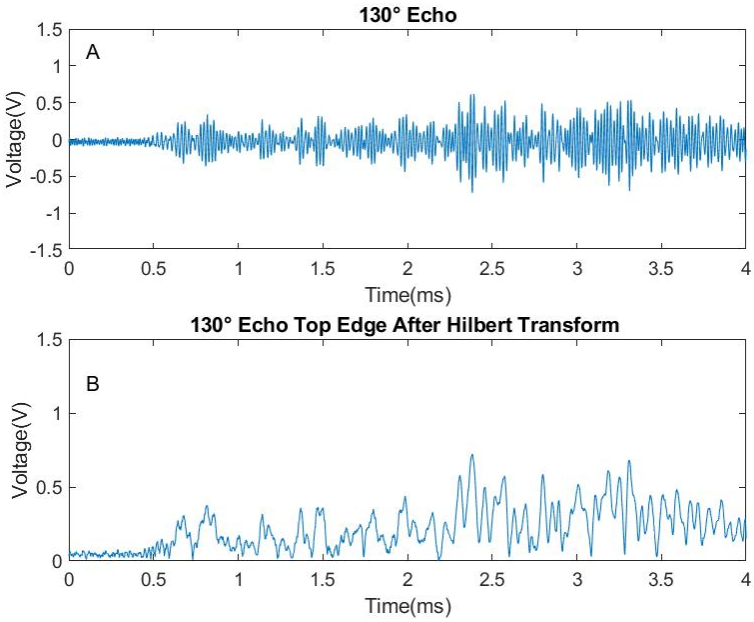

Figure 3.29: Reflected signal echo from three layers bush wall surface with grazing angle 130°,0.5 meter from bush wall at position 17.a) Entire reflected echo signal.b)Top edge of envelop from Echo by using Hilbert Transform

3.2.2 0.5 meter coherence results

For 0.5 meter coherence, the top side is the raw coherence from the collected echo data. However, since our experiment model were only using 20kHz to 105kHz chirp, therefore, the bottom side of the figure is the filtered result, which start from 20kHz and end with 105kHz. Based on the echo result, the initial guess would be that position 9 at 90 ° has the largest coherence magnitude, because position 9 at 90 ° has the most concentrated echo. However, the experimental results are not same as expected (Figure 3.34), there are not any clear tendency that shows 90 ° has the largest coherence. The summary of coherence with the chirp frequency range does not not show any linear relation that indicate coherence has relation with different grazing angle (Figure 3.40). According to the experimental result, echo has the largest coherence value at 75°and smallest coherence value at 105°. However, in the initial guess,those two positions should have similar value. Because those positions are in symmetrical positions to 90°grazing angle. In addition, the error bar of each position is significantly .

Coherence analysis result shows a better trend after Hilbert transform had been applied to the echo. The summary of Chirp frequency range coherence is shown in (Figure 3.41). In this result, the summary of coherence increases as the angle increases to 90 °, it decreases as the angle become larger than 90 °. However, at 75 ° and 105 °, these two position did not follow the initial guess. One possible assumption for this result would be that the distance between the sonar head faced and the bush wall is too close, therefore, some echoes are very similar at those two positions. Also, the error bar from after Hilbert transform is larger than the result before the Hilbert transform.

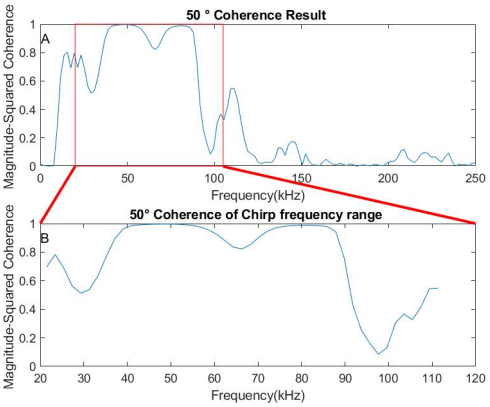

Figure 3.30: Reflected signal Coherence between N time and N+1 times from three layers bush wall surface with grazing angle 50°,0.5 meter from bush wall at position 1.a) Entire reflected signal echo coherence.b)Zoom in view of marked rectangular section where input signal range is from 20kHz to 105kHz

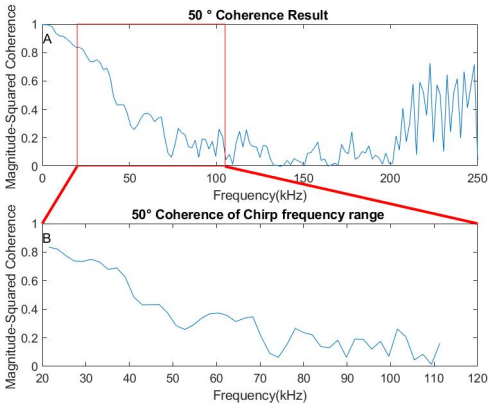

Figure 3.31: Reflected top edge of signal echo Coherence between N time and N+1 times from three layers bush wall surface with grazing angle 50°,0.5 meter from bush wall at position 1.a) Entire reflected signal echo coherence.b)Zoom in view of marked rectangular section where input signal range is from 20kHz to 105kHz

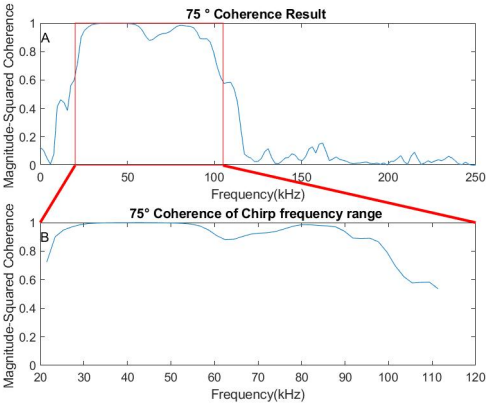

Figure 3.32: Reflected signal Coherence between N time and N+1 times from three layers bush wall surface with grazing angle 75°,0.5 meter from bush wall at position 6.a) Entire reflected signal echo coherence.b)Zoom in view of marked rectangular section where input signal range is from 20kHz to 105kHz

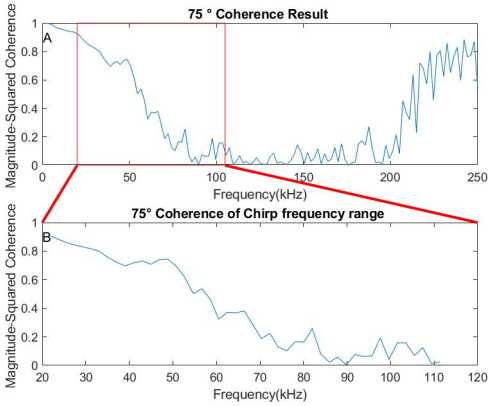

Figure 3.33: Reflected top edge of signal echo Coherence between N time and N+1 times from three layers bush wall surface with grazing angle 75°,0.5 meter from bush wall at position 6.a) Entire reflected signal echo coherence.b)Zoom in view of marked rectangular section where input signal range is from 20kHz to 105kHz

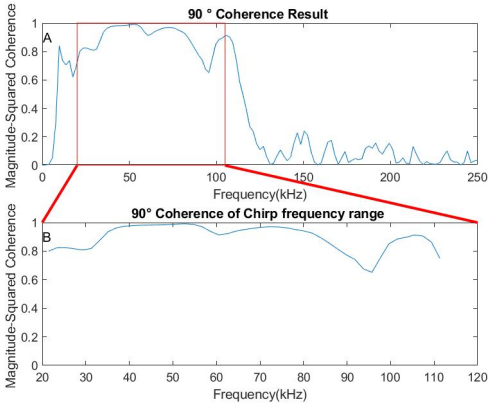

Figure 3.34: Reflected signal Coherence between N time and N+1 times from three layers bush wall surface with grazing angle 90°,0.5 meter from bush wall at position 9.a) Entire reflected signal echo coherence.b)Zoom in view of marked rectangular section where input signal range is from 20kHz to 105kHz

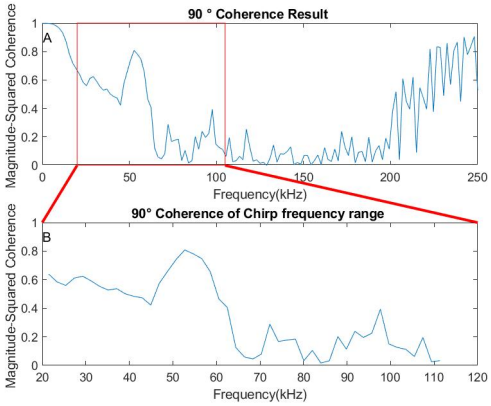

Figure 3.35: Reflected top edge of signal echo Coherence between N time and N+1 times from three layers bush wall surface with grazing angle 90°,0.5 meter from bush wall at position 9.a) Entire reflected signal echo coherence.b)Zoom in view of marked rectangular section where input signal range is from 20kHz to 105kHz

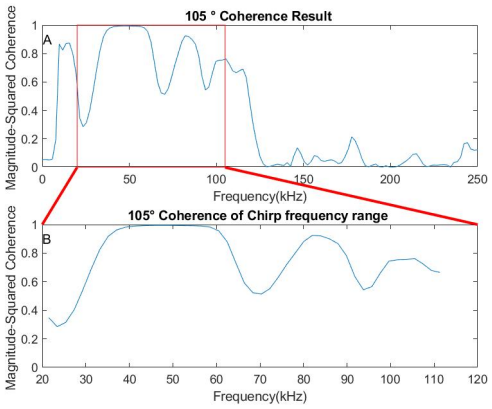

Figure 3.36: Reflected signal Coherence between N time and N+1 times from three layers bush wall surface with grazing angle 105°,0.5 meter from bush wall at position 12.a) Entire reflected signal echo coherence.b)Zoom in view of marked rectangular section where input signal range is from 20kHz to 105kHz

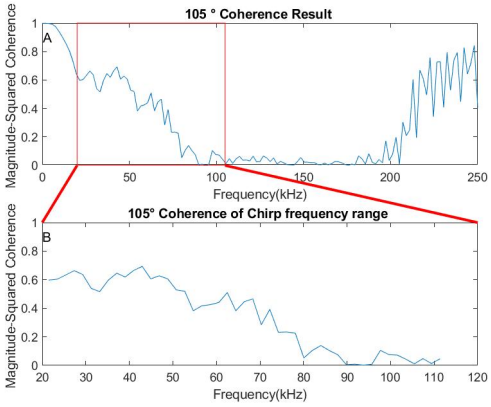

Figure 3.37: Reflected top edge of signal echo Coherence between N time and N+1 times from three layers bush wall surface with grazing angle 105°,0.5 meter from bush wall at position 12.a) Entire reflected signal echo coherence.b)Zoom in view of marked rectangular section where input signal range is from 20kHz to 105kHz

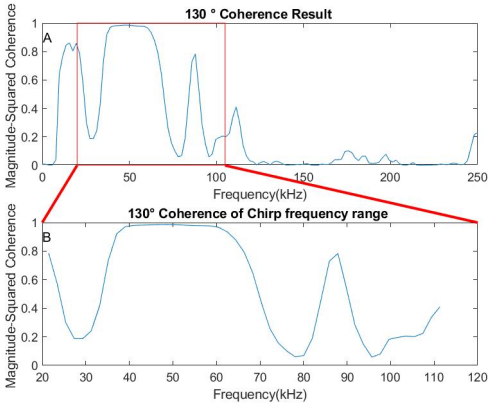

Figure 3.38: Reflected signal Coherence between N time and N+1 times from three layers bush wall surface with grazing angle 130°,0.5 meter from bush wall at position 17.a) Entire reflected signal echo coherence.b)Zoom in view of marked rectangular section where input signal range is from 20kHz to 105kHz

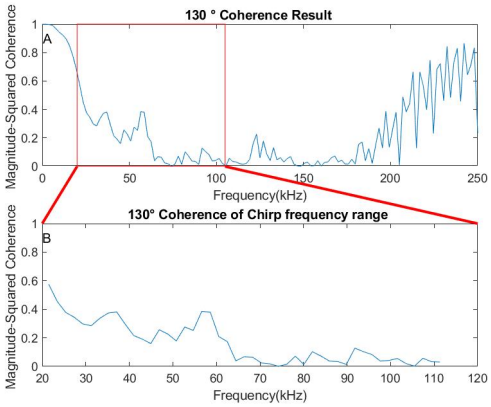

Figure 3.39: Reflected top edge of signal echo Coherence between N time and N+1 times from three layers bush wall surface with grazing angle 130°,0.5 meter from bush wall at position 17.a) Entire reflected signal echo coherence.b)Zoom in view of marked rectangular section where input signal range is from 20kHz to 105kHz

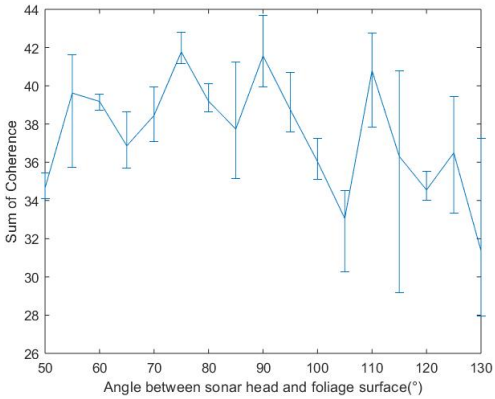

Figure 3.40: summary of Coherence at mean value with error bar of maximum and minimum when sonar head placed 0.5 meter away from bush wall

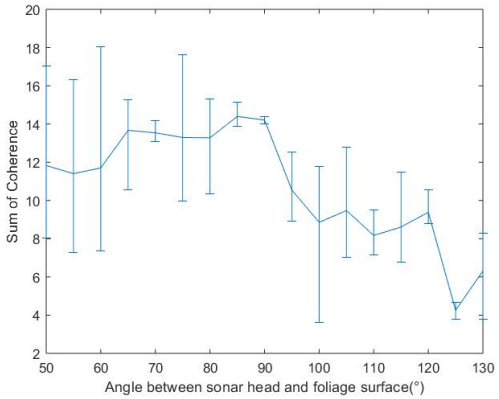

Figure 3.41: summary of top edge of echo Coherence At Mean Value with Error Bar of Maximum and Minimum when sonar head placed 0.5 meter away from bush wall

3.2.3 0.8 meter coherence results

In the 0.8 meter coherence result, the summary of the coherence result will be represented in this section, while the rest of the normal echo with different positions will be represented in Appendix II. According to the experimental result (Figure 3.42), when the position is at 90 °, it has the maximum coherence result, and the summary of coherence increases as angle increases to 90 °. Also the result decreases as angle changes from 90 ° to 130 °.There is a slightly clear pattern at the 0.8 meter coherence result, however, at 55 °and 120 °, these two positions are outliers. In addition, each position's error bar is huge, especially at 55°, 65°, 70°, 75°, 100°, 120° and 125°.

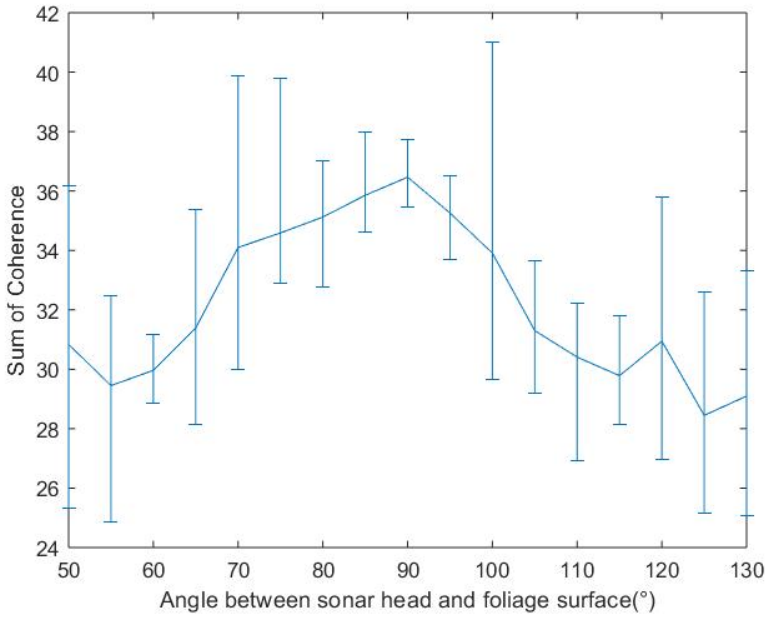

Figure 3.42: summary of Echo Coherence At Mean Value with Error Bar of Maximum and Minimum with 0.8 Meter Range

For the result after Hilbert transform. There is a clear summary of coherence increase pattern from 50 ° to 90 °, the coherence value increase as grazing angle increase. But from 90 ° to 130 °, there are outliers at 105°, 120° and 130° Figure 3.43. The result is still not symmetry,

nevertheless, the error bar of each position gets significantly improved.

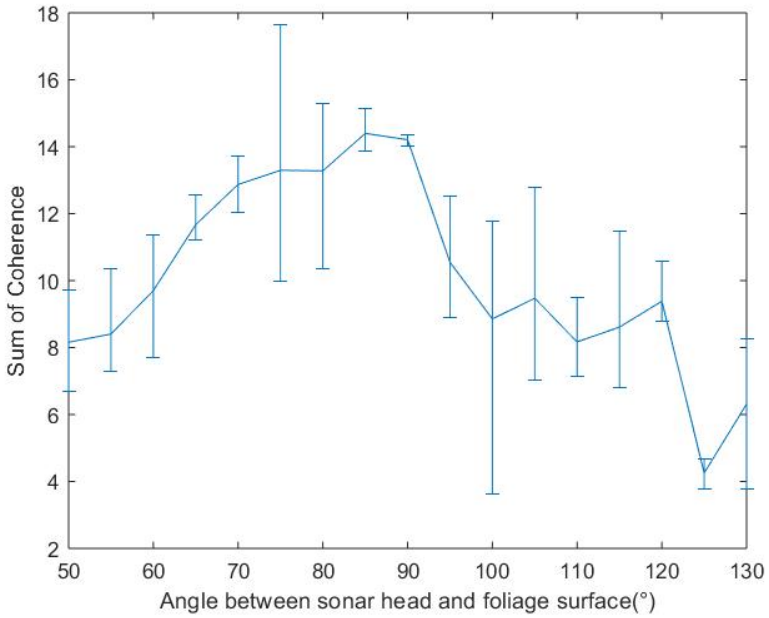

Figure 3.43: summary of Echo Edge Coherence At Mean Value With Error Bar of Maximum and Minimum with 0.8 Meter Range

3.3 Endura method results

For this experiment, a chrip signal from 20kHz to 105kHz had been used as acoustic signal, which means the wavelength of transducer is from 3.3 mm to 17mm. And the result of standard deviation for surface heights is 126 mm Figure (3.44). According to the figure, this result could fit into the Gaussian function, and the standard deviation of surface height happened at 126 mm mostly. The Kolmogorov-Smirnov shows the surface is following a Gaussian distribution, where the p-value shows fail to reject hypothesis Figure (3.45). Since the surface height is around 8 times of largest wavelength, at this point, the rough surface is used as a test model.

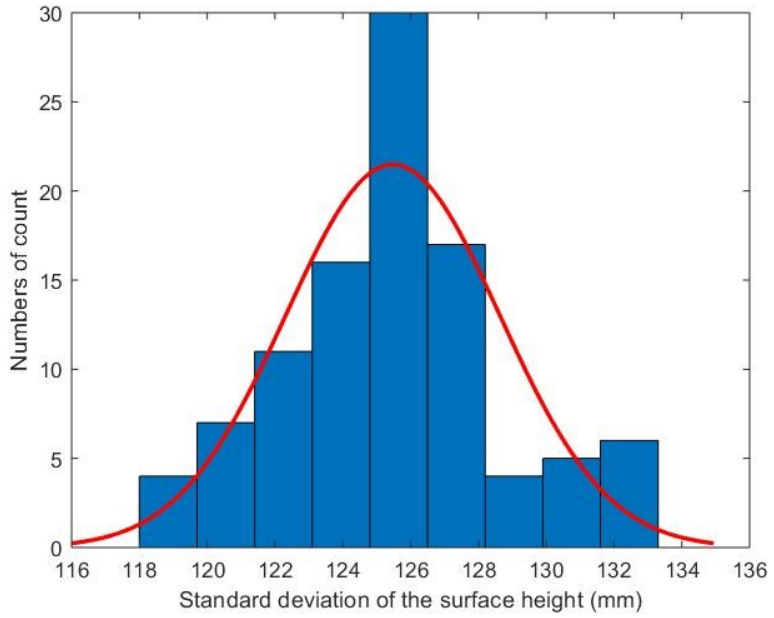

Figure 3.44: Normalized Gaussian Fit of standard deviation for surface heights by using sonar scan

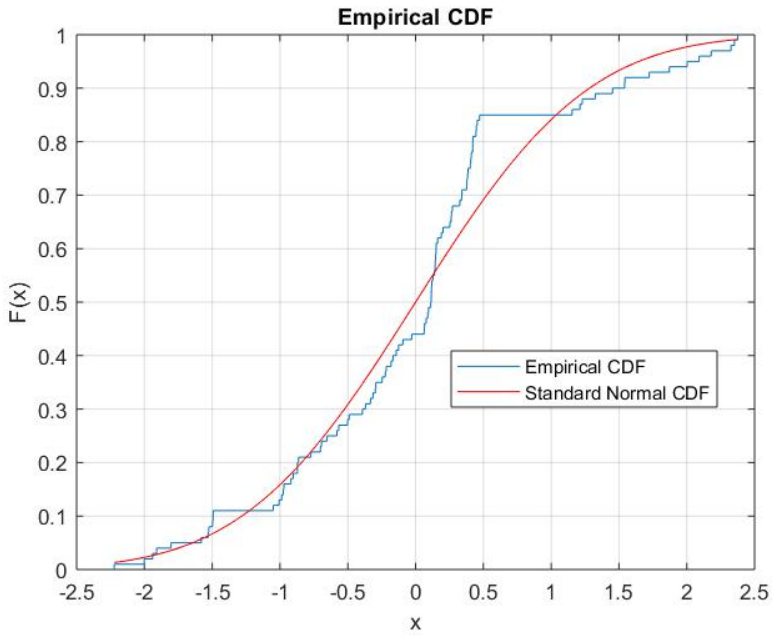

Figure 3.45: Kolmogorov-Smirnov(KS) test of Normalized Gaussian Fit of standard deviation for surface heights

According to Endura method with moderately rough surface, the energy increase as sonar head become closer to object, and the energy decrease as sonar head face away from object. For the rough surface, the energy would not change in a large amount at all position, but it would have a slight increase at 90 degree. Based on the experiment result 3.46, the energy result has a different trend comparing to method's result of the moderate rough, but it has a similar trend as method's result of the rough surface. According the method's equation describing moderately rough surface the 90 ° position's energy has 38.5 dB, and sonar head faced away object, which is 50 ° position's energy has 23.8 dB. Therefore, there are nearly 15 dB difference between two positions. In the other words, the 90 °'s receive signal should be 5.6 times stronger than the 50 °'s signal. Yet, this assumption does not fit in our experiment case(Figure 3.3 and figure 3.7). In the actual case, this experiment result is more similar to the rough surface's result but with a lower amplitude.

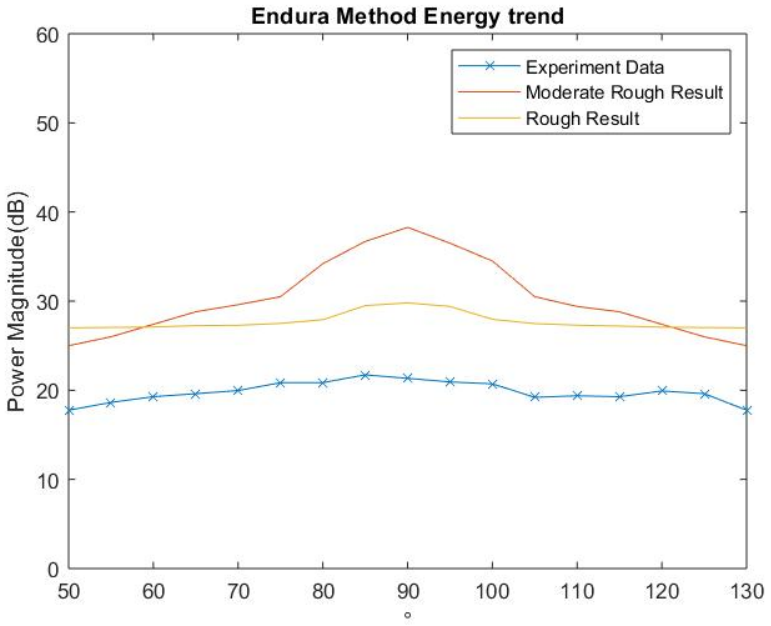

Figure 3.46: Reflected signal Echo Energy by using Endura Method from three layers bush wall surface with grazing angle from 50° to 130°,0.5 meter distance from bush wall.The red line represent the Moderate rough surface's equation result. The yellow line represent the rough surface's equation result. The blue line represent the experiment data result

For the duration equation, both moderate rough and rough surface share a same equation, therefore, the equation result should be same. Experimental result and Endura method's equation result are represented as figure 3.47. The duration result are very stable with low different value of each point, result are roughly symmetrical especially from 75 ° to 105 °. There are only two outliers in the experiment result, the first one is at 70 ° and second one is at 110 °, those two positions are also symmetrical to 90 ° grazing angle. Moreover, the error bar of each position are very impressive, especially from 75 ° to 105 °

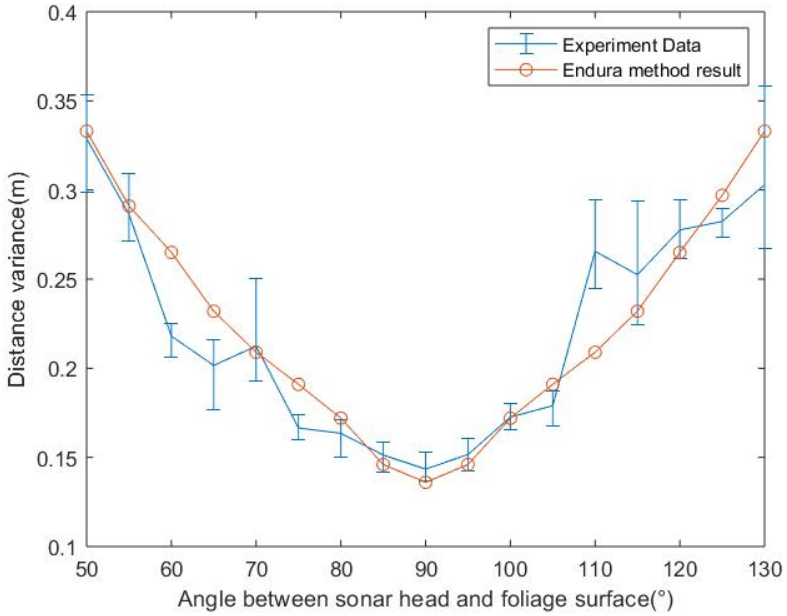

Figure 3.47: Reflected signal Echo Duration by using Endura Method from three layers bush wall surface with grazing angle from 50° to 130°,0.5 meter distance from bush wall.

A fit in equation has been generated based on the result and the error bar are also shown in the result figure. The third order of polynomial fitting function Figure (3.48) and fourth order of polynomial fitting equations Figure (3.49) are the chosen priority because of low calculation and suited for result. The 3rd order fitting equation is shown as equation (3.1) and 4th order fitting equation is shown as equation (3.2). Those two fitting function are based on normalized angle, which changed range from 50 ° to -1 and 130 ° to 1, respectively. Because normalized angle can significantly reduce computational time.

$$F(x) = -0.07096x^3 + 0.1631x^2 + 0.06033x + 0.1598 \tag{3.1}$$

$$F(x) = -0.07759x^4 - 0.07096x^3 + 0.237x^2 + 0.06033x + 0.1516 \tag{3.2}$$

A Monte Carlo simulation had been crated based on the fitting function and properties of duration data (mean value and standard deviation). Since the duration result are mostly

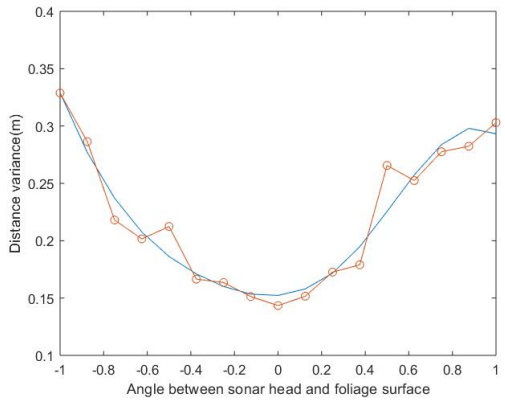

Figure 3.48: Third order of polynomial fitting function with R-value: 0.005

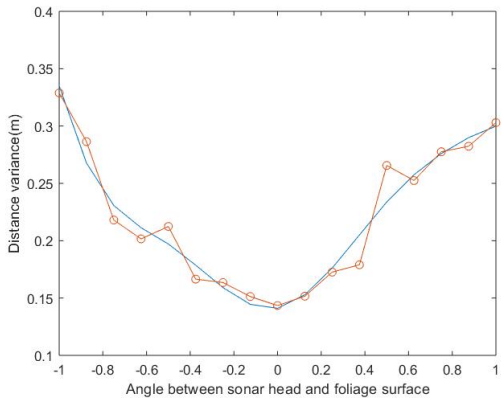

Figure 3.49: Fourth order of polynomial fitting function with R-value: 0.004

Gaussian distribution Figure (3.51) (some edge position may not be a Gaussian distribution because of result of KS test Figure (3.50)), a 100000 random samples, which followed a Gaussian distribution had generated 100000 random duration results. Those results applied into a inverse of polynomial function could get a position. The 55 ° Figure (3.52) and 80 ° Figure (3.53) results are shown below, rest could find in appendix. Since the random result is close to a Gaussian distribution, therefore, the difference of estimated position can be represented as result of standard derivation Figure (3.54). Since 50 °, 90 ° and 130 °grazing angle are the boundaries of fitting function, the estimate angle's standard deviation are extremely huge .The Monte carlo simulation could only estimate 55 ° to 85 ° and 90 ° to 130 ° position. The maximum of the standard deviation are at position 70 ° and 110 °, but still within 3 degree. Other positions are having standard deviation around 1 degree.

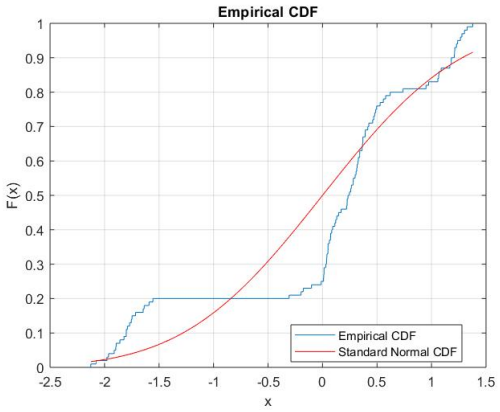

Figure 3.50: KS test for position 1 at 55 degree

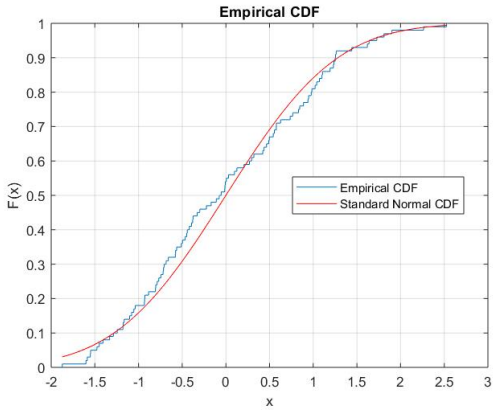

Figure 3.51: KS test for position 8 at 85 degree

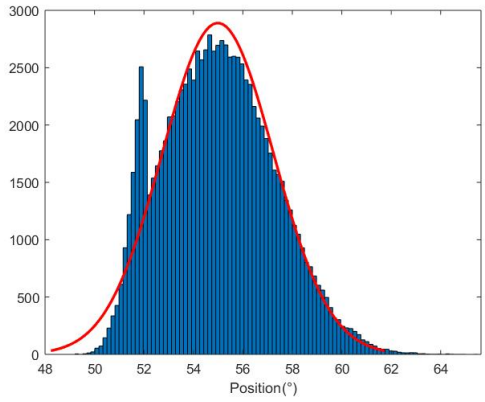

Figure 3.52: Position 2 at 55 ° result based on ten thousand random duration input

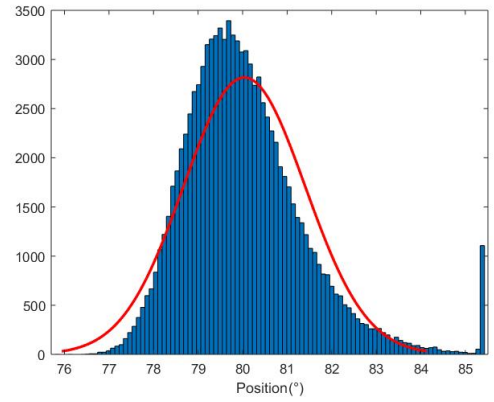

Figure 3.53: Position 1 at 80 ° result based on ten thousand random duration input

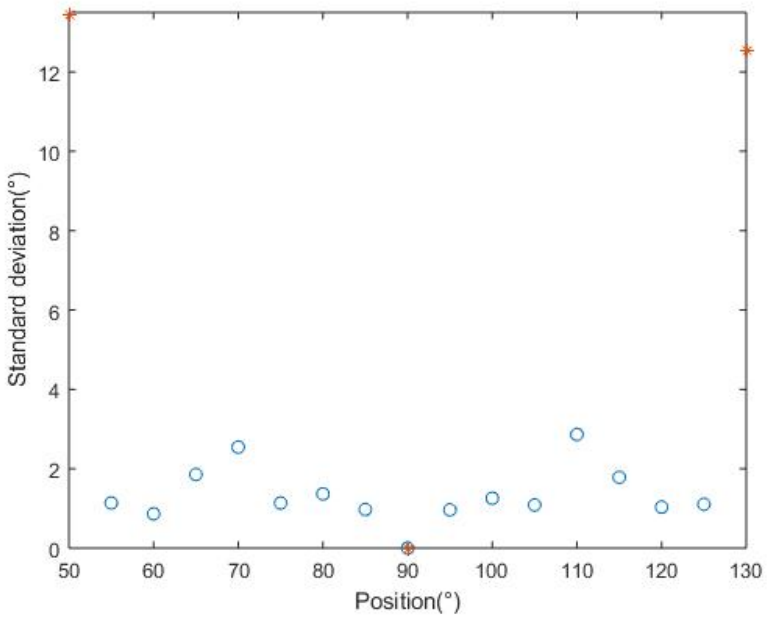

Figure 3.54: Standard deviation of Monte carlo simulation of each position with 100000 random input.Mark 'X' means the estimation is a bad estimation, Mark 'O' means the estimation is a good estimation

Chapter 4

Conclusions and Summary

4.1 Conclusion

With rapid development of autonomous flying drone, acoustic navigation would be an ever increasing popular technique for drone navigation. Therefore, the relationship between reflection from foliage with varying angles would be more useful in practical world. From the introduction section, an artificial sonar based drone is desired to perform as good as the bat's navigation behaviours, because the bat's autonomous navigation behaviours can be classified as a high level of autonomy. The primary purpose of this thesis is finding a sonar based technique that help drone reach a high level autonomy by analyzing the characteristics of each angle's acoustic signal reflection near a 3-D bush wall. As a result, any major findings need to be evaluated against practical world applications and bat's performance.

- The reflections from bush wall surfaces with varying grazing angle have various shapes. and these different shapes of echo tells sensor different target direction, which can classify as a sensory-motor level autonomy, and the echo results could potentially saves time and cost due to fast response that drone does not need any complicated math to calculate for next move. However, the experiment results tell us that the sensor being used in the experiment has a low repeatability of recognizing object direction. In conclusion, this product is not suggested to work on a sonar based autonomous drone.

Unless we have a bat-like acoustic sensor, which has a high repeatability. Because bats could repeatedly recognize object direction through echolocation during food acquisition process[39].

- Based on the result of coherence, the summary of coherence has a linear relation that 90° grazing angle has the largest magnitude of coherence. In the practical world, this finding can potentially help drone to avoid collision with any obstacles when reach a certain coherence value. However, the huge error bar and asymmetry result could cost drone on board system chaos, which is less desirable because a bat-like acoustic sensor should have stable judging system. Because bats have amazing accuracy target location through echolocation[32]. In conclusion, this finding illustrate grazing angle has linear relation with coherence magnitude. But this finding is useless in practical world, and perform poorly when compare to bat's navigation performance.

- Based on the result of the Endura method being applied to 3-D bush wall. The echo duration result has a linear relation with grazing angle, and the error within this linear relation is reasonable. Obviously, in piratical world, a low error and clear differences between each degree of angle would be an ideal case for an obstacle sensor. In addition, this method is more than a sensory-motor autonomy, because the computer not only detects objects, but also recognizes the fleet angle, which is an import factor for changing airline. Bats also have obstacle avoidance by using different echo duration[25], which is very similar to this experiment result. In conclusion, this finding is close to the desired values in the practical world's desire and almost the same as the bats' navigation behaviours.

In the three previous cases, a 3-D Endura method is more suitable to practical world's value and similar to bat's navigation behaviours. Because 3-D Endura method has more advantage

in achieving a lower error and getting a general value for all situation. Therefore, sonar based autonomy could use 3-D Endura method as a solution when the drone is in front of a layered bush wall .

4.2 Suggestions for future work

Future research work can be performed on a larger distance range and wider angle range. Also, smaller A/D converter is required in order to reduce the size of the on board system. This thesis is only a method to discuss the relevance between reflections from foliage with varying degrees. In the future version, a sensor could be designed based on this method, one possibility that it could collect data when the drone fly automatically in a forest by sensor and on board computer. Further research is needed in order to use better equipment and more data, for the final goal, autonomous drone could learn how to fly by big data learning and machine learning.

Chapter 5

Summary of achievements

5.1 Research achievements

This thesis has found a stable relation between bush wall reflected echo and variety of surface grazing angle. There are two major approaches to achieve final goal, and a sonar head also has been built to collect experimental data. In doing so, the following was achieved

- Design and built a working sonar head to collect data, which include emitter, emitter amplifier circuit, receiver, power distribution board, software development.
- Developed a method to test different grazing angle influence bush wall reflection echo
- Discovered a novel relation with different grazing angle's acoustic reflection from a 3-D bush wall
- Finding an effective method for sonar based autonomy with Endura method

5.2 Major Findings

- The 90° grazing angle, which is sonar head faced to bush wall has most contrasted echo, and when sonar head faced away bush wall, echo shape began to disperse.

- The top edge of 90° grazing angle has the largest summary of coherence, when sonar head placed 0.8 meter away from bush wall, it has better summary of coherence result than 0.5 meter's result. The top edge of echo, which is echo passed a Hilbert transform has better result than the original echo's result.

- A 3-D bush wall surface can be recognized as a moderately rough surface based on the surface height's standard deviation.

- Endura method can apply to a 3-D bush wall situation. Energy does not clearly change by each position in dB scale according to Endura method's result. However,echo duration get smaller when grazing angle increase from 50° to 90 ° and decrease from 90° to 130°.

Bibliography

[1] Anthony S. Acampora and Jack H. Winters. Three-dimensional ultrasonic vision for robotic applications. *IEEE Transactions on Pattern Analysis & Machine Intelligence*, (3):291–303, 1989.

[2] Huzefa Akbarally and Lindsay Kleeman. A sonar sensor for accurate 3d target localisation and classification. In *Robotics and Automation, 1995. Proceedings., 1995 IEEE International Conference on*, volume 3, pages 3003–3008. IEEE, 1995.

[3] Chris J Baker, Graeme E Smith, Alessio Balleri, Marc Holderied, and Hugh D Griffiths. Biomimetic echolocation with application to radar and sonar sensing. *Proceedings of the IEEE*, 102(4):447–458, 2014.

[4] Billur Barshan and Roman Kuc. A bat-like sonar system for obstacle localization. *IEEE Transactions on systems, man, and cybernetics*, 22(4):636–646, 1992.

[5] Troy E Beckert. Cognitive autonomy and self-evaluation in adolescence: A conceptual investigation and instrument development. *North American Journal of Psychology*, 9(3), 2007.

[6] Edward Bedrosian. A product theorem for hilbert transforms. 1962.

[7] Kurt Binder, Dieter Heermann, Lyle Roelofs, A John Mallinckrodt, and Susan McKay. Monte carlo simulation in statistical physics. *Computers in Physics*, 7(2):156–157, 1993.

[8] Johann Borenstein and Yoram Koren. Real-time obstacle avoidance for fast mobile robots. *IEEE Transactions on systems, Man, and Cybernetics*, 19(5):1179–1187, 1989.

[9] Johann Borenstein, Yoram Koren, et al. Histogramic in-motion mapping for mobile robot obstacle avoidance. *IEEE Transactions on Robotics and Automation*, 7(4):535–539, 1991.

[10] Philip Boucher. Domesticating the drone: the demilitarisation of unmanned aircraft for civil markets. *Science and engineering ethics*, 21(6):1393–1412, 2015.

[11] Oemuer Bozma and Roman Kuc. A physical model-based analysis of heterogeneous environments using sonar-endura method. *IEEE Transactions on Pattern Analysis and Machine Intelligence*, 16(5):497–506, 1994.

[12] Ömür Bozma and Roman Kuc. Building a sonar map in a specular environment using a single mobile sensor. *IEEE Transactions on Pattern Analysis & Machine Intelligence*, (12):1260–1269, 1991.

[13] G S Brown. Backscattering from a gaussian-distributed perfectly conducting rough surface. *IEEE Transactions on antennas and propagation*, 26(3):472–482, 1978.

[14] M Brown. Feature extraction techniques for recognizing solid objects with an ultrasonic range sensor. *IEEE Journal on Robotics and Automation*, 1(4):191–205, 1985.

[15] Ryan A Chisholm, Jinqiang Cui, Shawn KY Lum, and Ben M Chen. Uav lidar for below-canopy forest surveys. *Journal of Unmanned Vehicle Systems*, 1(01):61–68, 2013.

[16] Kwangsu Cho, Minhee Cho, and Jongwoo Jeon. Fly a drone safely: Evaluation of an embodied egocentric drone controller interface. *Interacting with computers*, 29(3):345–354, 2017.

[17] BM Costa, TA Battista, and SJ Pittman. Comparative evaluation of airborne lidar and ship-based multibeam sonar bathymetry and intensity for mapping coral reef ecosystems. *Remote Sensing of Environment*, 113(5):1082–1100, 2009.

[18] J Crowley. Navigation for an intelligent mobile robot. *IEEE Journal on Robotics and Automation*, 1(1):31–41, 1985.

[19] J Dugundji. Envelopes and pre-envelopes of real waveforms. *IRE Transactions on Information Theory*, 4(1):53–57, 1958.

[20] Carl Eckart. The scattering of sound from the sea surface. *The Journal of the Acoustical Society of America*, 25(3):566–570, 1953.

[21] Alberto Elfes. Sonar-based real-world mapping and navigation. *IEEE Journal on Robotics and Automation*, 3(3):249–265, 1987.

[22] Dario Floreano and Robert J Wood. Science, technology and the future of small autonomous drones. *Nature*, 521(7553):460, 2015.

[23] Dario Floreano, Jean-Christophe Zufferey, Mandyam V Srinivasan, and Charlie Ellington. *Flying insects and robots*. Springer, 2009.

[24] Donald R Griffin and Robert Galambos. The sensory basis of obstacle avoidance by flying bats. *Journal of Experimental zoology*, 86(3):481–506, 1941.

[25] Robert A Grummon and Alvin Novick. Obstacle avoidance in the bat, macrotus mexicanus. *Physiological Zoology*, 36(4):361–369, 1963.

[26] Tomáš Krajník, Vojtěch Vonásek, Daniel Fišer, and Jan Faigl. Ar-drone as a platform for robotic research and education. In *International conference on research and education in robotics*, pages 172–186. Springer, 2011.

[27] Roman Kuc. Three-dimensional tracking using qualitative bionic sonar. *Robotics and Autonomous Systems*, 11(3-4):213–219, 1993.

[28] Roman Kuc and Victor Brian Viard. A physically based navigation strategy for sonar-guided vehicles. *The international journal of robotics research*, 10(2):75–87, 1991.

[29] John J Leonard and Hugh F Durrant-Whyte. *Directed sonar sensing for mobile robot navigation*, volume 175. Springer Science & Business Media, 2012.

[30] Chen Ming, Anupam Kumar Gupta, Ruijin Lu, Hongxiao Zhu, and Rolf Müller. A computational model for biosonar echoes from foliage. *PloS one*, 12(8):e0182824, 2017.

[31] Chen Ming, Hongxiao Zhu, and Rolf Müller. A simplified model of biosonar echoes from foliage and the properties of natural foliages. *PloS one*, 12(12):e0189824, 2017.

[32] Golrokh Mirzaei, Mohammad Wadood Majid, Mohsin M Jamali, Jeremy Ross, J Frizado, Peter V Gorsevski, and V Bingman. The application of evolutionary neural network for bat echolocation calls recognition. In *Neural Networks (IJCNN), The 2011 International Joint Conference on*, pages 1106–1111. IEEE, 2011.

[33] Rolf Müller and Roman Kuc. Foliage echoes: a probe into the ecological acoustics of bat echolocation. *The Journal of the Acoustical Society of America*, 108(2):836–845, 2000.

[34] JI Nelson, PA Salin, MH-J Munk, M Arzi, and J Bullier. Spatial and temporal coherence in cortico-cortical connections: a cross-correlation study in areas 17 and 18 in the cat. *Visual neuroscience*, 9(1):21–37, 1992.

[35] Emanuel Parzen. On estimation of a probability density function and mode. *The annals of mathematical statistics*, 33(3):1065–1076, 1962.

[36] Jonas Reijniers and Herbert Peremans. Towards a theory of how bats navigate through foliage. In *Proc. of the 8th Int. Conf. on the Simulation of Adaptive Behaviour*, pages 77–86, 2004.

[37] Wolfgang D Rencken. Autonomous sonar navigation in indoor, unknown and unstructured environments. In *Proceedings of IEEE/RSJ International Conference on Intelligent Robots and Systems (IROS'94)*, volume 1, pages 431–438. IEEE, 1994.

[38] Sebastian Scherer, Sanjiv Singh, Lyle Chamberlain, and Srikanth Saripalli. Flying fast and low among obstacles. In *Robotics and Automation, 2007 IEEE International Conference on*, pages 2023–2029. IEEE, 2007.

[39] Hans-Ulrich Schnitzler, Cynthia F Moss, and Annette Denzinger. From spatial orientation to food acquisition in echolocating bats. *Trends in Ecology & Evolution*, 18(8):386–394, 2003.

[40] James A Simmons. Echolocation in bats: signal processing of echoes for target range. *Science*, 171(3974):925–928, 1971.

[41] Eric I Thorsos. The validity of the kirchhoff approximation for rough surface scattering using a gaussian roughness spectrum. *The Journal of the Acoustical Society of America*, 83(1):78–92, 1988.

[42] Nicolas Vandapel, James Kuffner, and Omead Amidi. Planning 3-d path networks in unstructured environments. In *Robotics and Automation, 2005. ICRA 2005. Proceedings of the 2005 IEEE International Conference on*, pages 4624–4629. IEEE, 2005.

[43] Ben Verboom, Arjan M Boonman, and Herman JGA Limpens. Acoustic perception of landscape elements by the pond bat (myotis dasycneme). *Journal of Zoology*, 248(1):59–66, 1999.

[44] Talbot H Waterman. *Animal navigation*. Scientific American Library New York, 1989.

[45] Jie Zhang, Bruce W Drinkwater, and Paul D Wilcox. Effect of roughness on imaging and

sizing rough crack-like defects using ultrasonic arrays. *IEEE transactions on ultrasonics, ferroelectrics, and frequency control*, 59(5), 2012.

Appendices

Appendix A

First Appendix

A.1 Section one:Other Position Echo Result

A.1.1 0.5 meter Echo

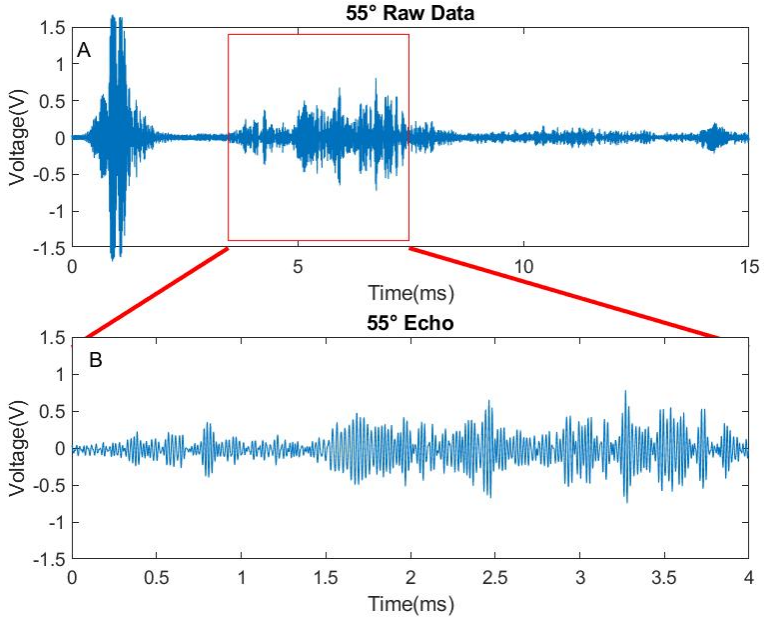

Figure A.1: Reflected signal from one layer bush wall surface with grazing angle 55°,0.5 meter from bush wall at position 2.a) Entire reflected signal.b)Zoom in view of marked rectangular section

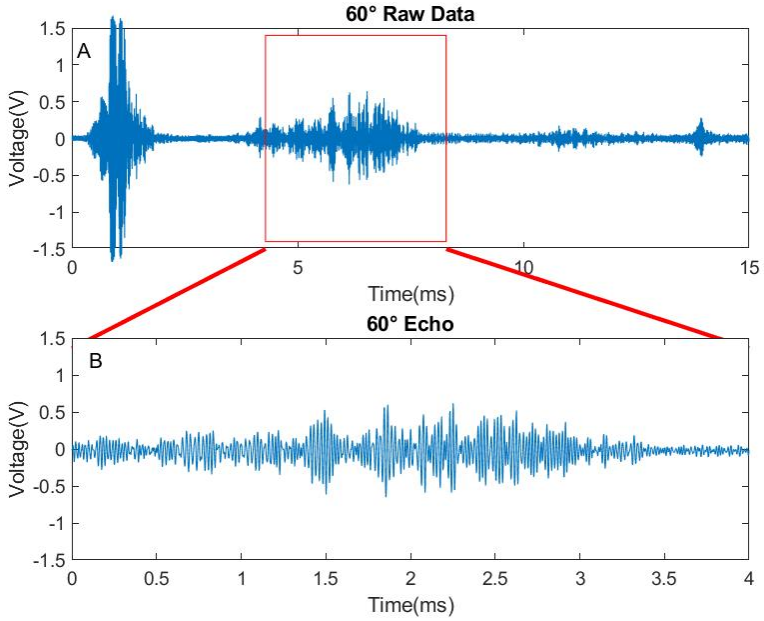

Figure A.2: Reflected signal from one layer bush wall surface with grazing angle 60°,0.5 meter from bush wall at position 3.a) Entire reflected signal.b)Zoom in view of marked rectangular section

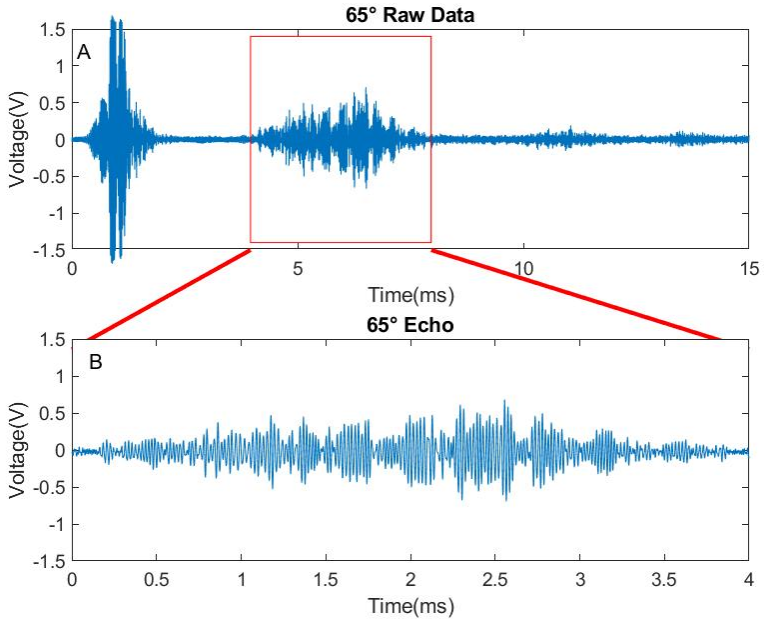

Figure A.3: Reflected signal from one layer bush wall surface with grazing angle 65°,0.5 meter from bush wall at position 4.a) Entire reflected signal.b)Zoom in view of marked rectangular section

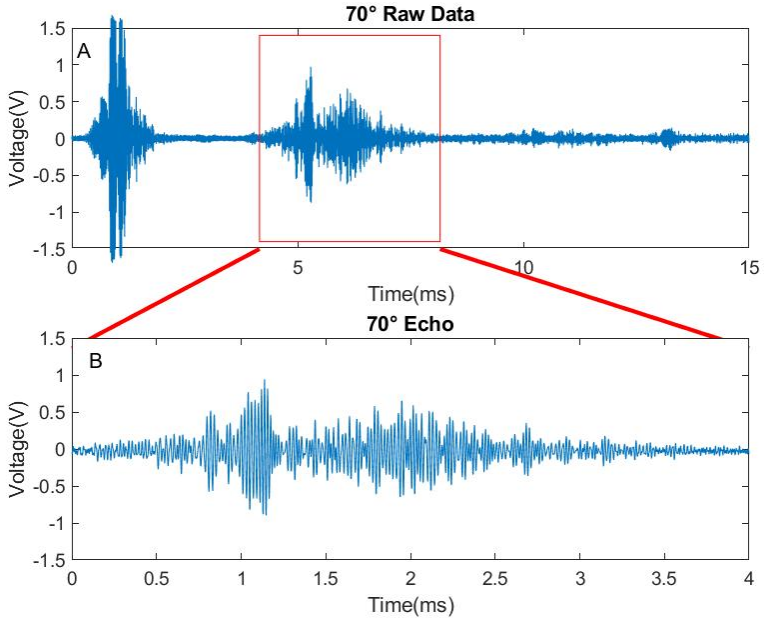

Figure A.4: Reflected signal from one layer bush wall surface with grazing angle 70°,0.5 meter from bush wall at position 5.a) Entire reflected signal.b)Zoom in view of marked rectangular section

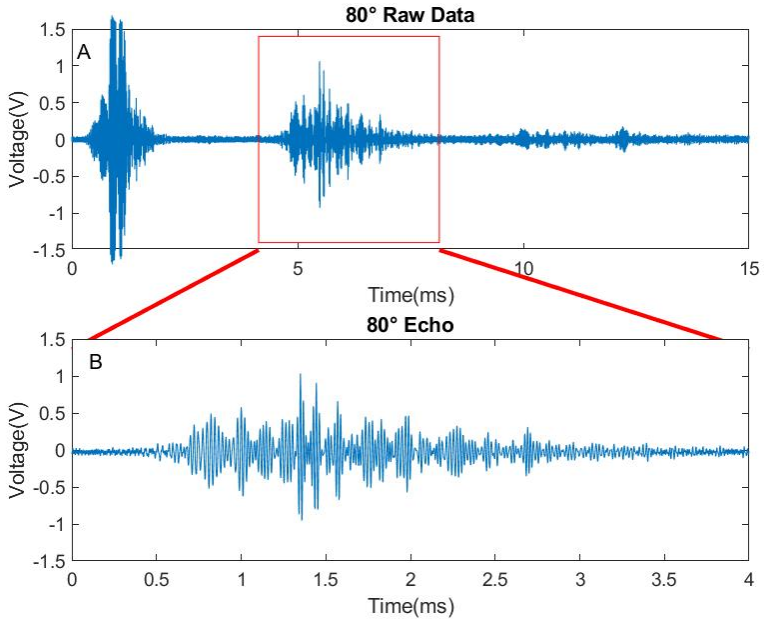

Figure A.5: Reflected signal from one layer bush wall surface with grazing angle 80°,0.5 meter from bush wall at position 7.a) Entire reflected signal.b)Zoom in view of marked rectangular section

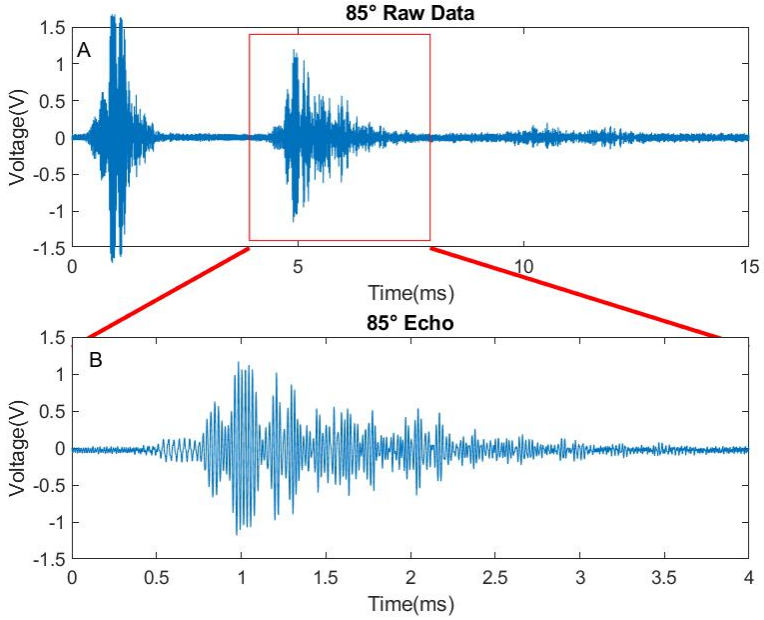

Figure A.6: Reflected signal from one layer bush wall surface with grazing angle 85°,0.5 meter from bush wall at position 8.a) Entire reflected signal.b)Zoom in view of marked rectangular section

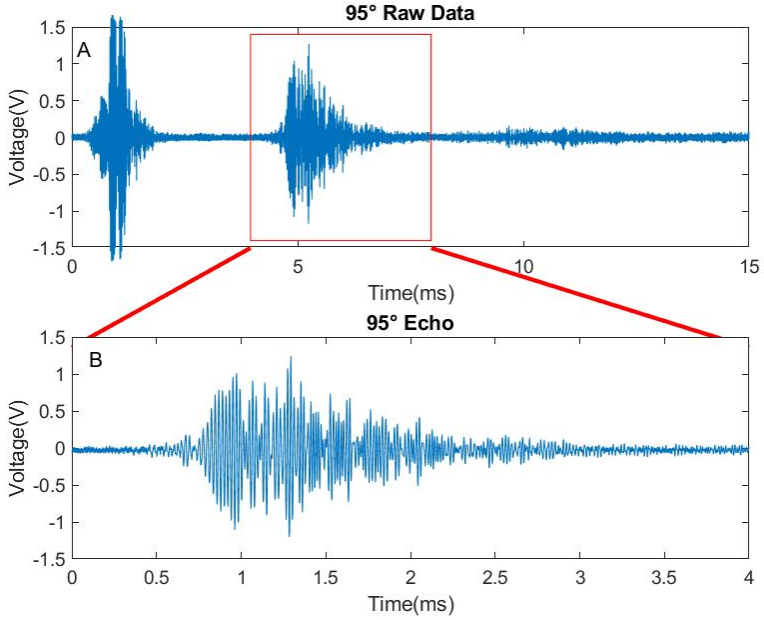

Figure A.7: Reflected signal from one layer bush wall surface with grazing angle 95°,0.5 meter from bush wall at position 10.a) Entire reflected signal.b)Zoom in view of marked rectangular section

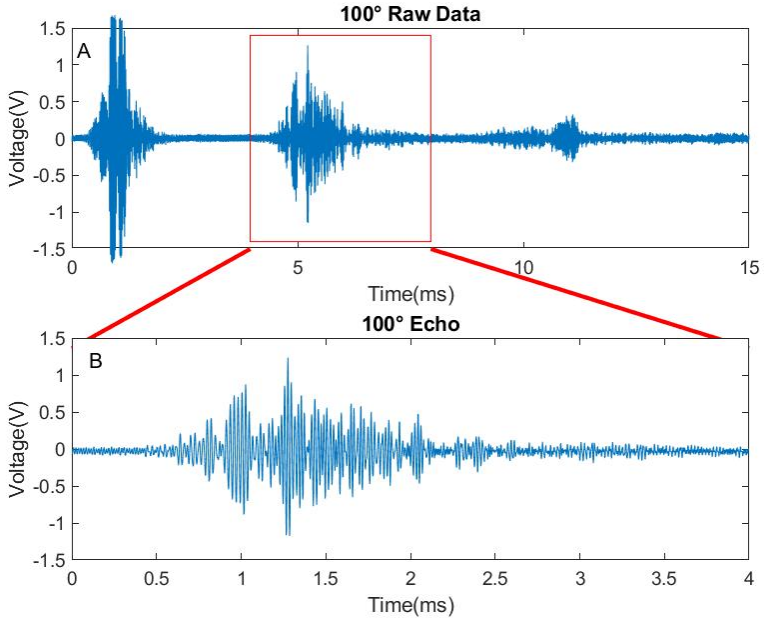

Figure A.8: Reflected signal from one layer bush wall surface with grazing angle 100°,0.5 meter from bush wall at position 11.a) Entire reflected signal.b)Zoom in view of marked rectangular section

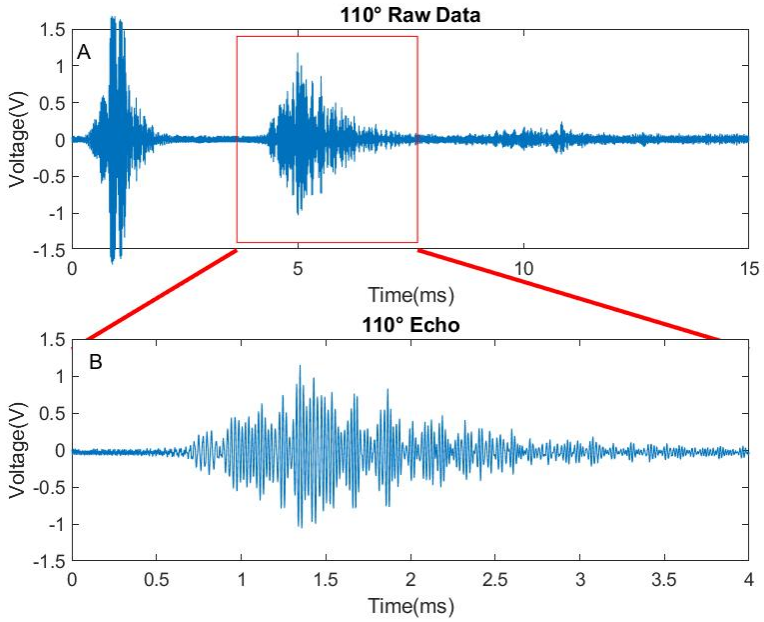

Figure A.9: Reflected signal from one layer bush wall surface with grazing angle 110°,0.5 meter from bush wall at position 13.a) Entire reflected signal.b)Zoom in view of marked rectangular section

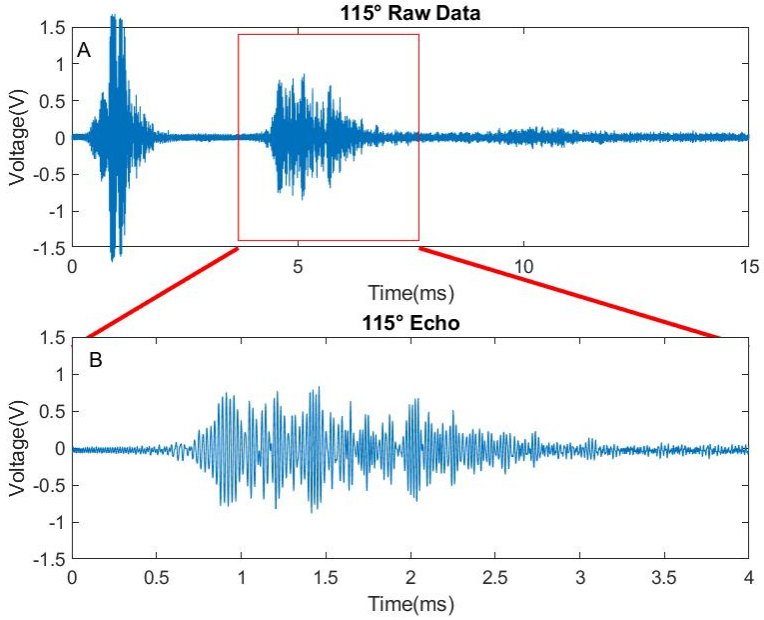

Figure A.10: Reflected signal from one layer bush wall surface with grazing angle 115°,0.5 meter from bush wall at position 14.a) Entire reflected signal.b)Zoom in view of marked rectangular section

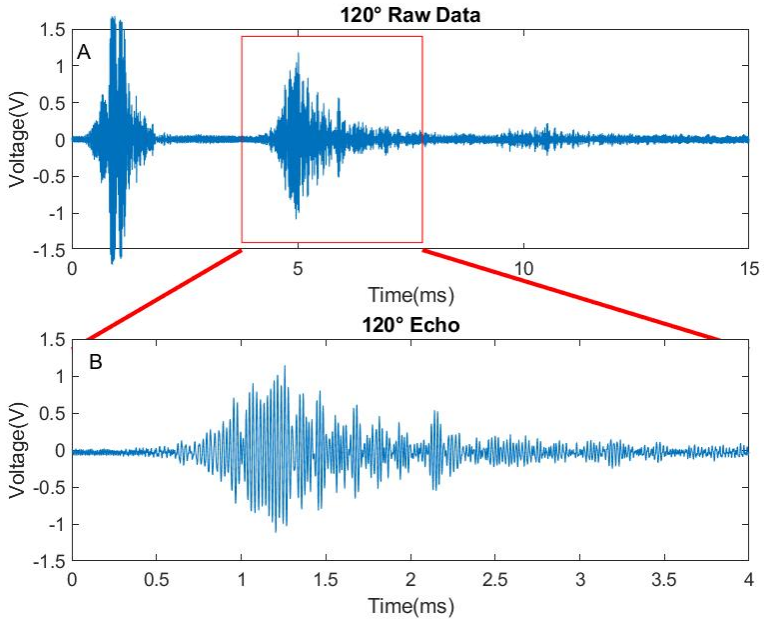

Figure A.11: Reflected signal from one layer bush wall surface with grazing angle 120°,0.5 meter from bush wall at position 15.a) Entire reflected signal.b)Zoom in view of marked rectangular section

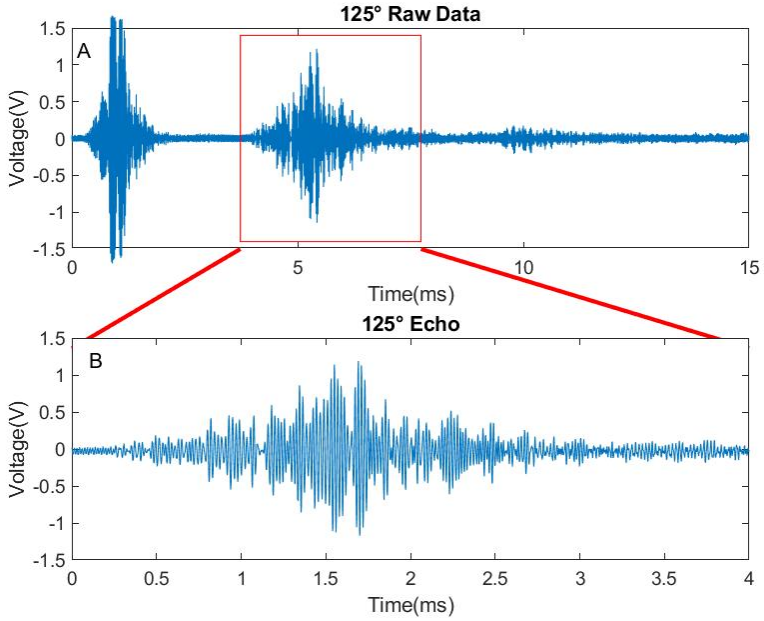

Figure A.12: Reflected signal from two layers bush wall surface with grazing angle 125°,0.5 meter from bush wall at position 16.a) Entire reflected signal.b)Zoom in view of marked rectangular section

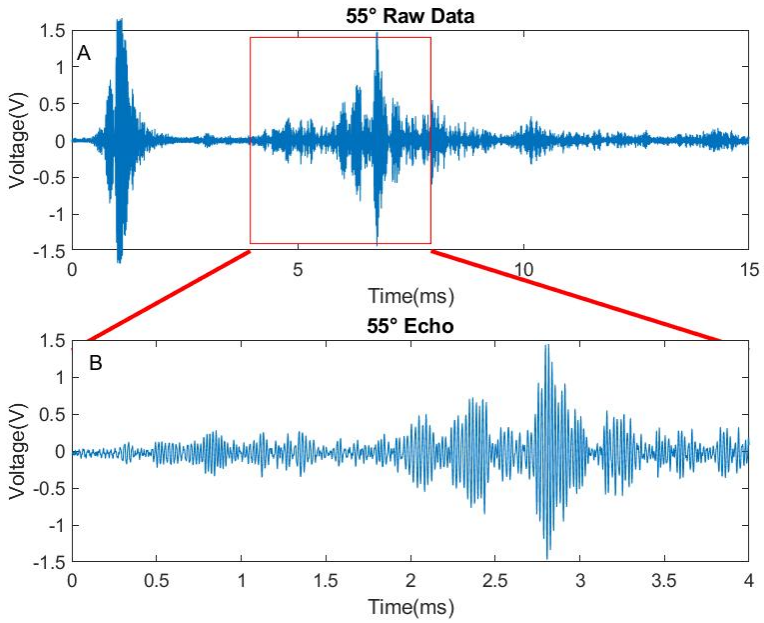

Figure A.13: Reflected signal from two layers bush wall surface with grazing angle 55°,0.5 meter from bush wall at position 2.a) Entire reflected signal.b)Zoom in view of marked rectangular section

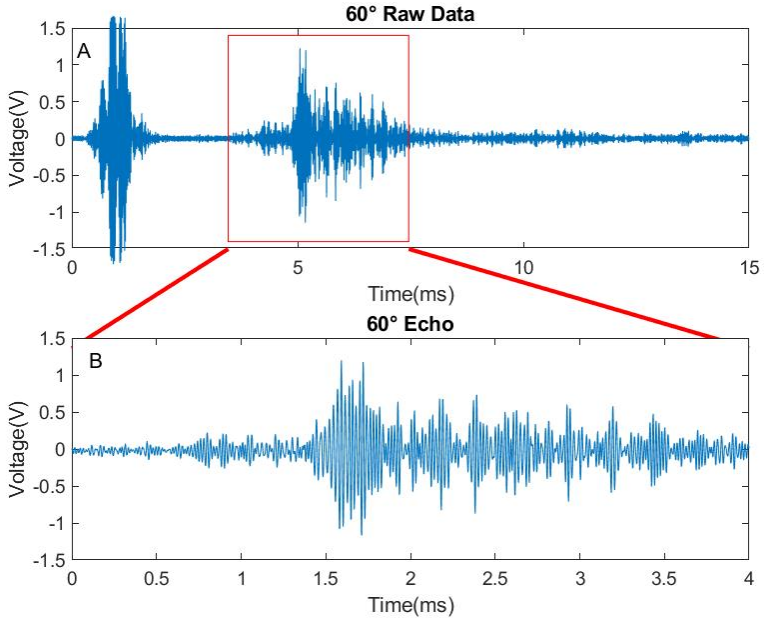

Figure A.14: Reflected signal from two layers bush wall surface with grazing angle 60°,0.5 meter from bush wall at position 3.a) Entire reflected signal.b)Zoom in view of marked rectangular section

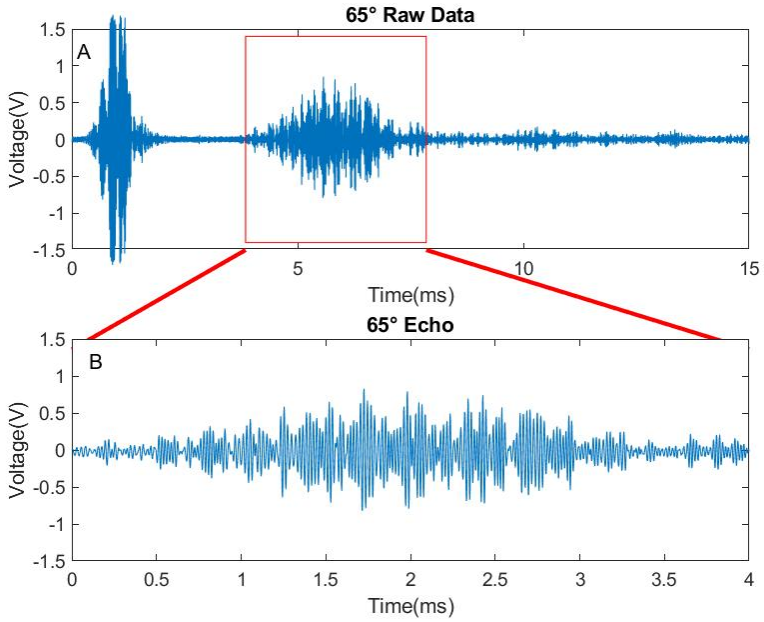

Figure A.15: Reflected signal from two layers bush wall surface with grazing angle 65°,0.5 meter from bush wall at position 4.a) Entire reflected signal.b)Zoom in view of marked rectangular section

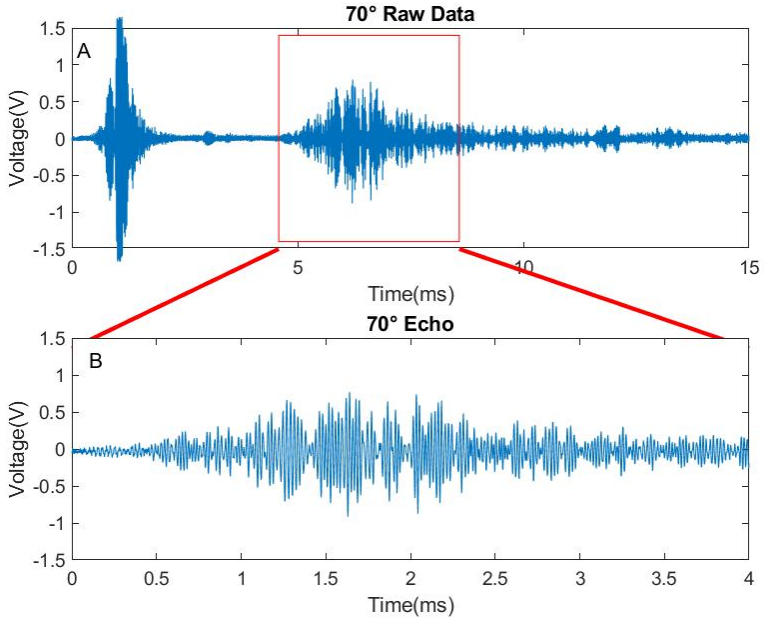

Figure A.16: Reflected signal from two layers bush wall surface with grazing angle 70°,0.5 meter from bush wall at position 5.a) Entire reflected signal.b)Zoom in view of marked rectangular section

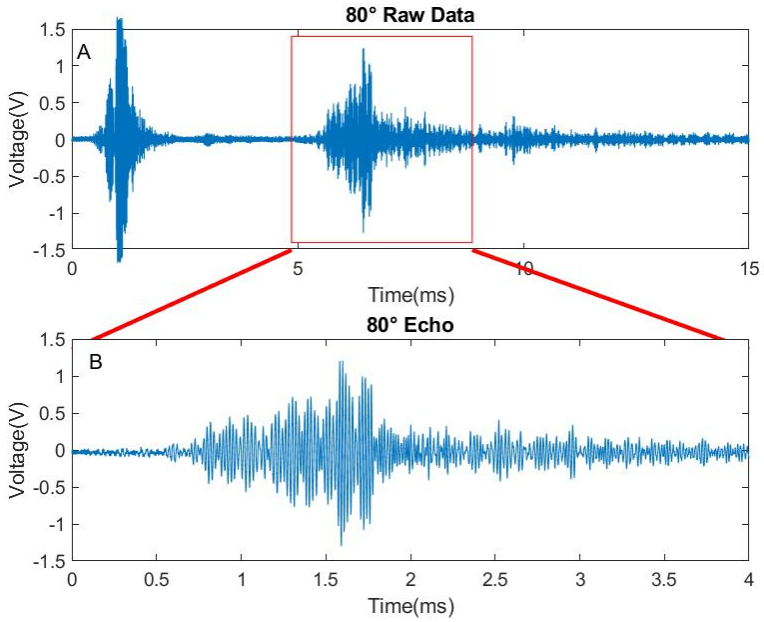

Figure A.17: Reflected signal from two layers bush wall surface with grazing angle 80°,0.5 meter from bush wall at position 7.a) Entire reflected signal.b)Zoom in view of marked rectangular section

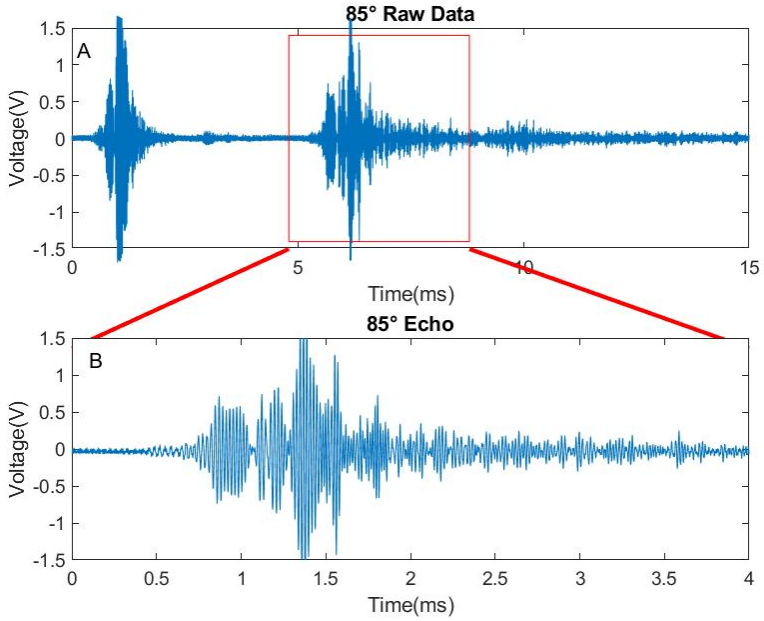

Figure A.18: Reflected signal from two layers bush wall surface with grazing angle 85°,0.5 meter from bush wall at position 8.a) Entire reflected signal.b)Zoom in view of marked rectangular section

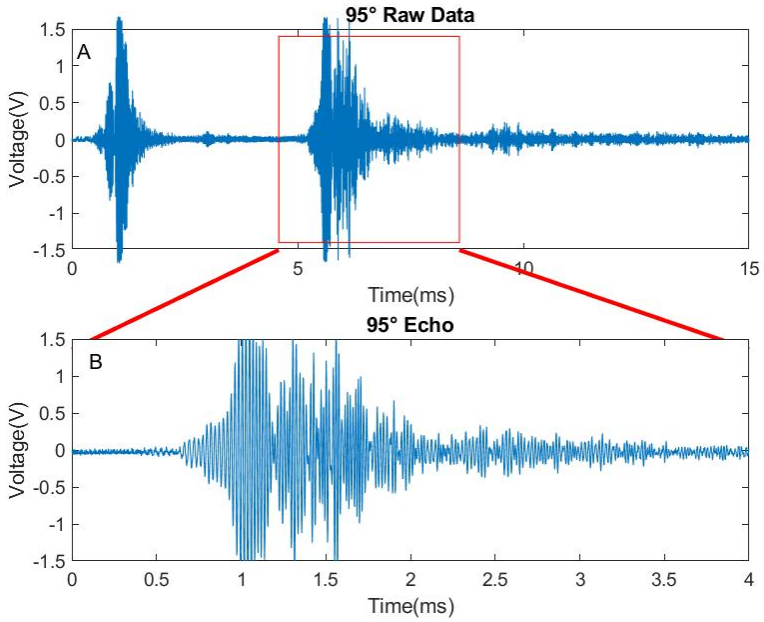

Figure A.19: Reflected signal from two layers bush wall surface with grazing angle 95°,0.5 meter from bush wall at position 10.a) Entire reflected signal.b)Zoom in view of marked rectangular section

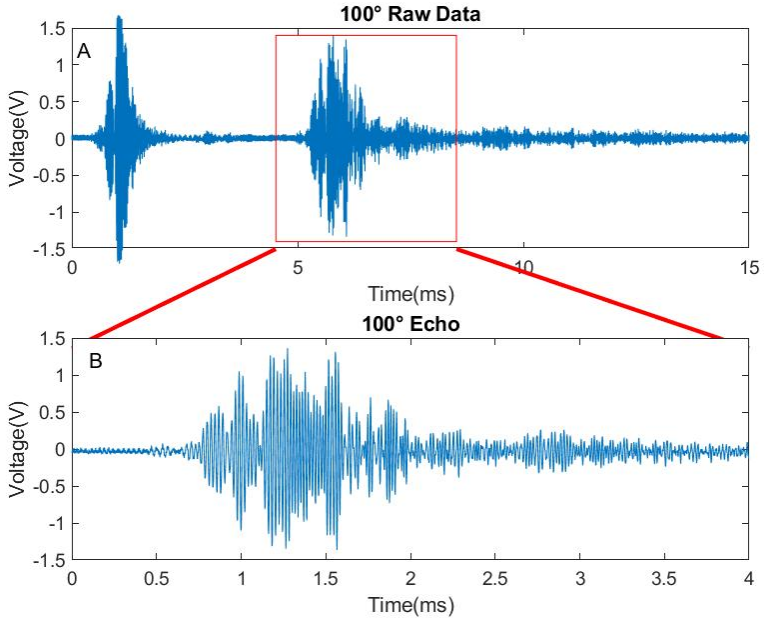

Figure A.20: Reflected signal from two layers bush wall surface with grazing angle 100°,0.5 meter from bush wall at position 11.a) Entire reflected signal.b)Zoom in view of marked rectangular section

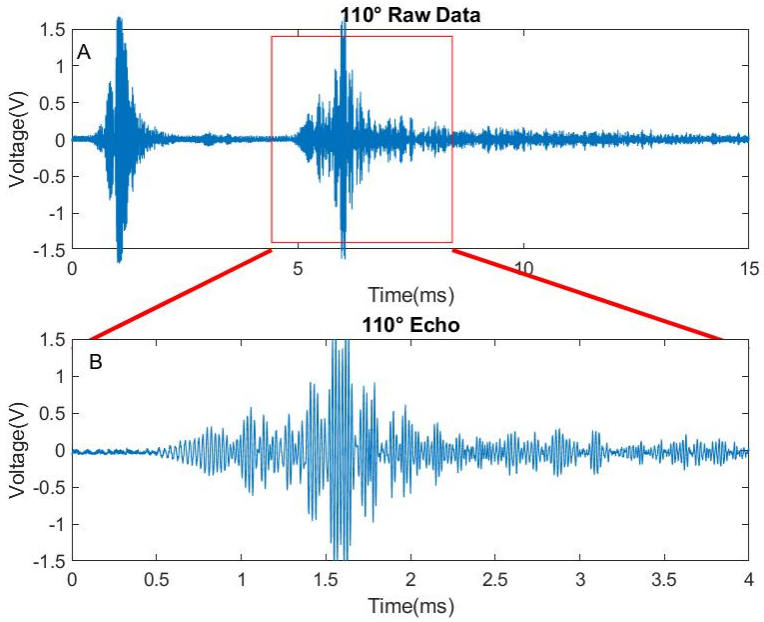

Figure A.21: Reflected signal from two layers bush wall surface with grazing angle 110°,0.5 meter from bush wall at position 13.a) Entire reflected signal.b)Zoom in view of marked rectangular section

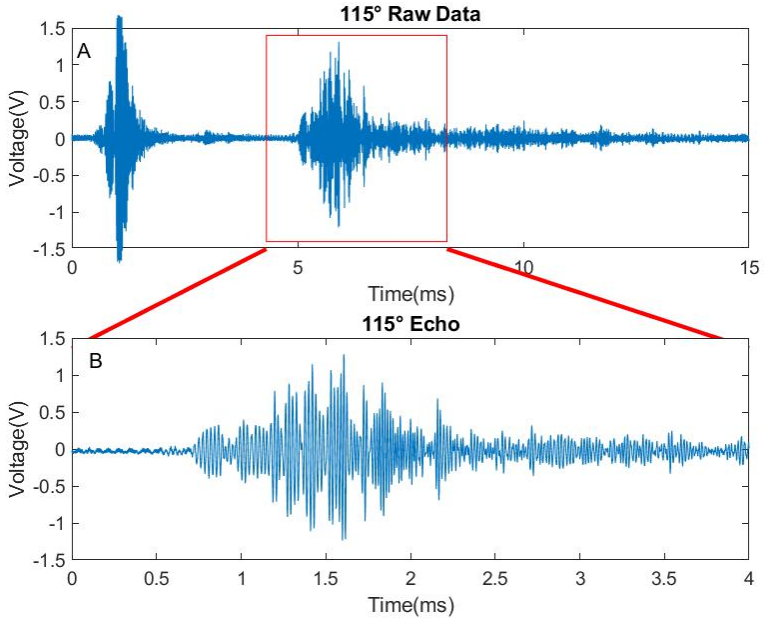

Figure A.22: Reflected signal from two layers bush wall surface with grazing angle 115°,0.5 meter from bush wall at position 14.a) Entire reflected signal.b)Zoom in view of marked rectangular section

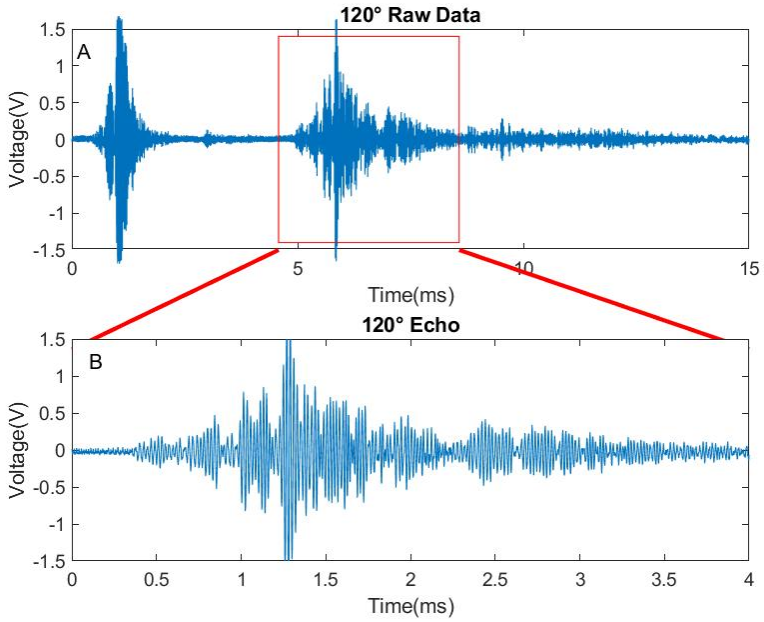

Figure A.23: Reflected signal from two layers bush wall surface with grazing angle 120°,0.5 meter from bush wall at position 15.a) Entire reflected signal.b)Zoom in view of marked rectangular section

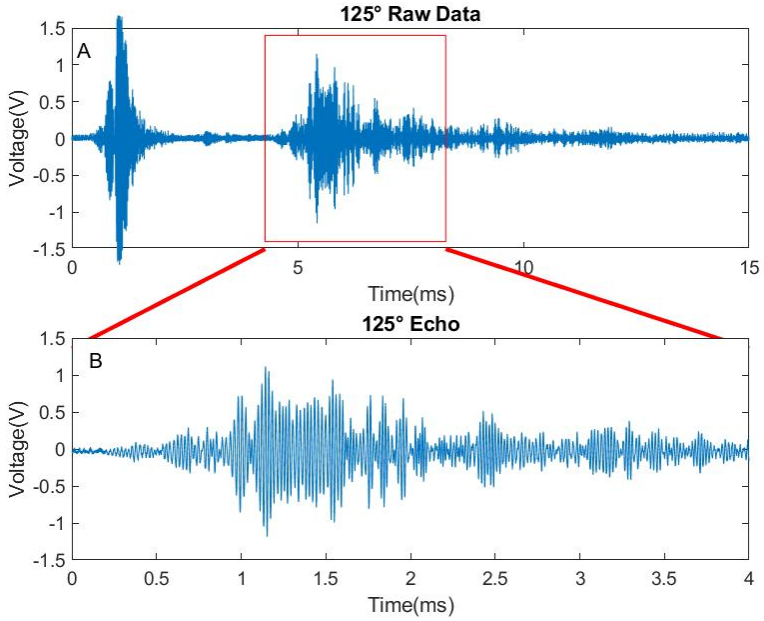

Figure A.24: Reflected signal from two layers bush wall surface with grazing angle 125°,0.5 meter from bush wall at position 16.a) Entire reflected signal.b)Zoom in view of marked rectangular section

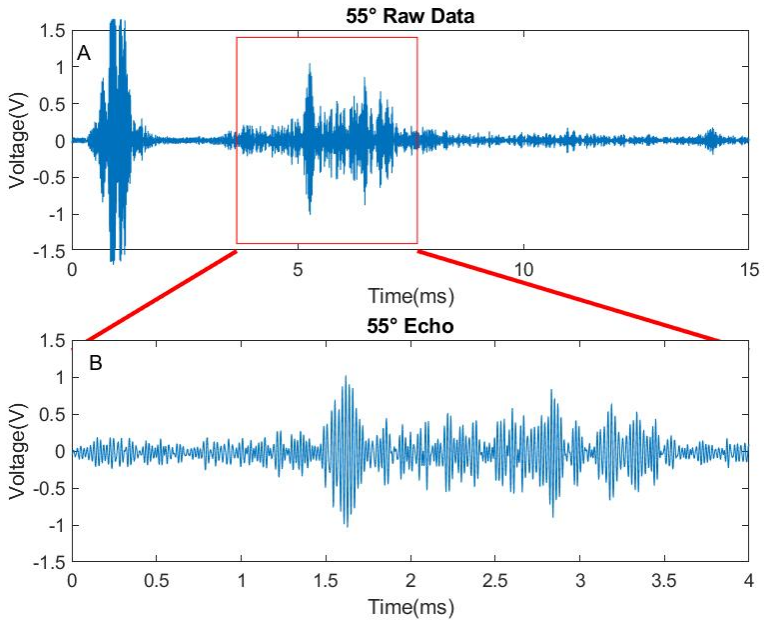

Figure A.25: Reflected signal from three layers bush wall surface with grazing angle 55°,0.5 meter from bush wall at position 2.a) Entire reflected signal.b)Zoom in view of marked rectangular section

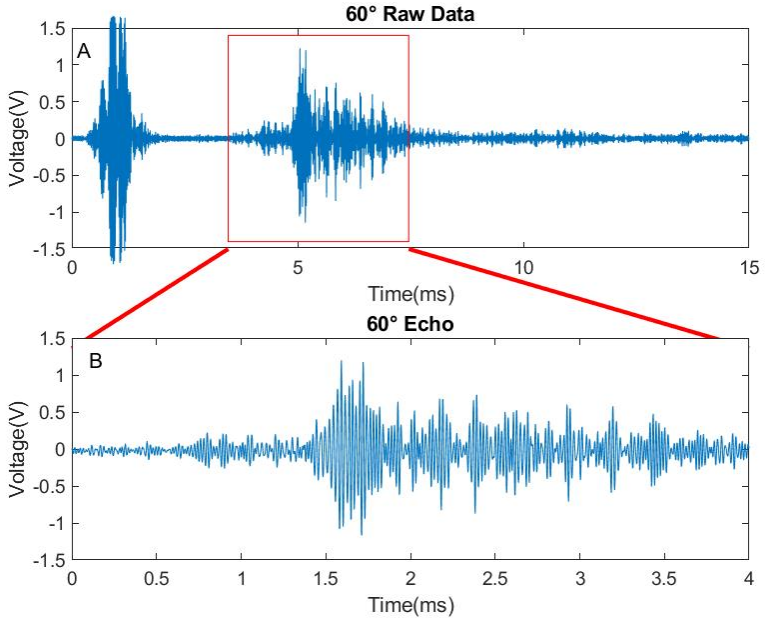

Figure A.26: Reflected signal from three layers bush wall surface with grazing angle 60°,0.5 meter from bush wall at position 3.a) Entire reflected signal.b)Zoom in view of marked rectangular section

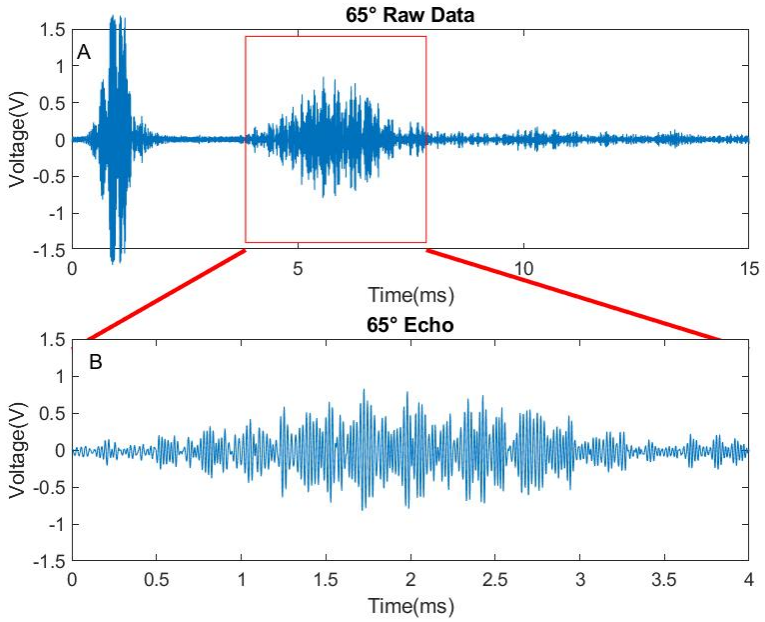

Figure A.27: Reflected signal from three layers bush wall surface with grazing angle 65°,0.5 meter from bush wall at position 4.a) Entire reflected signal.b)Zoom in view of marked rectangular section

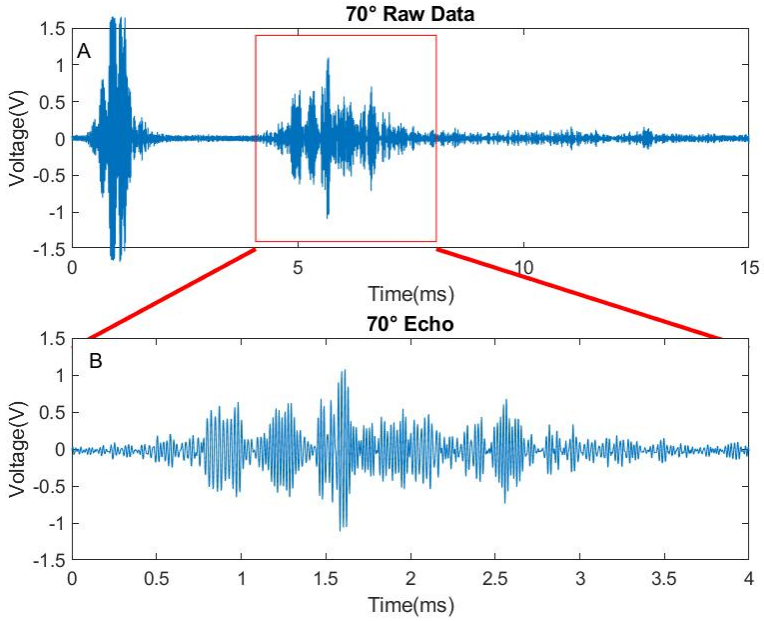

Figure A.28: Reflected signal from three layers bush wall surface with grazing angle 70°,0.5 meter from bush wall at position 5.a) Entire reflected signal.b)Zoom in view of marked rectangular section

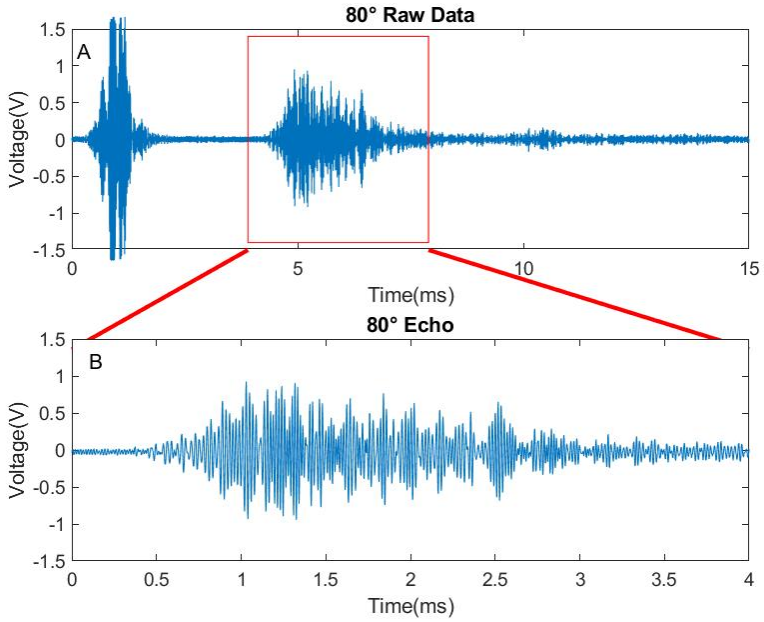

Figure A.29: Reflected signal from three layers bush wall surface with grazing angle 80°,0.5 meter from bush wall at position 7.a) Entire reflected signal.b)Zoom in view of marked rectangular section

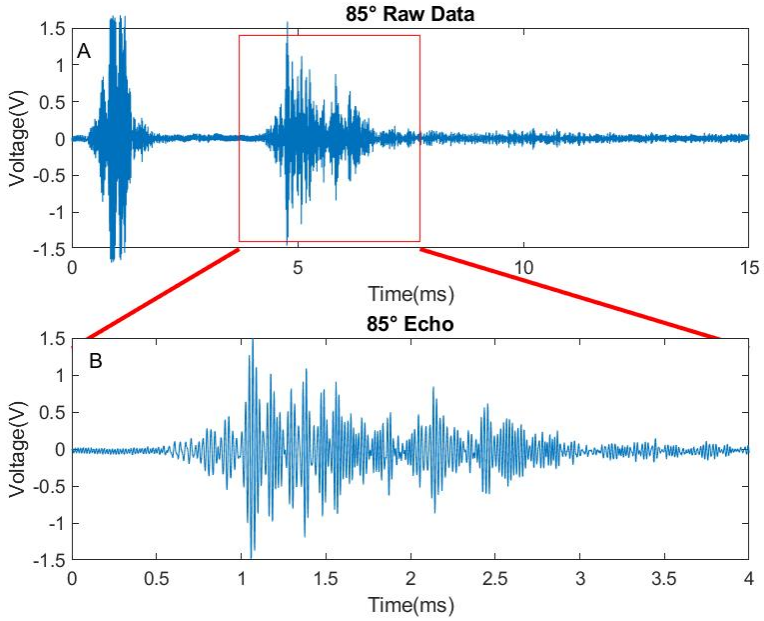

Figure A.30: Reflected signal from three layers bush wall surface with grazing angle 85°,0.5 meter from bush wall at position 8.a) Entire reflected signal.b)Zoom in view of marked rectangular section

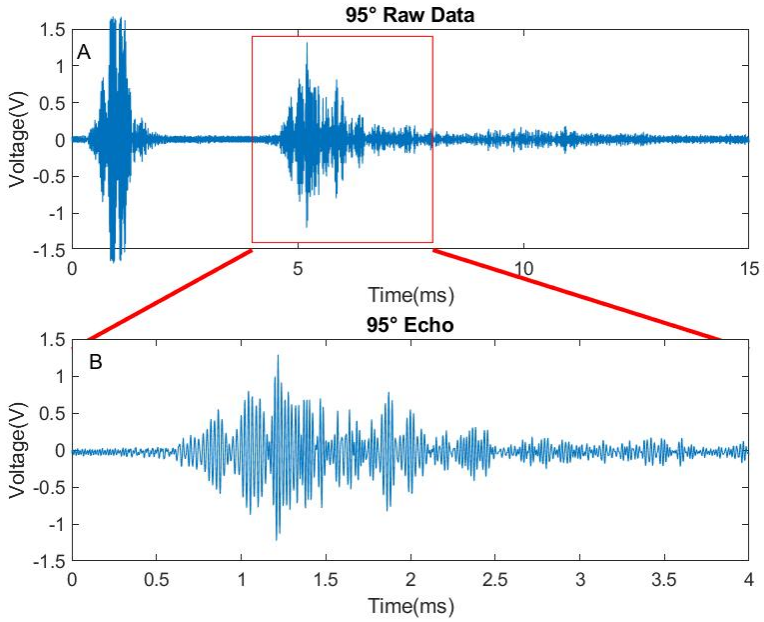

Figure A.31: Reflected signal from three layers bush wall surface with grazing angle 95°,0.5 meter from bush wall at position 10.a) Entire reflected signal.b)Zoom in view of marked rectangular section

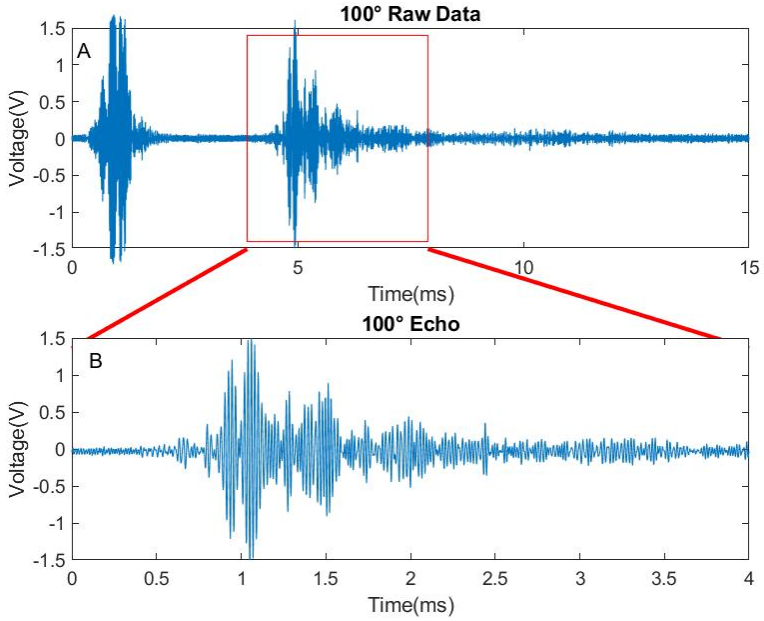

Figure A.32: Reflected signal from three layers bush wall surface with grazing angle 100°,0.5 meter from bush wall at position 11.a) Entire reflected signal.b)Zoom in view of marked rectangular section

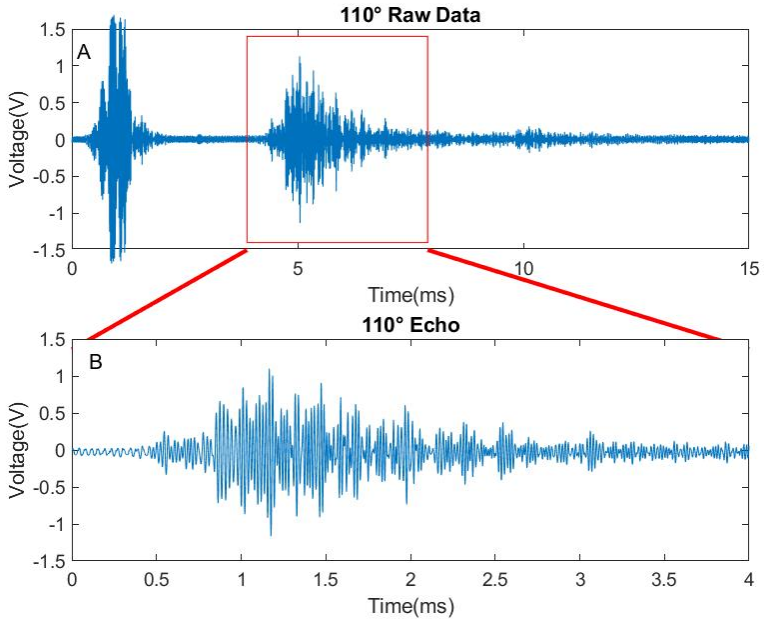

Figure A.33: Reflected signal from three layers bush wall surface with grazing angle 110°,0.5 meter from bush wall at position 13.a) Entire reflected signal.b)Zoom in view of marked rectangular section

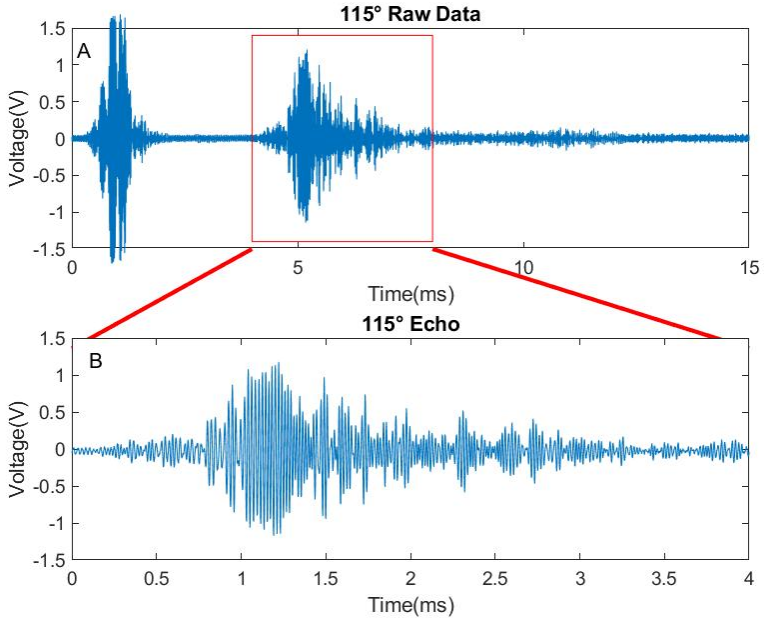

Figure A.34: Reflected signal from three layers bush wall surface with grazing angle 115°,0.5 meter from bush wall at position 14.a) Entire reflected signal.b)Zoom in view of marked rectangular section

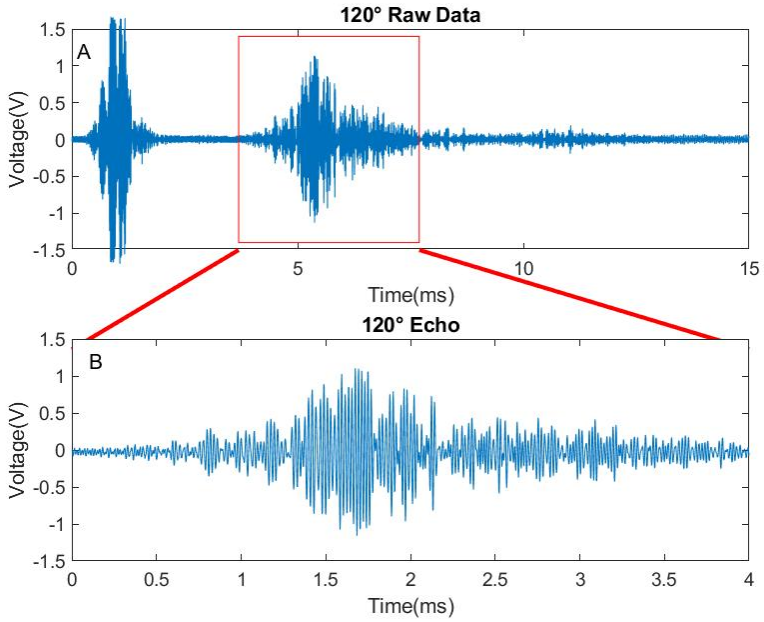

Figure A.35: Reflected signal from three layers bush wall surface with grazing angle 120°,0.5 meter from bush wall at position 15.a) Entire reflected signal.b)Zoom in view of marked rectangular section

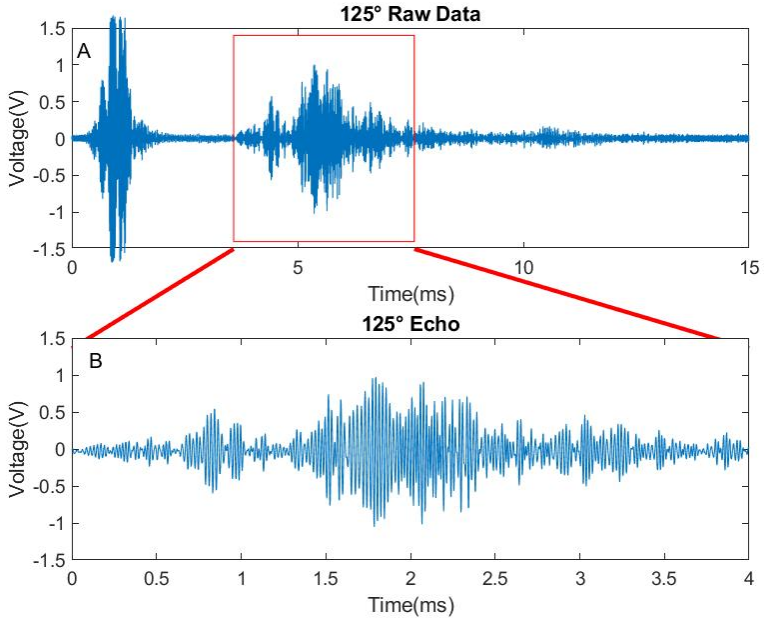

Figure A.36: Reflected signal from two layers bush wall surface with grazing angle 125°,0.5 meter from bush wall at position 16.a) Entire reflected signal.b)Zoom in view of marked rectangular section

A.1.2 0.8 meter Echo

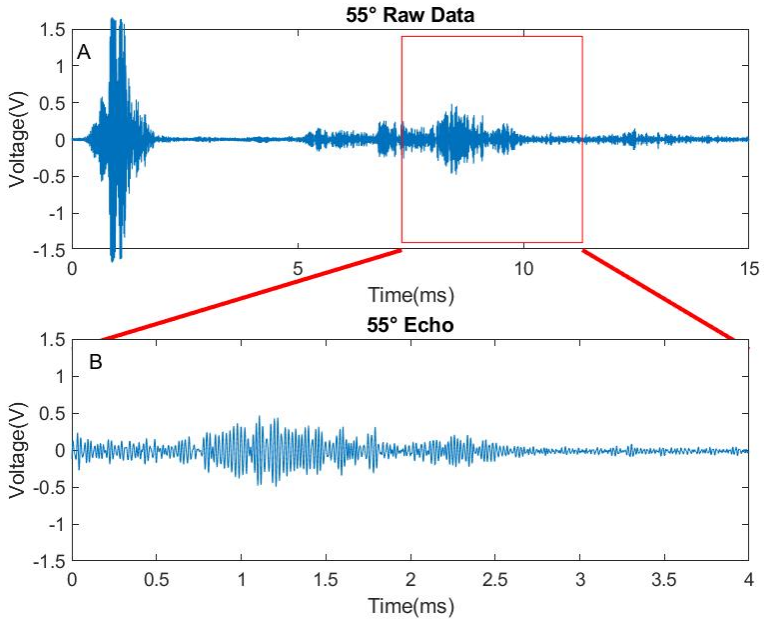

Figure A.37: Reflected signal from one layer bush wall surface with grazing angle 55°,0.5 meter from bush wall at position 2.a) Entire reflected signal.b)Zoom in view of marked rectangular section

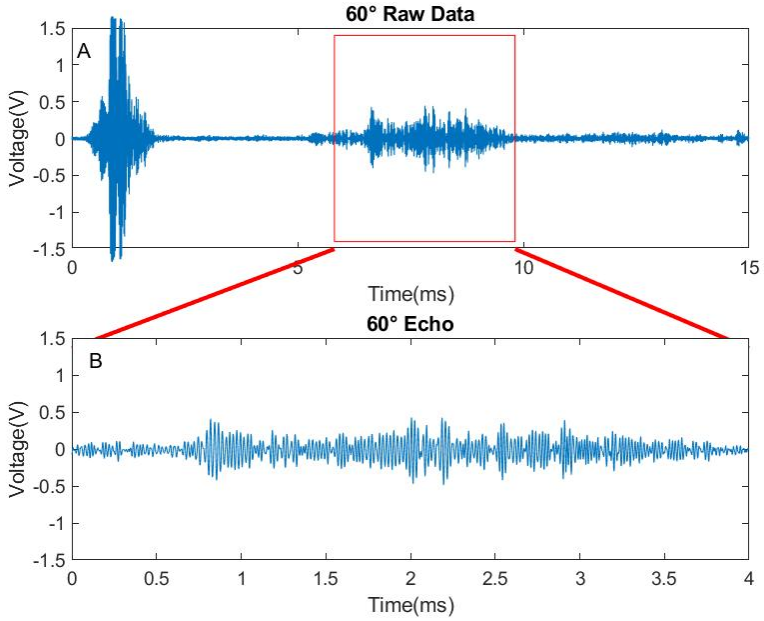

Figure A.38: Reflected signal from one layer bush wall surface with grazing angle 60°,0.5 meter from bush wall at position 3.a) Entire reflected signal.b)Zoom in view of marked rectangular section

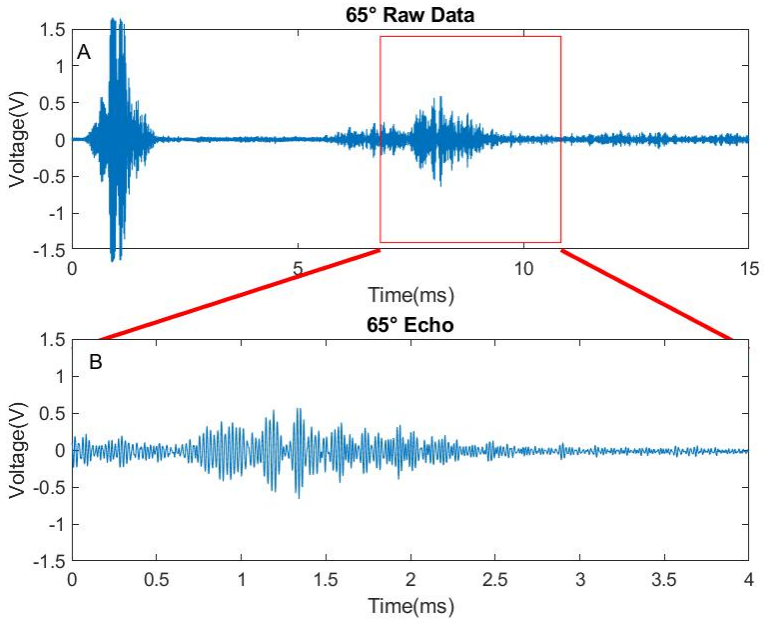

Figure A.39: Reflected signal from one layer bush wall surface with grazing angle 65°,0.5 meter from bush wall at position 4.a) Entire reflected signal.b)Zoom in view of marked rectangular section

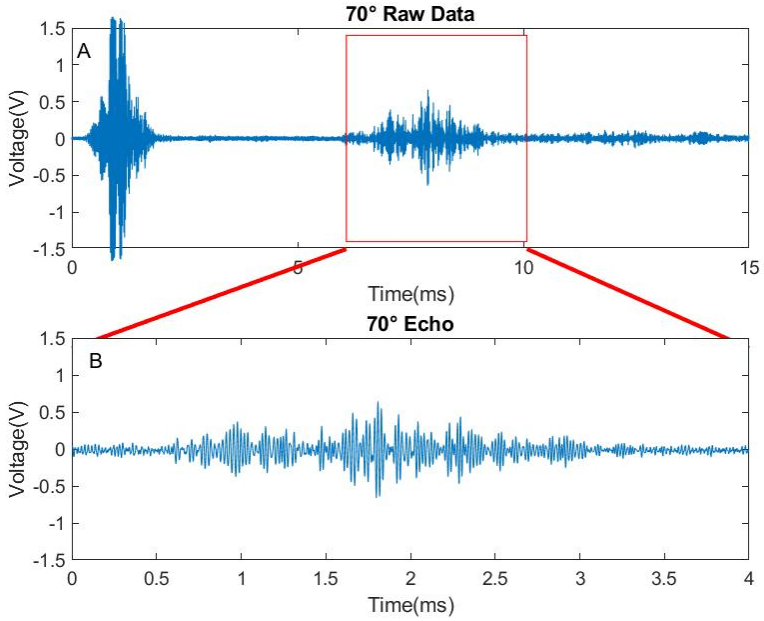

Figure A.40: Reflected signal from one layer bush wall surface with grazing angle 70°,0.5 meter from bush wall at position 5.a) Entire reflected signal.b)Zoom in view of marked rectangular section

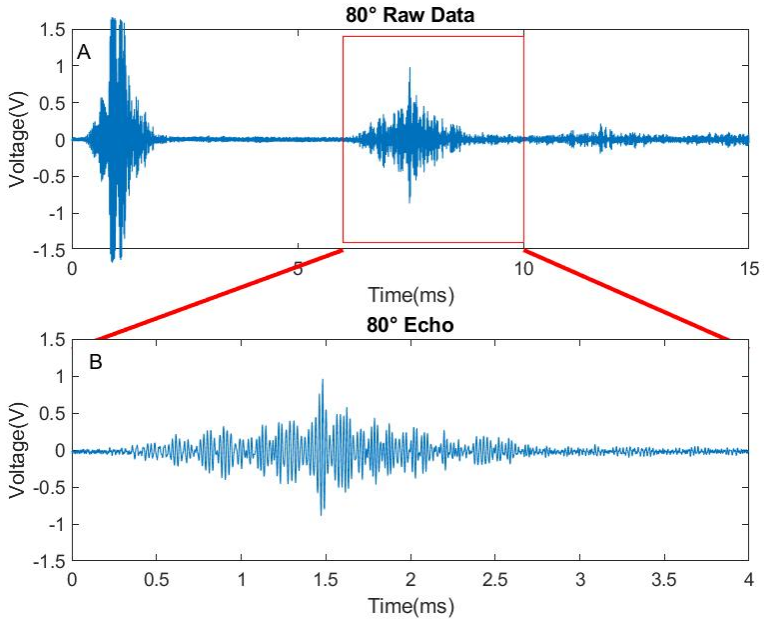

Figure A.41: Reflected signal from one layer bush wall surface with grazing angle 80°,0.5 meter from bush wall at position 7.a) Entire reflected signal.b)Zoom in view of marked rectangular section

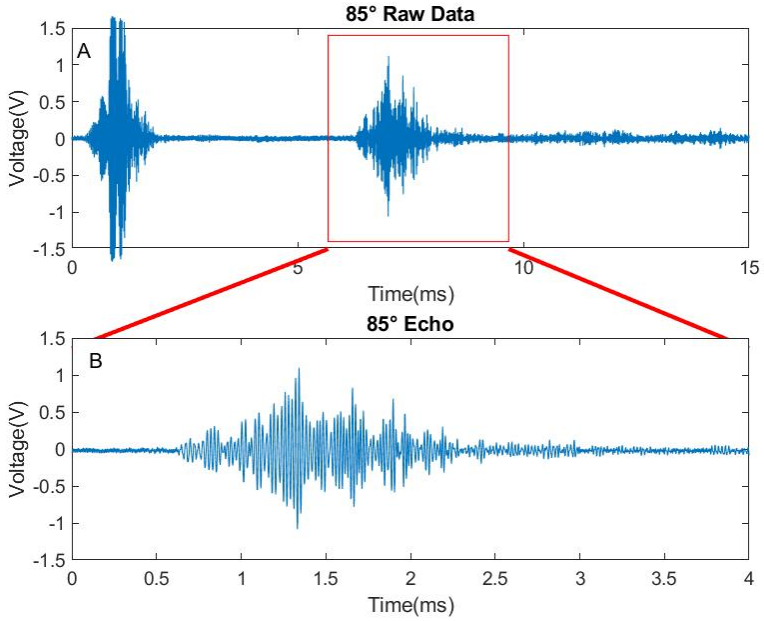

Figure A.42: Reflected signal from one layer bush wall surface with grazing angle 85°,0.5 meter from bush wall at position 8.a) Entire reflected signal.b)Zoom in view of marked rectangular section

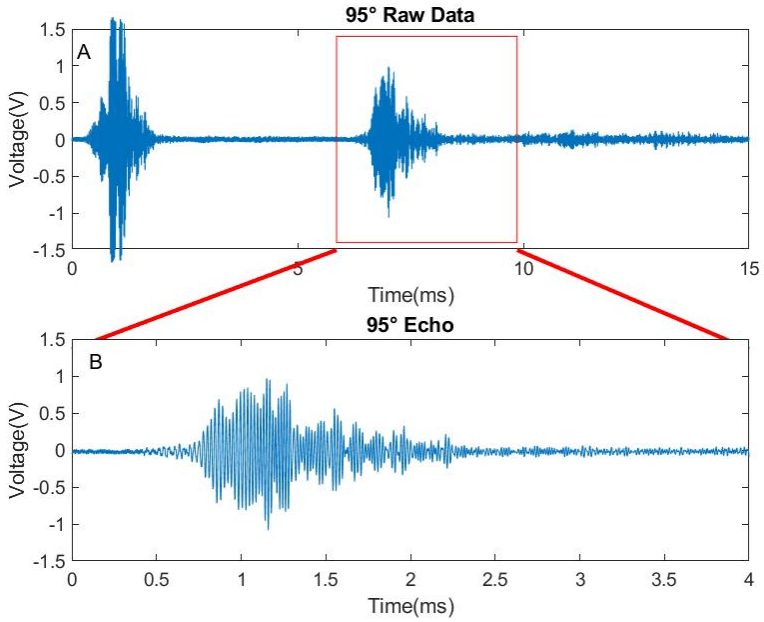

Figure A.43: Reflected signal from one layer bush wall surface with grazing angle 95°,0.5 meter from bush wall at position 10.a) Entire reflected signal.b)Zoom in view of marked rectangular section

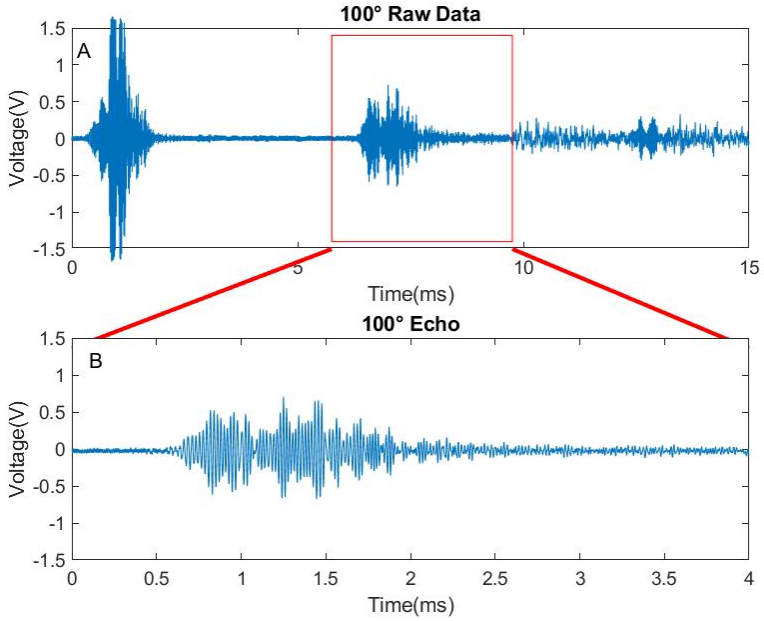

Figure A.44: Reflected signal from one layer bush wall surface with grazing angle 100°,0.5 meter from bush wall at position 11.a) Entire reflected signal.b)Zoom in view of marked rectangular section

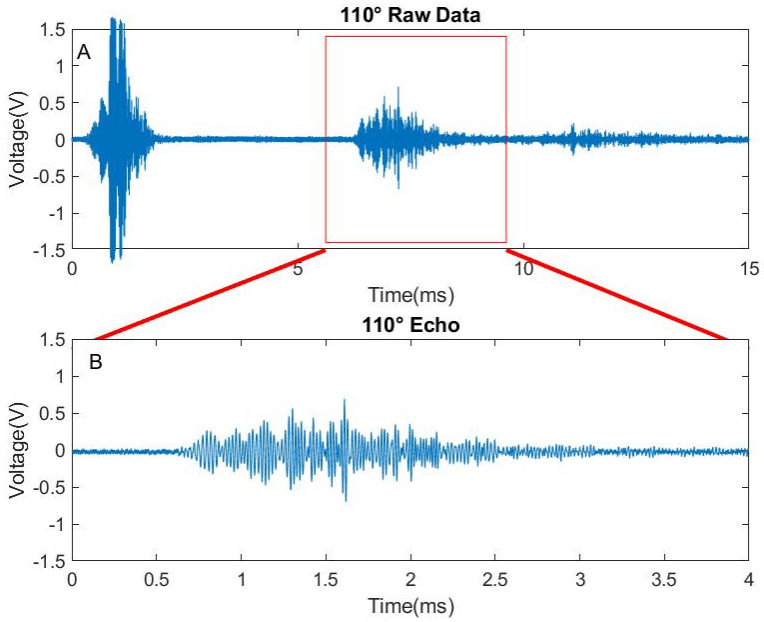

Figure A.45: Reflected signal from one layer bush wall surface with grazing angle 110°,0.5 meter from bush wall at position 13.a) Entire reflected signal.b)Zoom in view of marked rectangular section

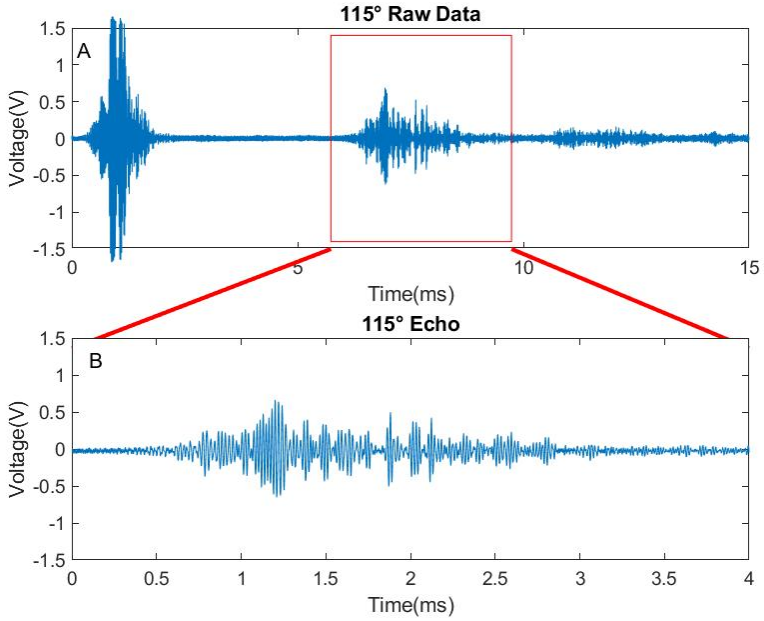

Figure A.46: Reflected signal from one layer bush wall surface with grazing angle 115°,0.5 meter from bush wall at position 14.a) Entire reflected signal.b)Zoom in view of marked rectangular section

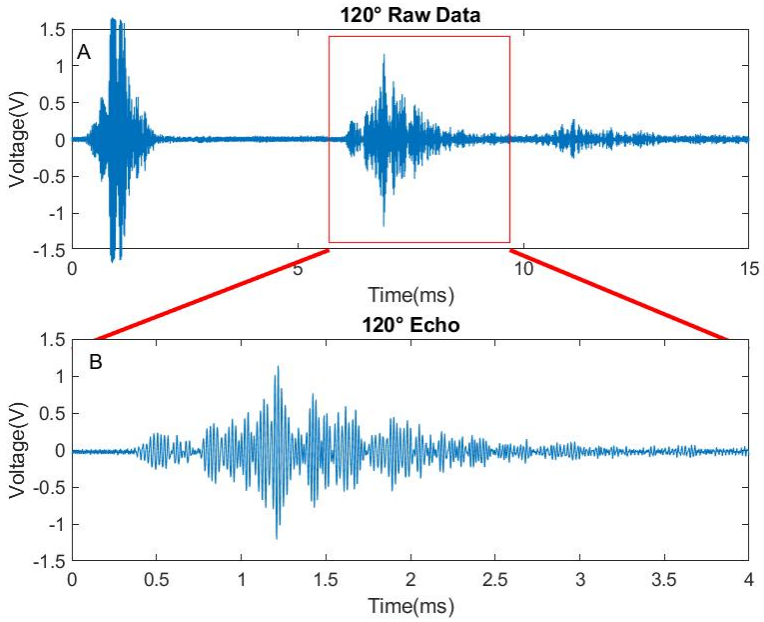

Figure A.47: Reflected signal from one layer bush wall surface with grazing angle 120°,0.5 meter from bush wall at position 15.a) Entire reflected signal.b)Zoom in view of marked rectangular section

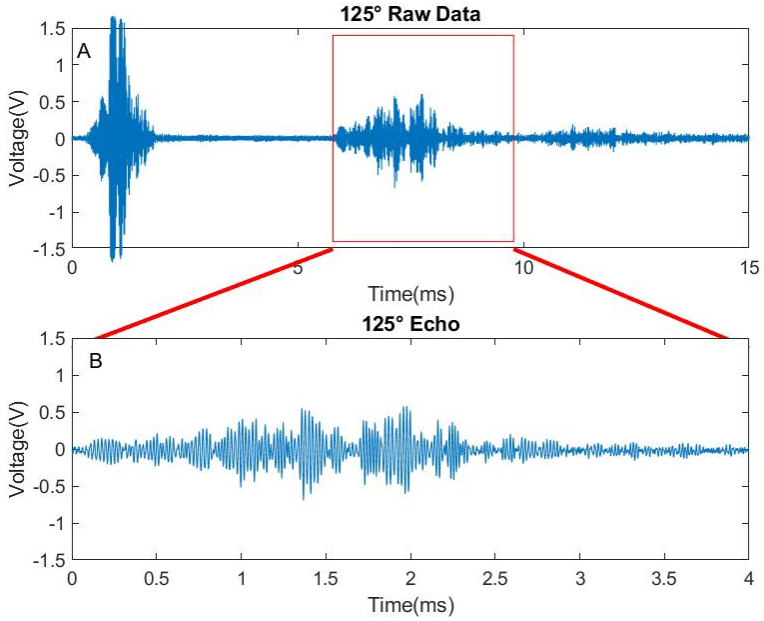

Figure A.48: Reflected signal from two layers bush wall surface with grazing angle 125°,0.5 meter from bush wall at position 16.a) Entire reflected signal.b)Zoom in view of marked rectangular section

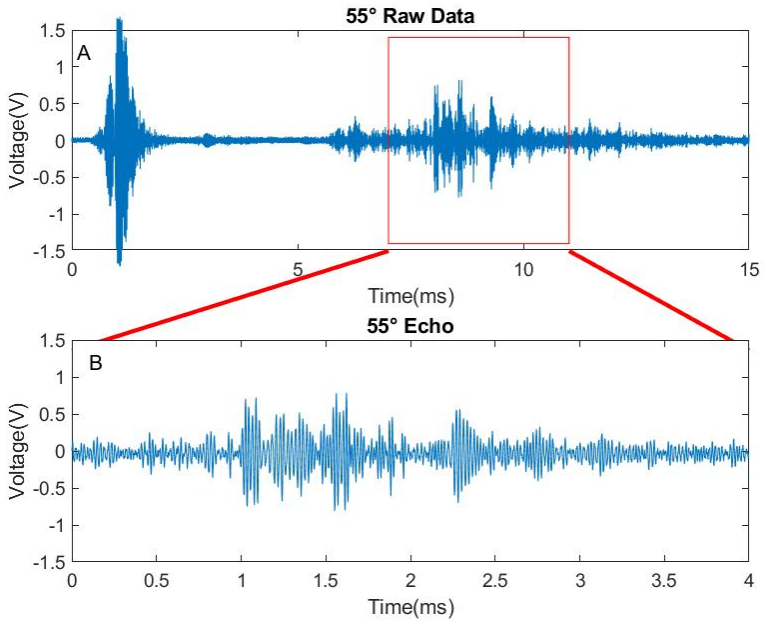

Figure A.49: Reflected signal from two layers bush wall surface with grazing angle 55°,0.5 meter from bush wall at position 2.a) Entire reflected signal.b)Zoom in view of marked rectangular section

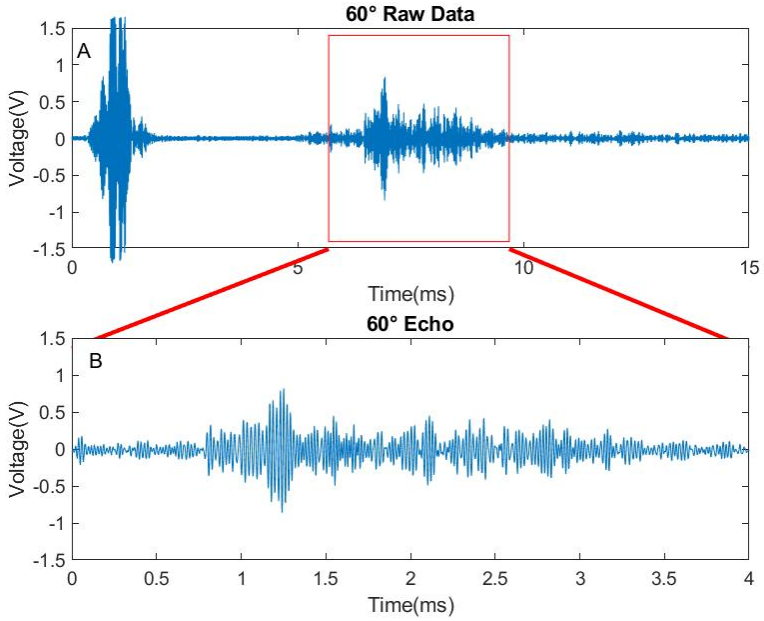

Figure A.50: Reflected signal from two layers bush wall surface with grazing angle 60°,0.5 meter from bush wall at position 3.a) Entire reflected signal.b)Zoom in view of marked rectangular section

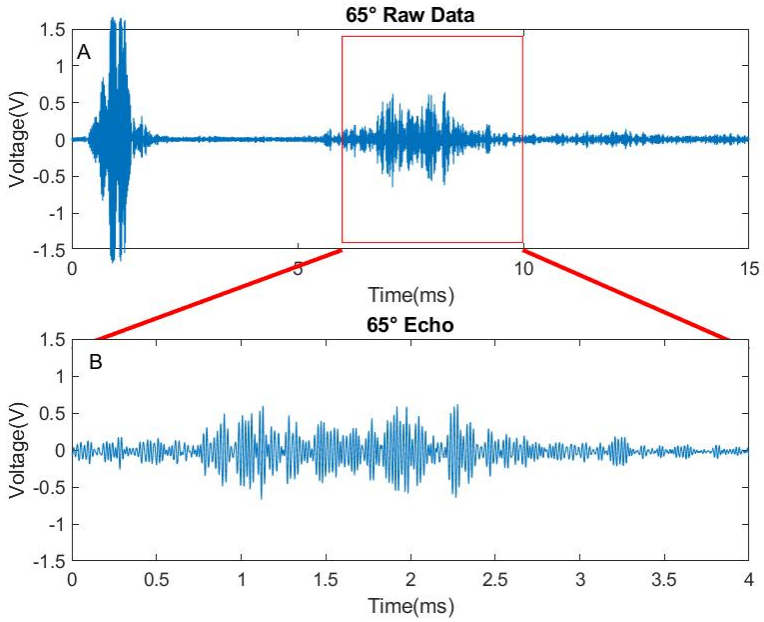

Figure A.51: Reflected signal from two layers bush wall surface with grazing angle 65°,0.5 meter from bush wall at position 4.a) Entire reflected signal.b)Zoom in view of marked rectangular section

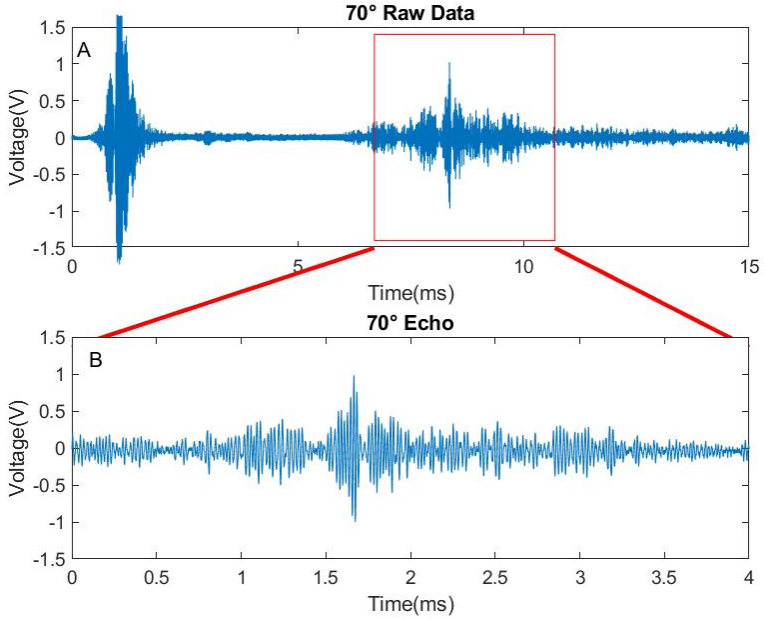

Figure A.52: Reflected signal from two layers bush wall surface with grazing angle 70°,0.5 meter from bush wall at position 5.a) Entire reflected signal.b)Zoom in view of marked rectangular section

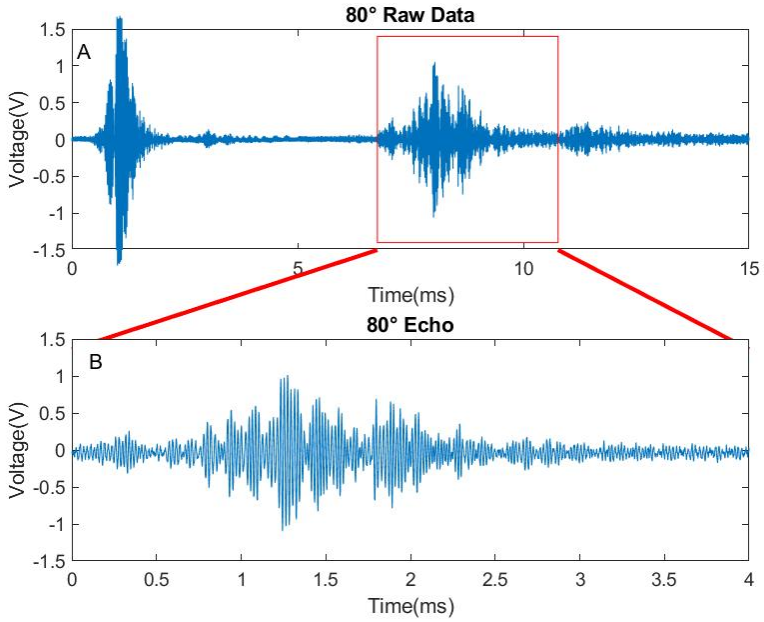

Figure A.53: Reflected signal from two layers bush wall surface with grazing angle 80°,0.5 meter from bush wall at position 7.a) Entire reflected signal.b)Zoom in view of marked rectangular section

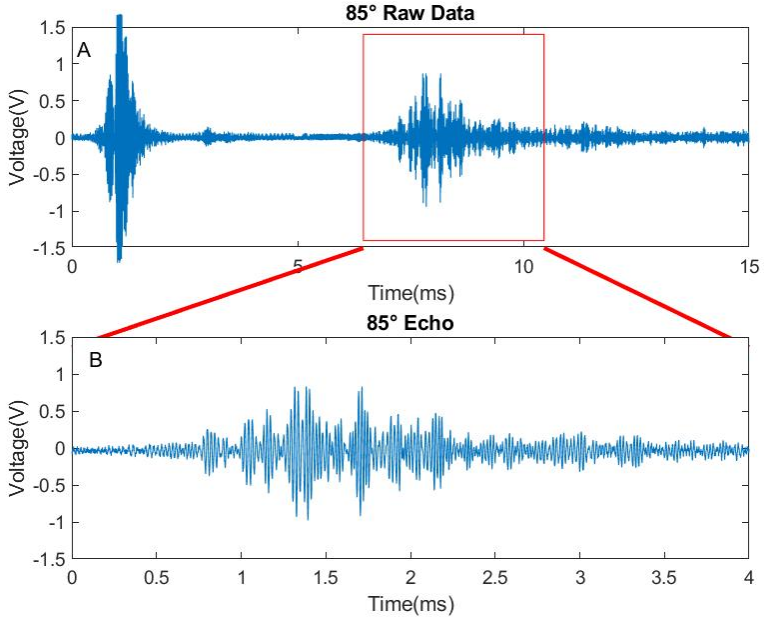

Figure A.54: Reflected signal from two layers bush wall surface with grazing angle 85°,0.5 meter from bush wall at position 8.a) Entire reflected signal.b)Zoom in view of marked rectangular section

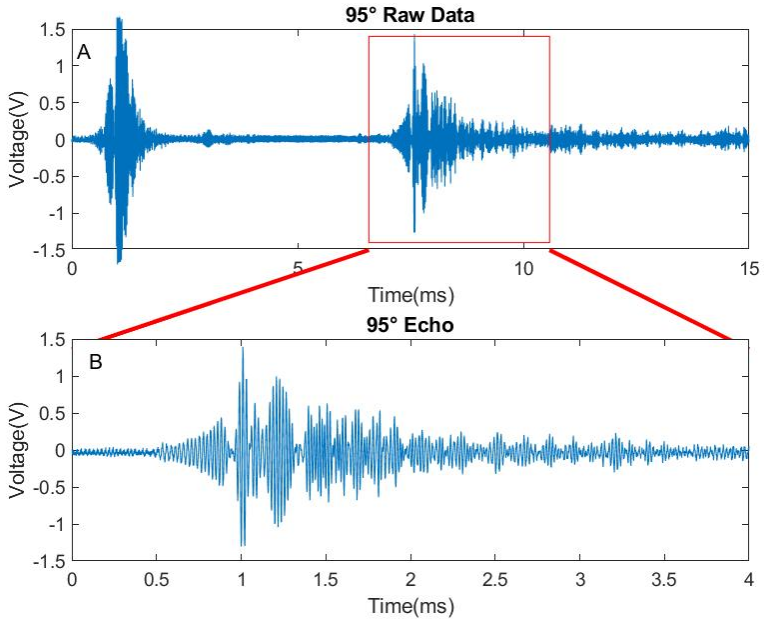

Figure A.55: Reflected signal from two layers bush wall surface with grazing angle 95°,0.5 meter from bush wall at position 10.a) Entire reflected signal.b)Zoom in view of marked rectangular section

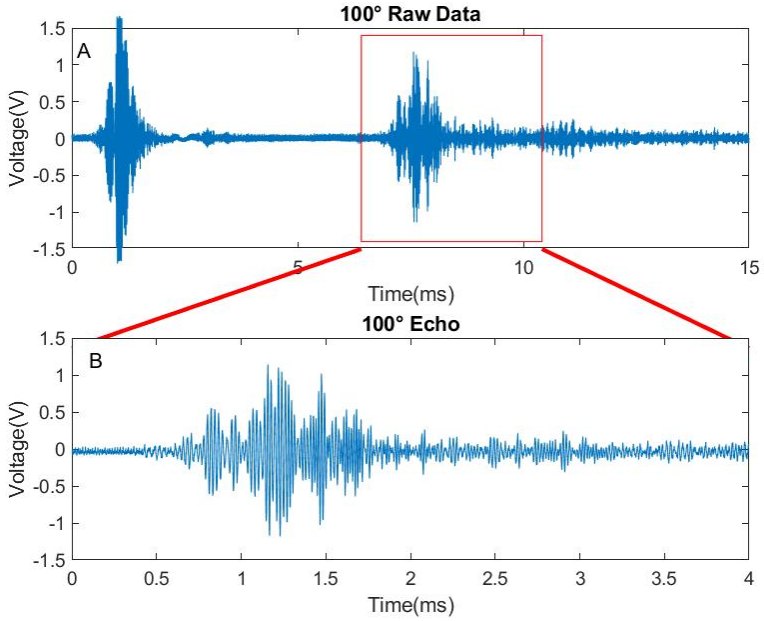

Figure A.56: Reflected signal from two layers bush wall surface with grazing angle 100°,0.5 meter from bush wall at position 11.a) Entire reflected signal.b)Zoom in view of marked rectangular section

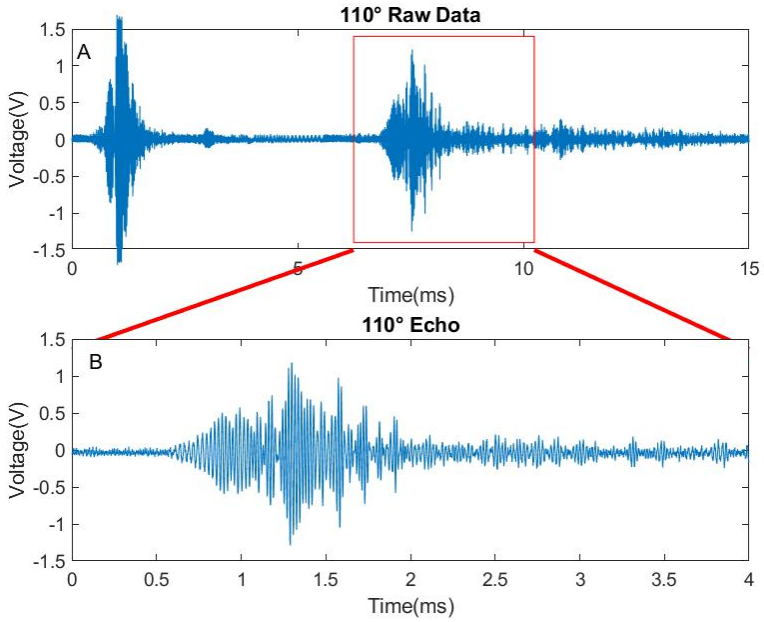

Figure A.57: Reflected signal from two layers bush wall surface with grazing angle 110°,0.5 meter from bush wall at position 13.a) Entire reflected signal.b)Zoom in view of marked rectangular section

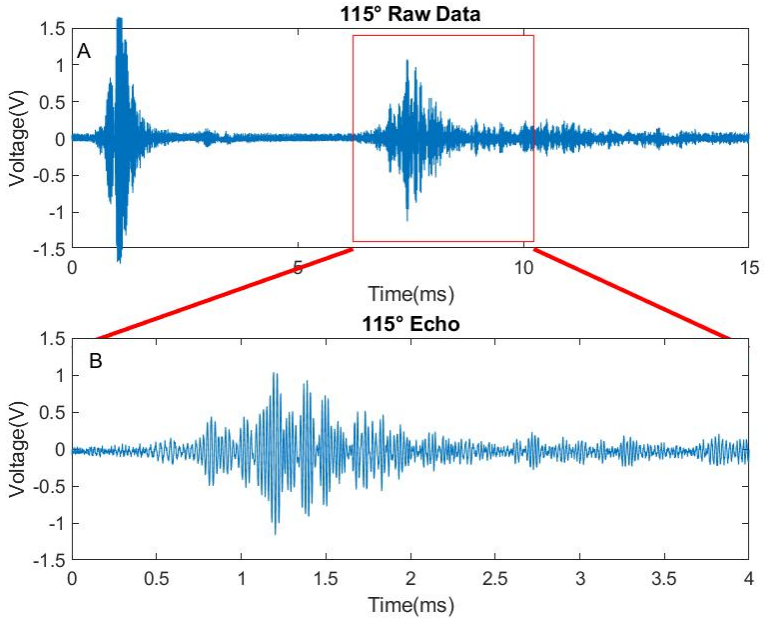

Figure A.58: Reflected signal from two layers bush wall surface with grazing angle 115°,0.5 meter from bush wall at position 14.a) Entire reflected signal.b)Zoom in view of marked rectangular section

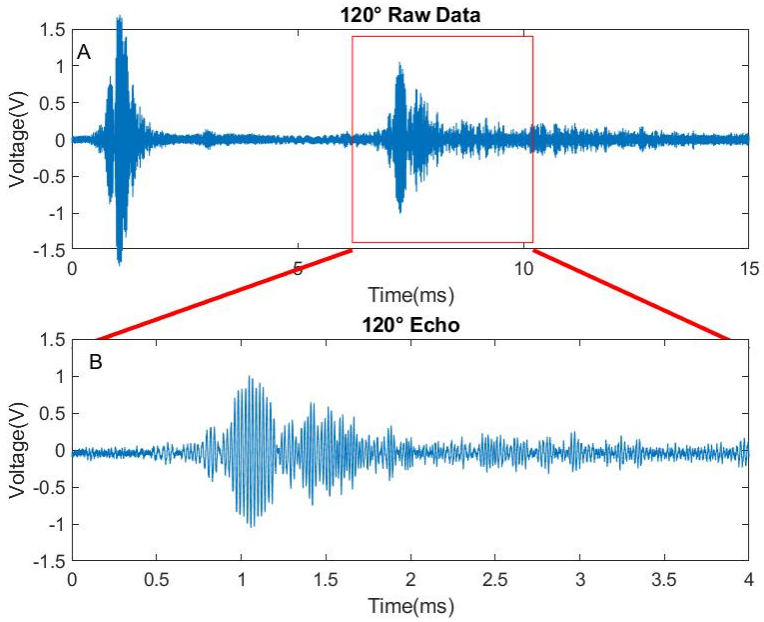

Figure A.59: Reflected signal from two layers bush wall surface with grazing angle 120°,0.5 meter from bush wall at position 15.a) Entire reflected signal.b)Zoom in view of marked rectangular section

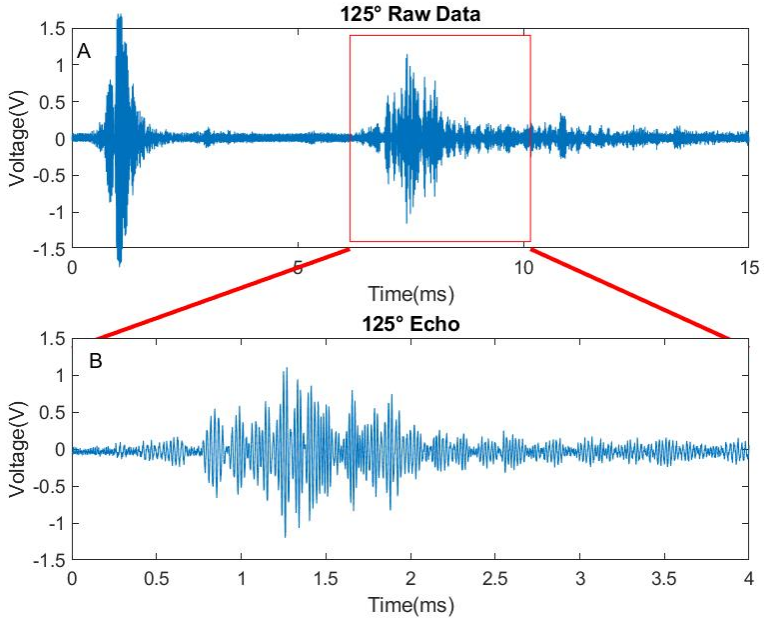

Figure A.60: Reflected signal from two layers bush wall surface with grazing angle 125°,0.5 meter from bush wall at position 16.a) Entire reflected signal.b)Zoom in view of marked rectangular section

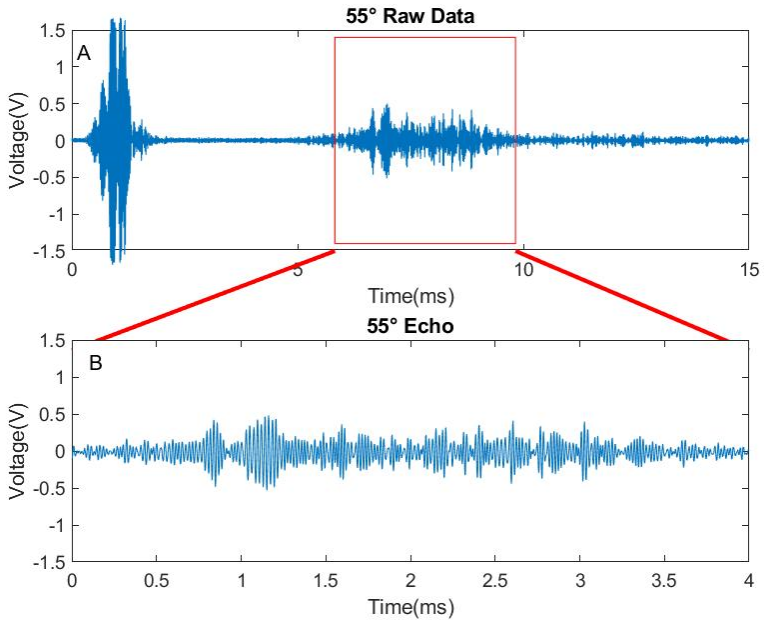

Figure A.61: Reflected signal from three layers bush wall surface with grazing angle 55°,0.5 meter from bush wall at position 2.a) Entire reflected signal.b)Zoom in view of marked rectangular section

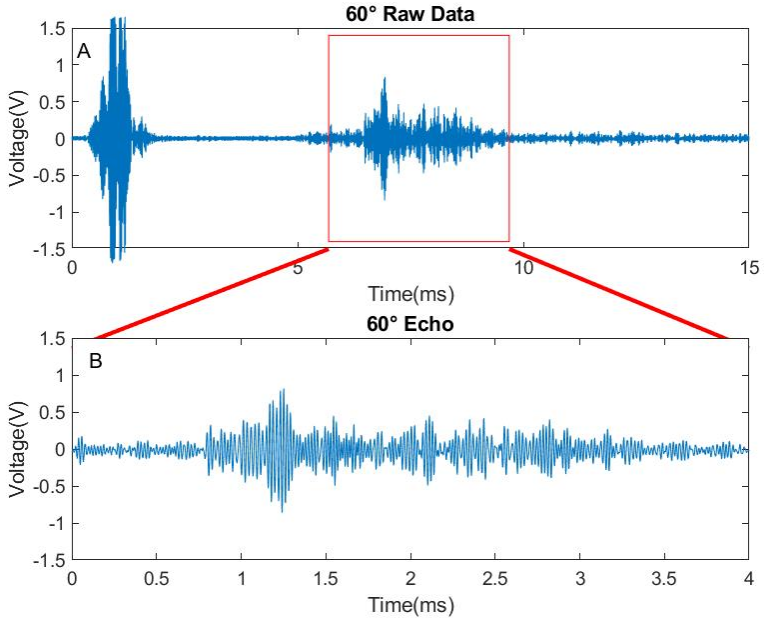

Figure A.62: Reflected signal from three layers bush wall surface with grazing angle 60°,0.5 meter from bush wall at position 3.a) Entire reflected signal.b)Zoom in view of marked rectangular section

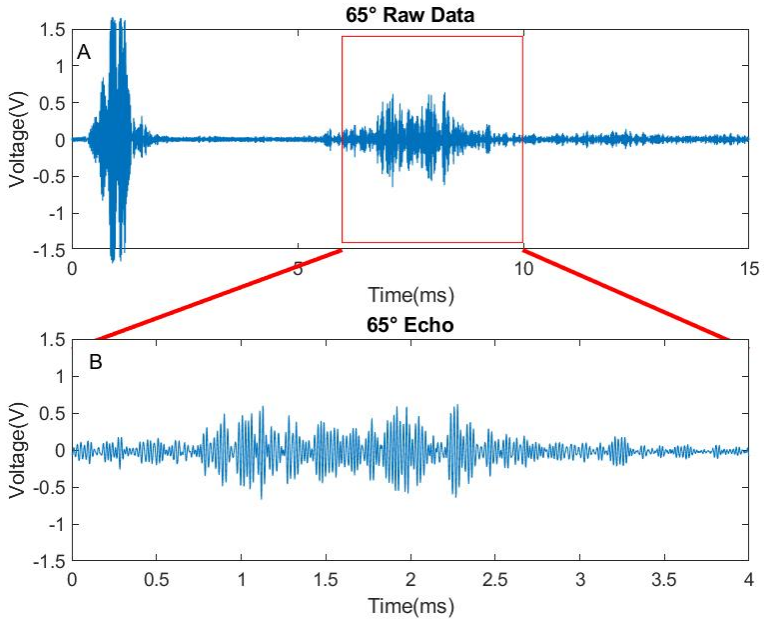

Figure A.63: Reflected signal from three layers bush wall surface with grazing angle 65°,0.5 meter from bush wall at position 4.a) Entire reflected signal.b)Zoom in view of marked rectangular section

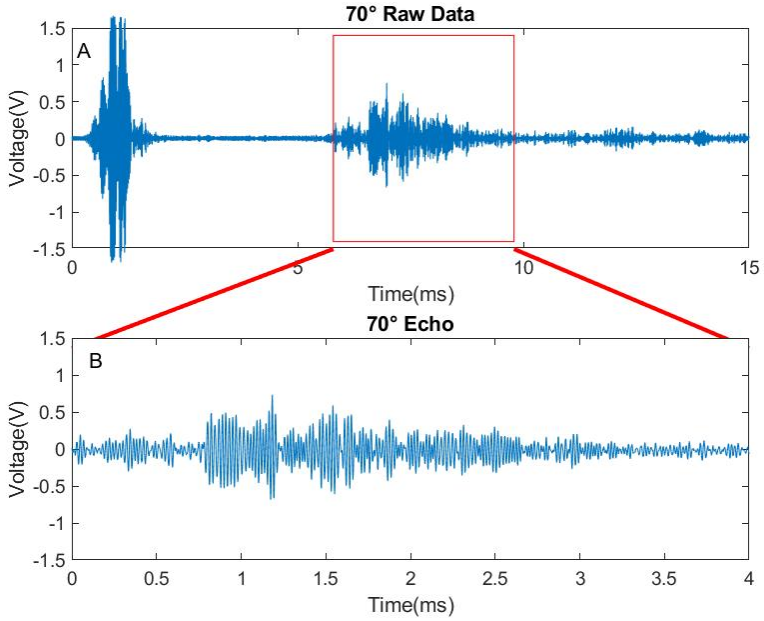

Figure A.64: Reflected signal from three layers bush wall surface with grazing angle 70°,0.5 meter from bush wall at position 5.a) Entire reflected signal.b)Zoom in view of marked rectangular section

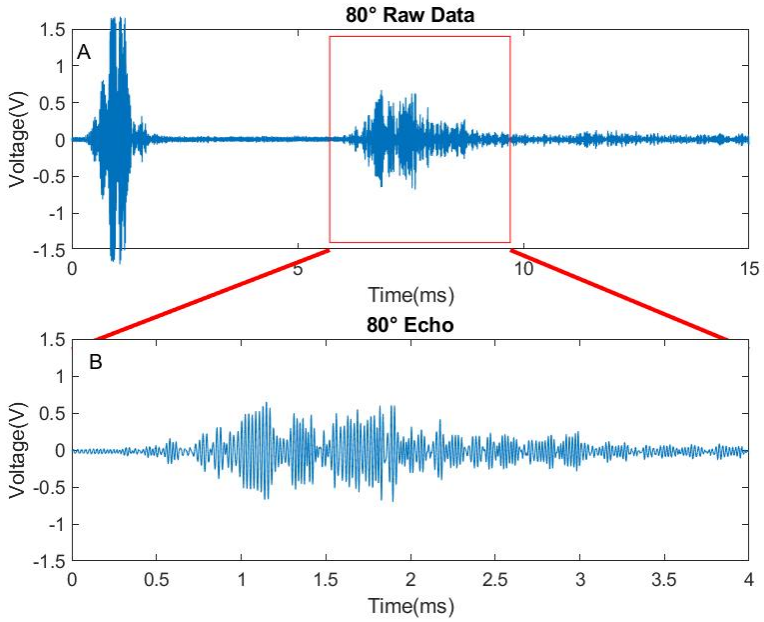

Figure A.65: Reflected signal from three layers bush wall surface with grazing angle 80°,0.5 meter from bush wall at position 7.a) Entire reflected signal.b)Zoom in view of marked rectangular section

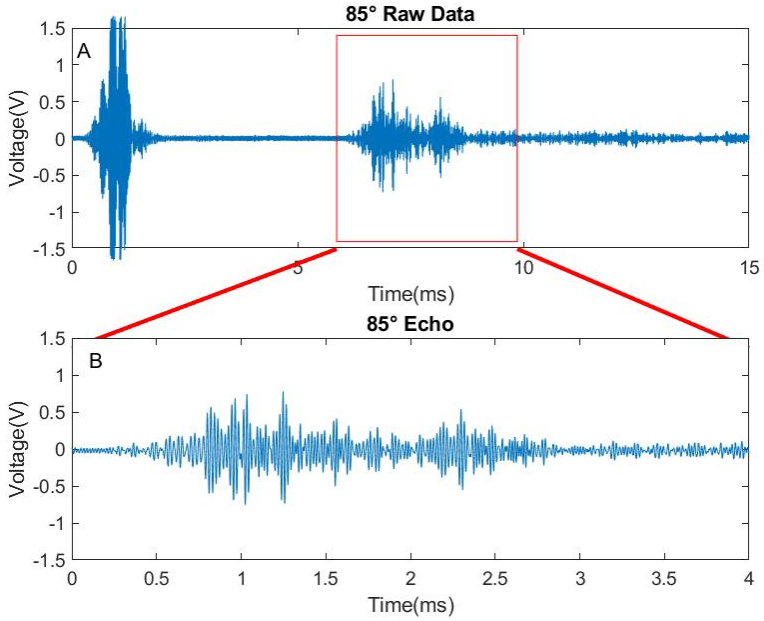

Figure A.66: Reflected signal from three layers bush wall surface with grazing angle 85°,0.5 meter from bush wall at position 8.a) Entire reflected signal.b)Zoom in view of marked rectangular section

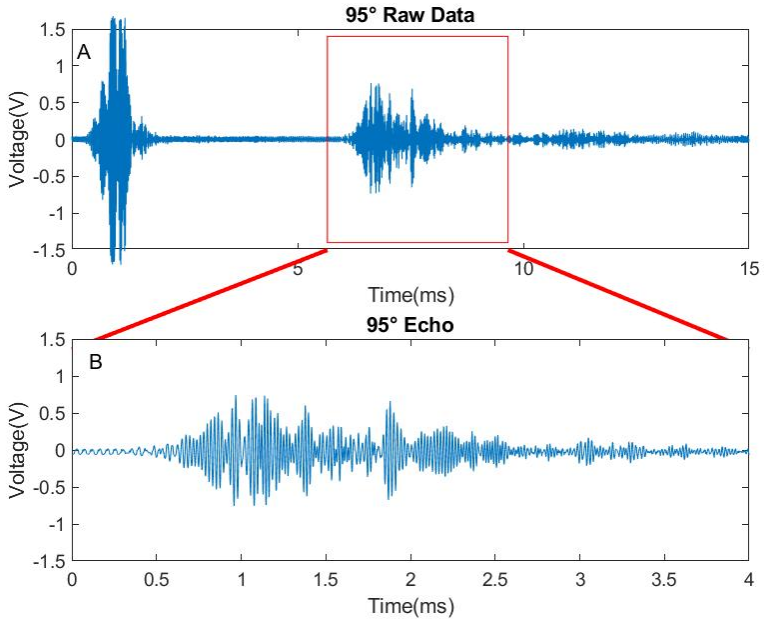

Figure A.67: Reflected signal from three layers bush wall surface with grazing angle 95°,0.5 meter from bush wall at position 10.a) Entire reflected signal.b)Zoom in view of marked rectangular section

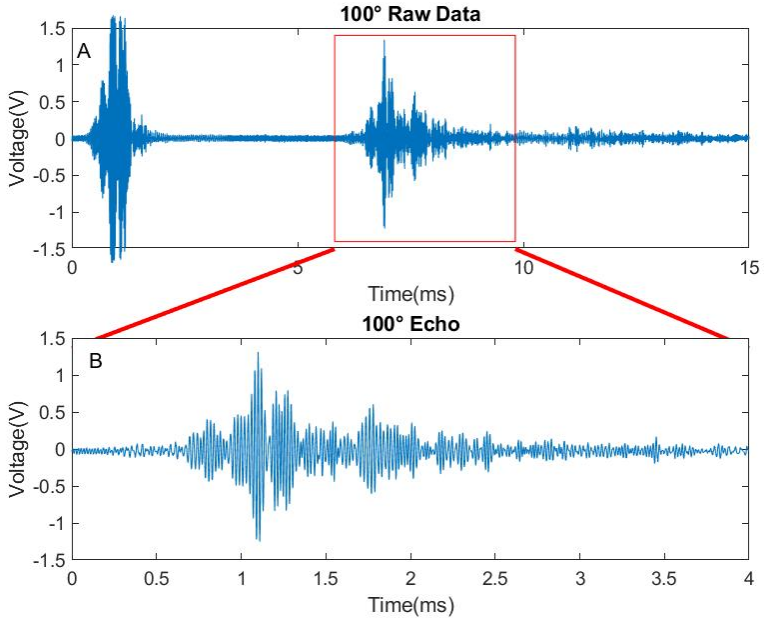

Figure A.68: Reflected signal from three layers bush wall surface with grazing angle 100°,0.5 meter from bush wall at position 11.a) Entire reflected signal.b)Zoom in view of marked rectangular section

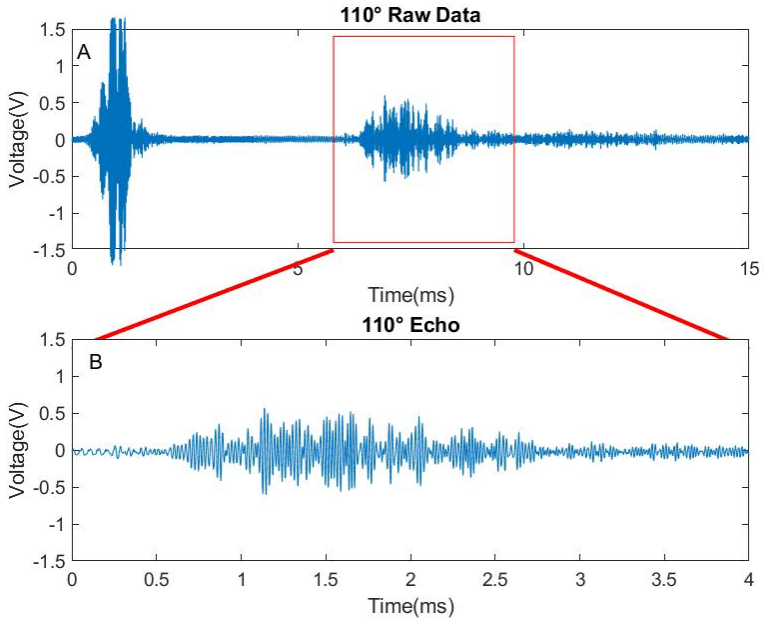

Figure A.69: Reflected signal from three layers bush wall surface with grazing angle 110°,0.5 meter from bush wall at position 13.a) Entire reflected signal.b)Zoom in view of marked rectangular section

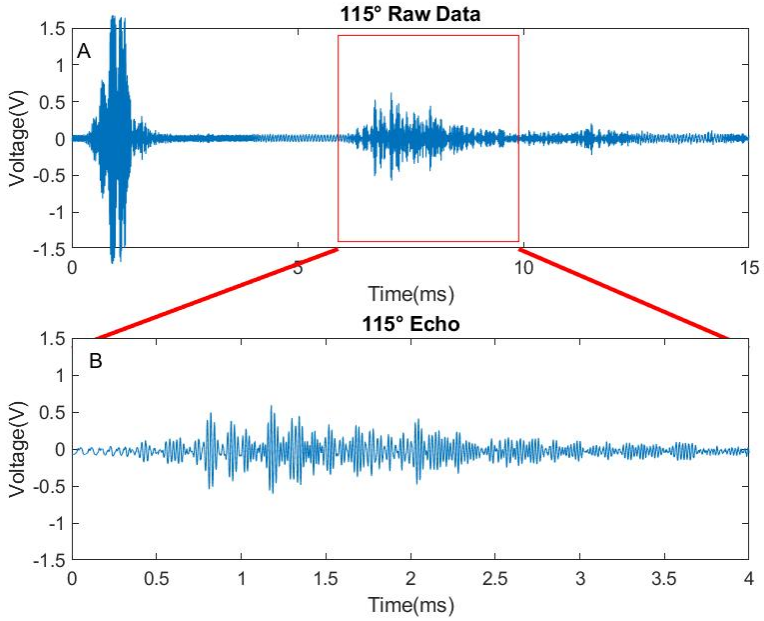

Figure A.70: Reflected signal from three layers bush wall surface with grazing angle 115°,0.5 meter from bush wall at position 14.a) Entire reflected signal.b)Zoom in view of marked rectangular section

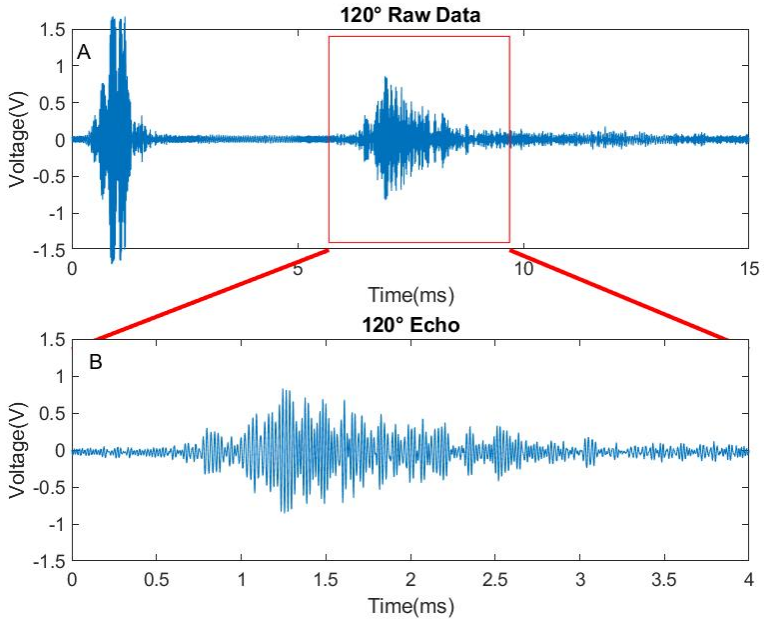

Figure A.71: Reflected signal from three layers bush wall surface with grazing angle 120°,0.5 meter from bush wall at position 15.a) Entire reflected signal.b)Zoom in view of marked rectangular section

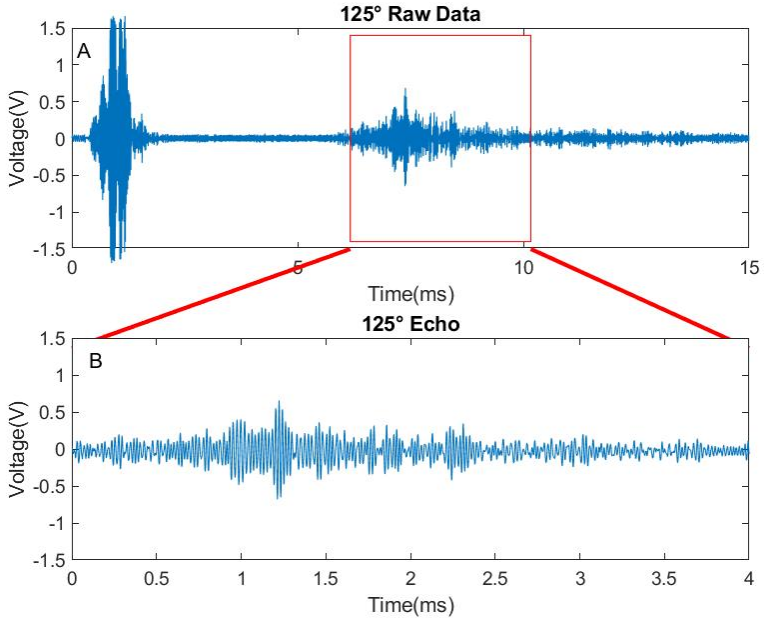

Figure A.72: Reflected signal from two layers bush wall surface with grazing angle 125°,0.5 meter from bush wall at position 16.a) Entire reflected signal.b)Zoom in view of marked rectangular section

A.1.3 0.5 Meter Coherence Result

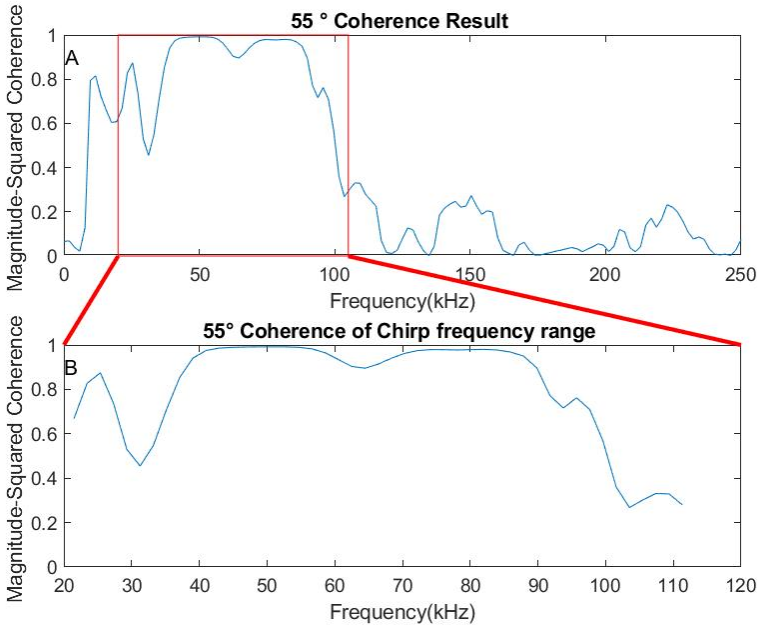

Figure A.73: Reflected signal Coherence between N time and N+1 times from three layers bush wall surface with grazing angle 55°,0.5 meter from bush wall at position 2.a) Entire reflected signal echo coherence.b)Zoom in view of marked rectangular section where input signal range is from 20kHz to 105kHz

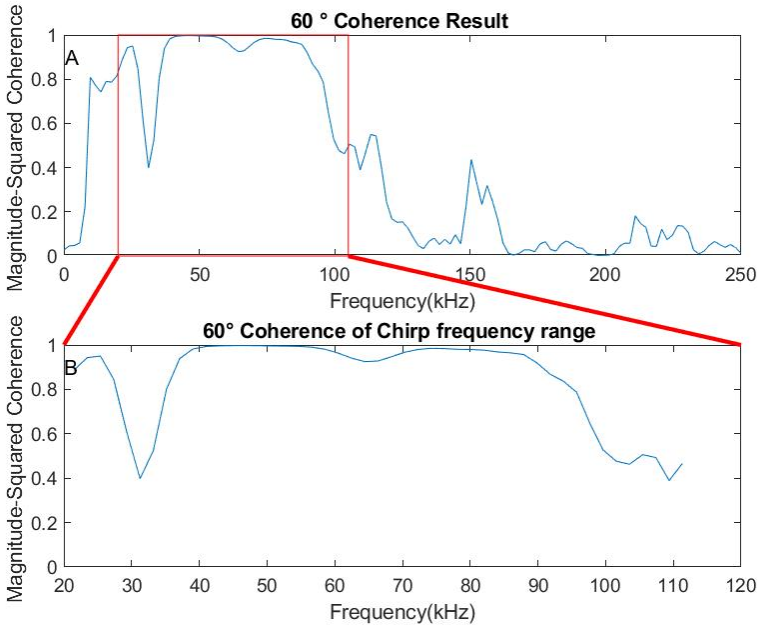

Figure A.74: Reflected signal Coherence between N time and N+1 times from three layers bush wall surface with grazing angle 60°,0.5 meter from bush wall at position 3.a) Entire reflected signal echo coherence.b)Zoom in view of marked rectangular section where input signal range is from 20kHz to 105kHz

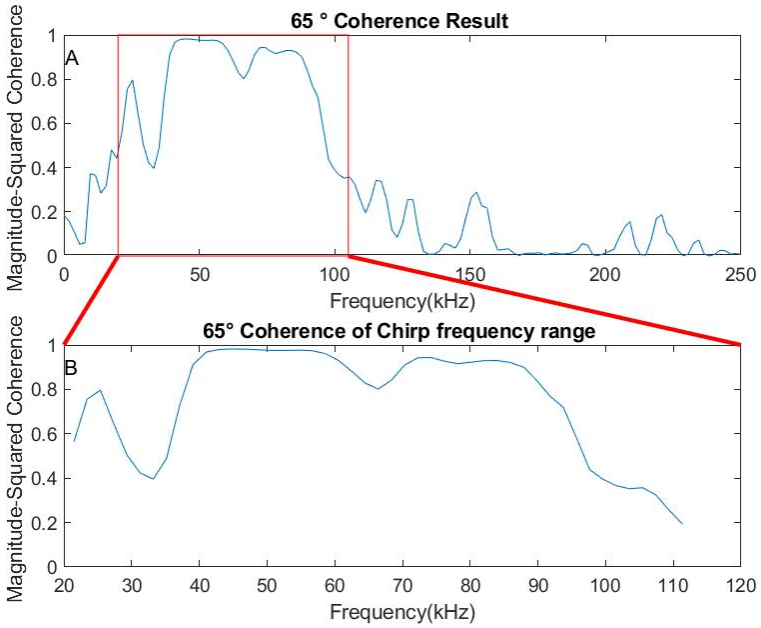

Figure A.75: Reflected signal Coherence between N time and N+1 times from three layers bush wall surface with grazing angle 65°,0.5 meter from bush wall at position 4.a) Entire reflected signal echo coherence.b)Zoom in view of marked rectangular section where input signal range is from 20kHz to 105kHz

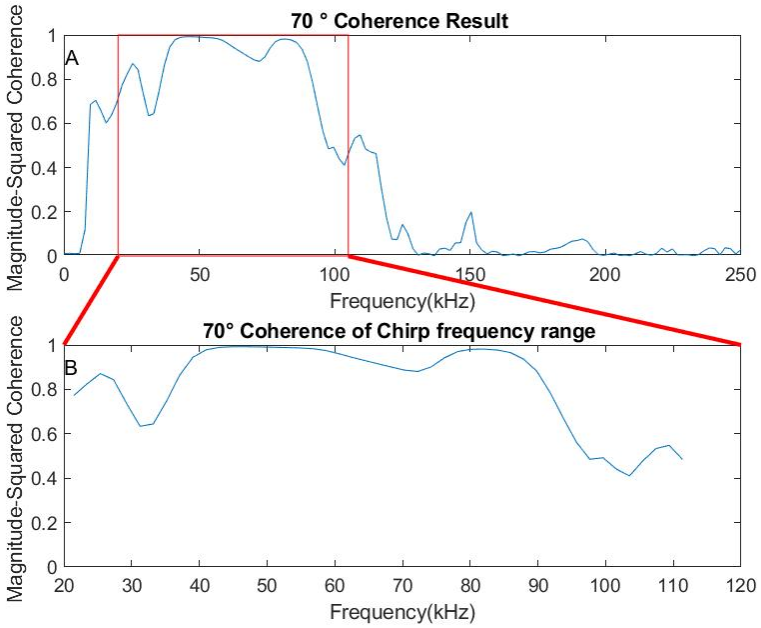

Figure A.76: Reflected signal Coherence between N time and N+1 times from three layers bush wall surface with grazing angle 70°,0.5 meter from bush wall at position 5.a) Entire reflected signal echo coherence.b)Zoom in view of marked rectangular section where input signal range is from 20kHz to 105kHz

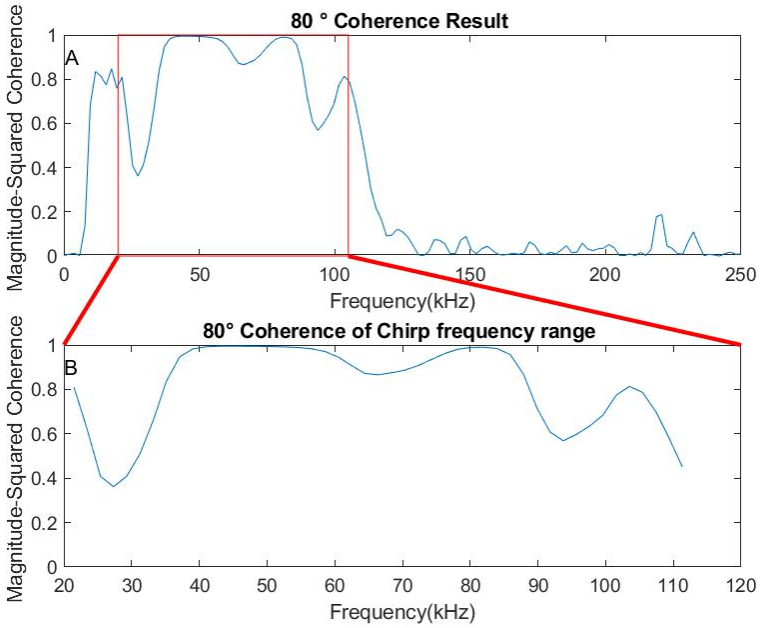

Figure A.77: Reflected signal Coherence between N time and N+1 times from three layers bush wall surface with grazing angle 80°,0.5 meter from bush wall at position 7.a) Entire reflected signal echo coherence.b)Zoom in view of marked rectangular section where input signal range is from 20kHz to 105kHz

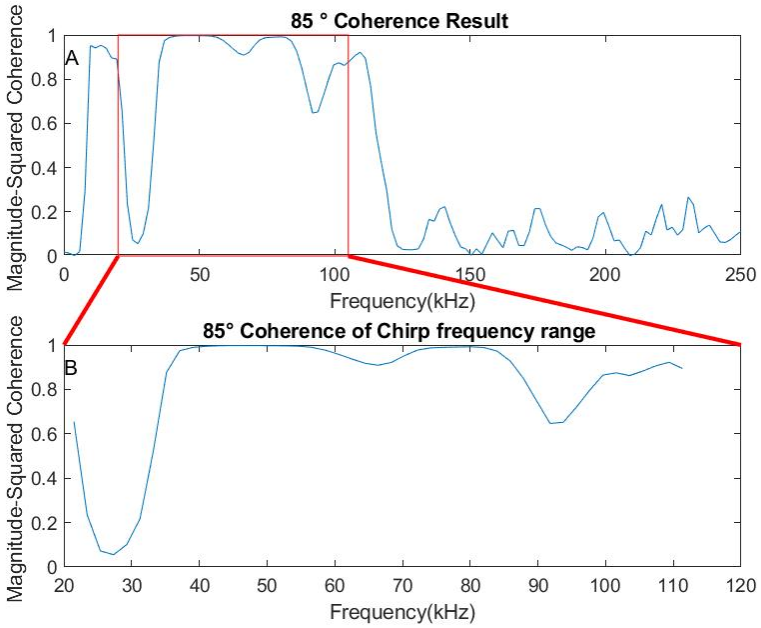

Figure A.78: Reflected signal Coherence between N time and N+1 times from three layers bush wall surface with grazing angle 85°,0.5 meter from bush wall at position 8.a) Entire reflected signal echo coherence.b)Zoom in view of marked rectangular section where input signal range is from 20kHz to 105kHz

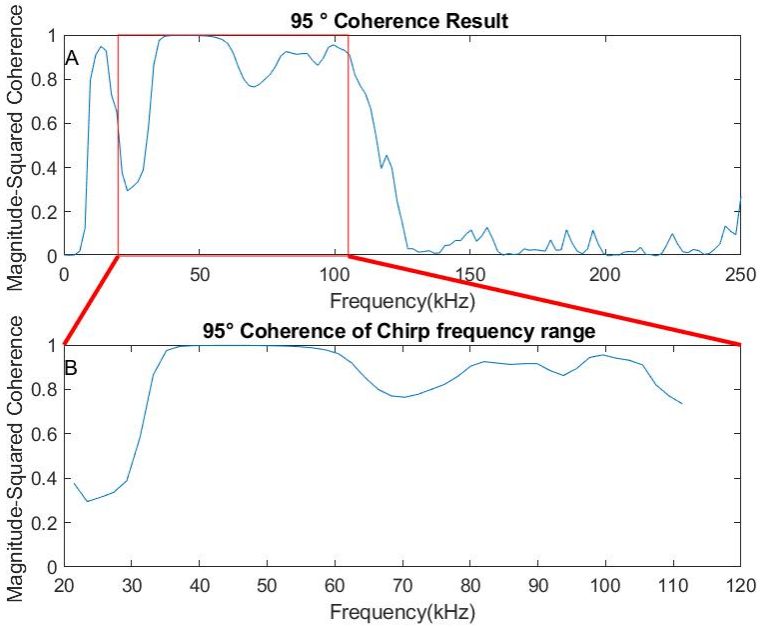

Figure A.79: Reflected signal Coherence between N time and N+1 times from three layers bush wall surface with grazing angle 95°,0.5 meter from bush wall at position 10.a) Entire reflected signal echo coherence.b)Zoom in view of marked rectangular section where input signal range is from 20kHz to 105kHz

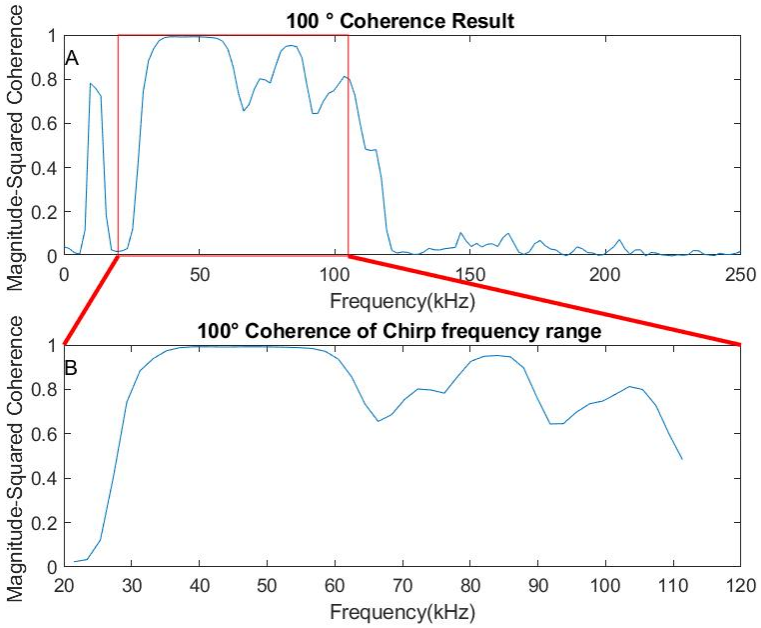

Figure A.80: Reflected signal Coherence between N time and N+1 times from three layers bush wall surface with grazing angle 100°,0.5 meter from bush wall at position 11.a) Entire reflected signal echo coherence.b)Zoom in view of marked rectangular section where input signal range is from 20kHz to 105kHz

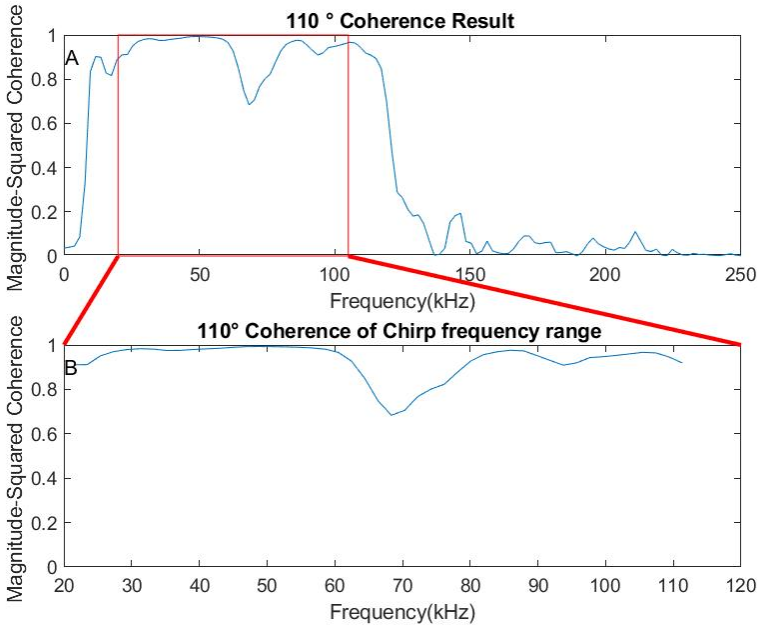

Figure A.81: Reflected signal Coherence between N time and N+1 times from three layers bush wall surface with grazing angle 110°,0.5 meter from bush wall at position 13.a) Entire reflected signal echo coherence.b)Zoom in view of marked rectangular section where input signal range is from 20kHz to 105kHz

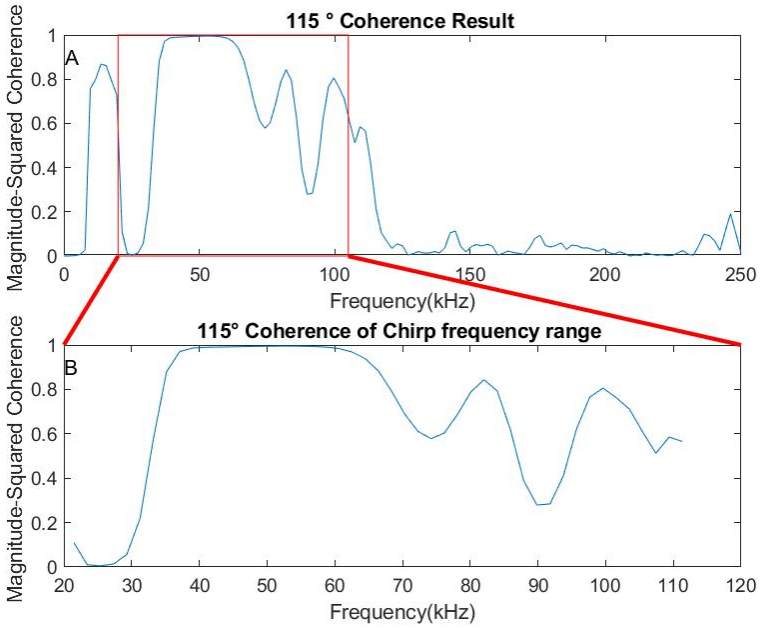

Figure A.82: Reflected signal Coherence between N time and N+1 times from three layers bush wall surface with grazing angle 115°,0.5 meter from bush wall at position 14.a) Entire reflected signal echo coherence.b)Zoom in view of marked rectangular section where input signal range is from 20kHz to 105kHz

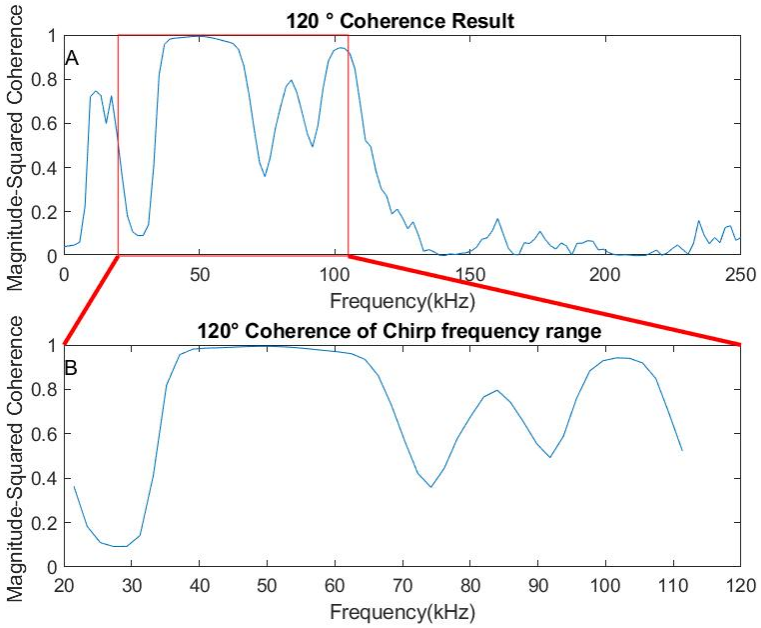

Figure A.83: Reflected signal Coherence between N time and N+1 times from three layers bush wall surface with grazing angle 120°,0.5 meter from bush wall at position 15.a) Entire reflected signal echo coherence.b)Zoom in view of marked rectangular section where input signal range is from 20kHz to 105kHz

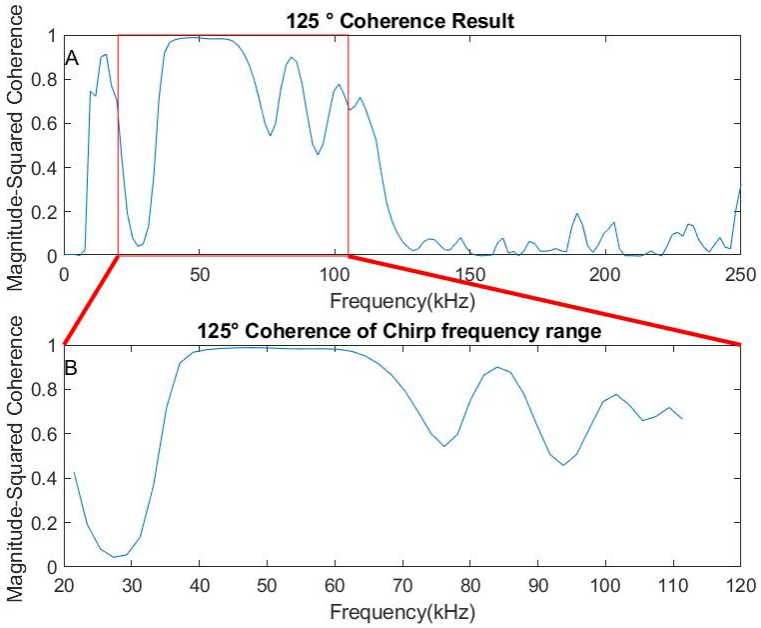

Figure A.84: Reflected signal Coherence between N time and N+1 times from three layers bush wall surface with grazing angle 125°,0.5 meter from bush wall at position 16.a) Entire reflected signal echo coherence.b)Zoom in view of marked rectangular section where input signal range is from 20kHz to 105kHz

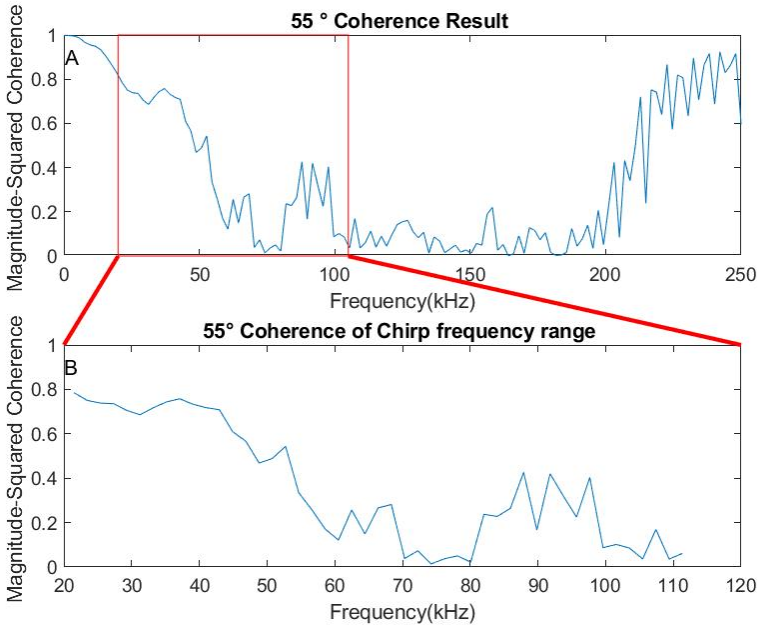

Figure A.85: Reflected top edge of signal echo Coherence between N time and N+1 times from three layers bush wall surface with grazing angle 55°,0.5 meter from bush wall at position 2.a) Entire reflected signal echo coherence.b)Zoom in view of marked rectangular section where input signal range is from 20kHz to 105kHz

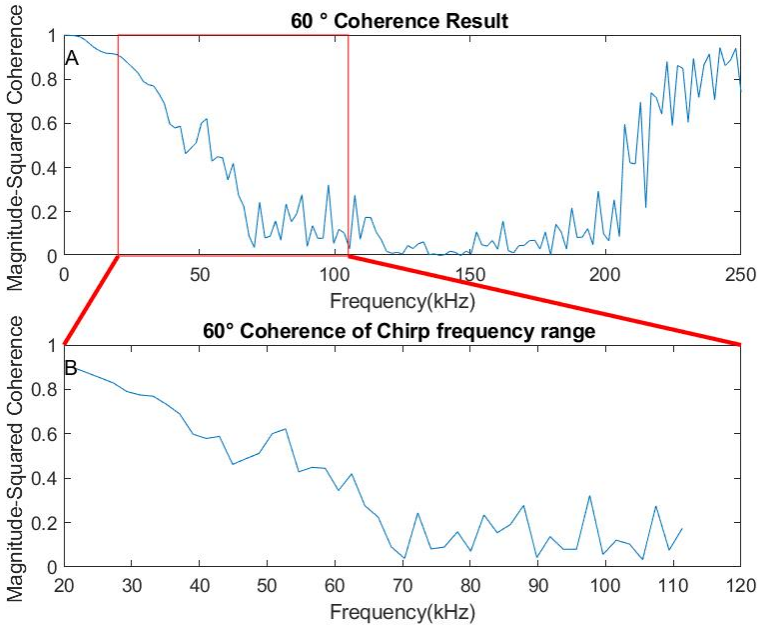

Figure A.86: Reflected top edge of signal echo Coherence between N time and N+1 times from three layers bush wall surface with grazing angle 60°,0.5 meter from bush wall at position 3.a) Entire reflected signal echo coherence.b)Zoom in view of marked rectangular section where input signal range is from 20kHz to 105kHz

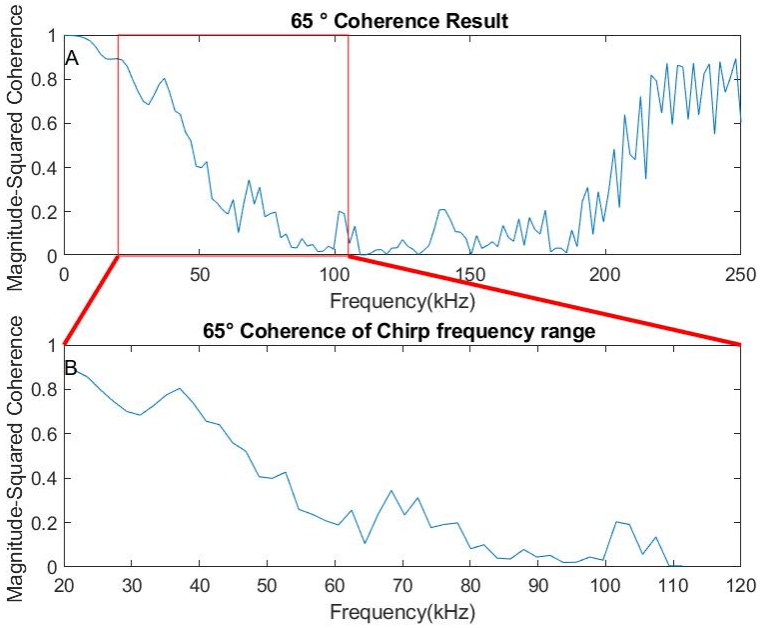

Figure A.87: Reflected top edge of signal echo Coherence between N time and N+1 times from three layers bush wall surface with grazing angle 65°,0.5 meter from bush wall at position 4.a) Entire reflected signal echo coherence.b)Zoom in view of marked rectangular section where input signal range is from 20kHz to 105kHz

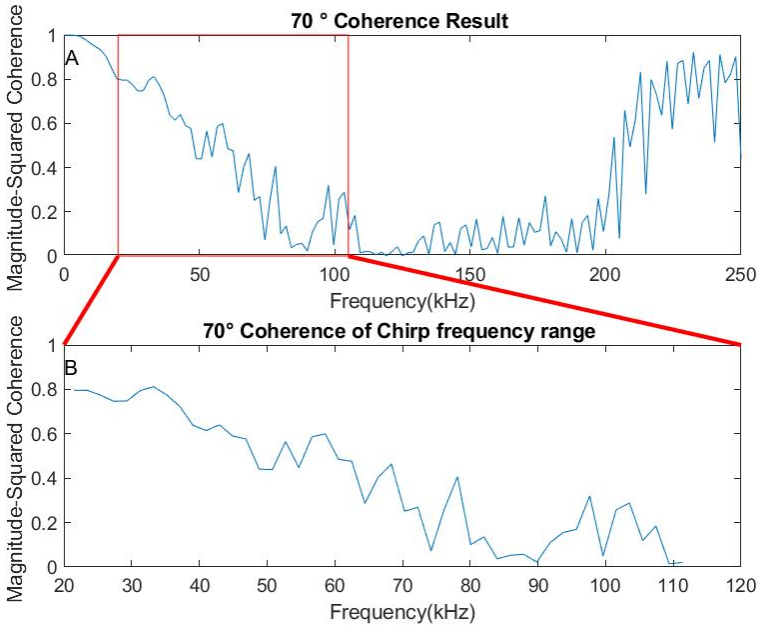

Figure A.88: Reflected top edge of signal echo Coherence between N time and N+1 times from three layers bush wall surface with grazing angle 70°,0.5 meter from bush wall at position 5.a) Entire reflected signal echo coherence.b)Zoom in view of marked rectangular section where input signal range is from 20kHz to 105kHz

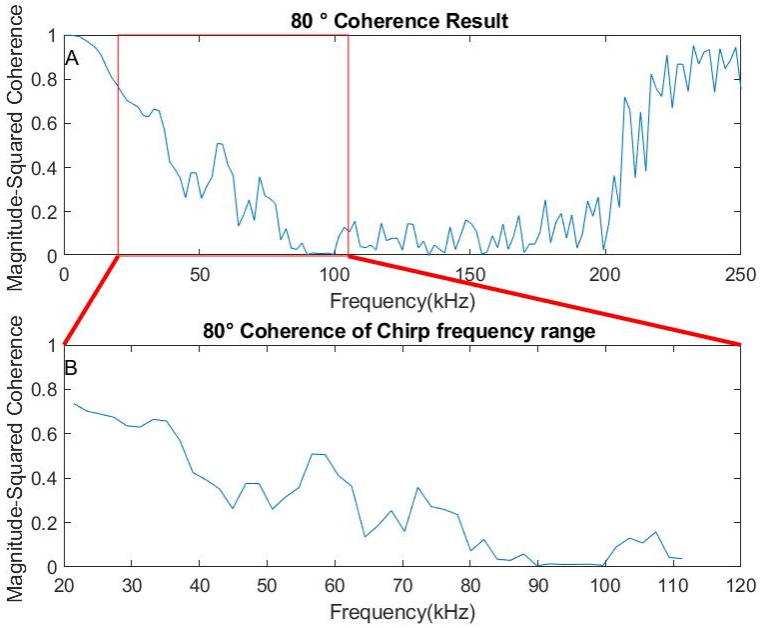

Figure A.89: Reflected top edge of signal echo Coherence between N time and N+1 times from three layers bush wall surface with grazing angle 80°,0.5 meter from bush wall at position 7.a) Entire reflected signal echo coherence.b)Zoom in view of marked rectangular section where input signal range is from 20kHz to 105kHz

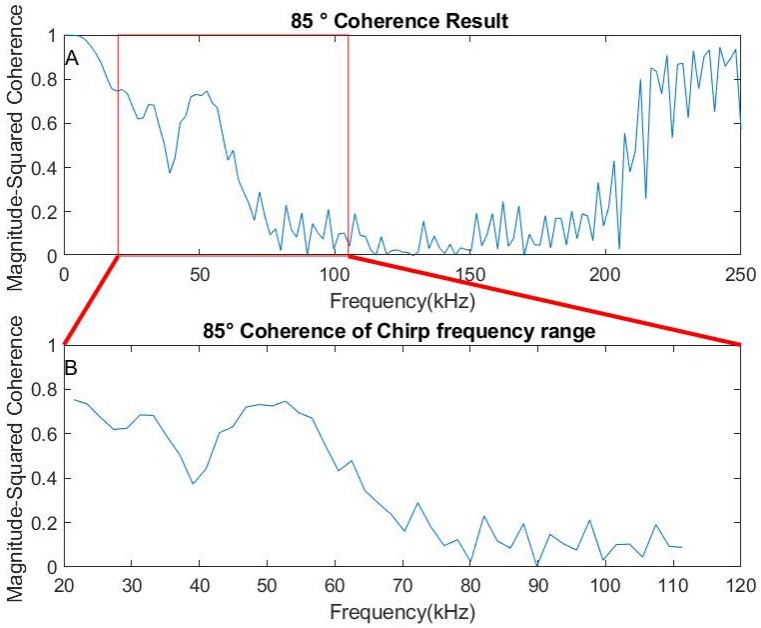

Figure A.90: Reflected top edge of signal echo Coherence between N time and N+1 times from three layers bush wall surface with grazing angle 85°,0.5 meter from bush wall at position 8.a) Entire reflected signal echo coherence.b)Zoom in view of marked rectangular section where input signal range is from 20kHz to 105kHz

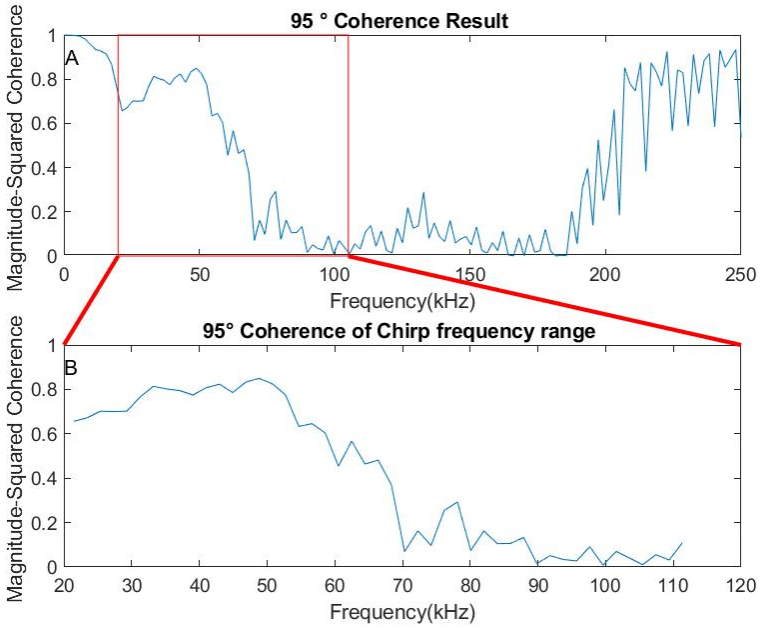

Figure A.91: Reflected top edge of signal echo Coherence between N time and N+1 times from three layers bush wall surface with grazing angle 95°,0.5 meter from bush wall at position 10.a) Entire reflected signal echo coherence.b)Zoom in view of marked rectangular section where input signal range is from 20kHz to 105kHz

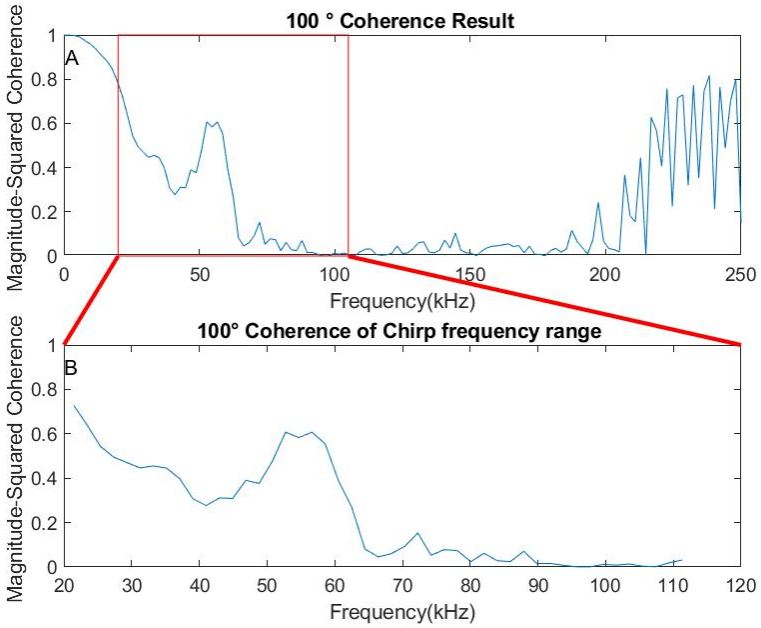

Figure A.92: Reflected top edge of signal echo Coherence between N time and N+1 times from three layers bush wall surface with grazing angle 100°,0.5 meter from bush wall at position 11.a) Entire reflected signal echo coherence.b)Zoom in view of marked rectangular section where input signal range is from 20kHz to 105kHz

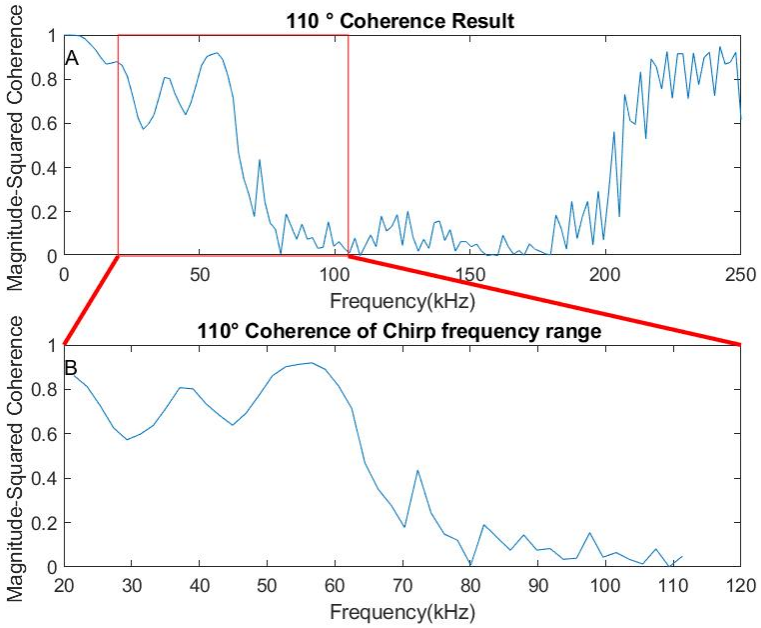

Figure A.93: Reflected top edge of signal echo Coherence between N time and N+1 times from three layers bush wall surface with grazing angle 110°,0.5 meter from bush wall at position 13.a) Entire reflected signal echo coherence.b)Zoom in view of marked rectangular section where input signal range is from 20kHz to 105kHz

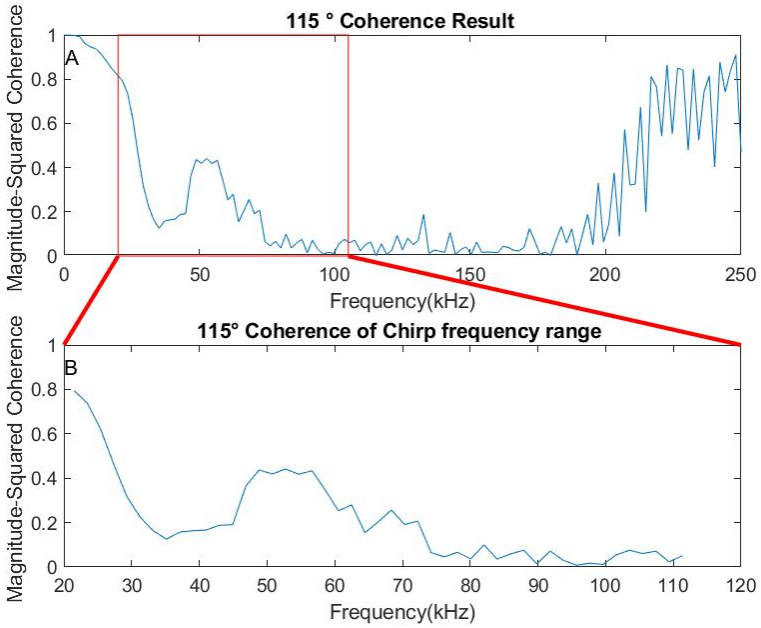

Figure A.94: Reflected top edge of signal echo Coherence between N time and N+1 times from three layers bush wall surface with grazing angle 115°,0.5 meter from bush wall at position 14.a) Entire reflected signal echo coherence.b)Zoom in view of marked rectangular section where input signal range is from 20kHz to 105kHz

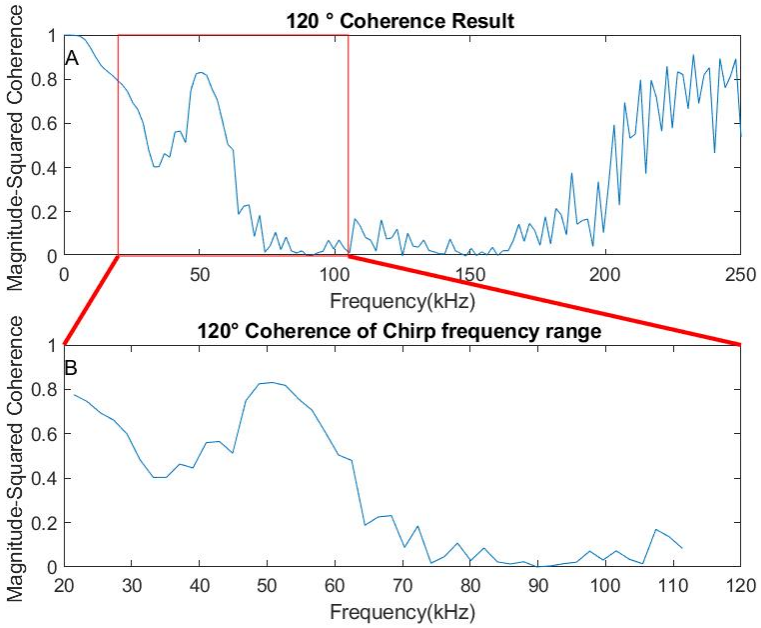

Figure A.95: Reflected top edge of signal echo Coherence between N time and N+1 times from three layers bush wall surface with grazing angle 120°,0.5 meter from bush wall at position 15.a) Entire reflected signal echo coherence.b)Zoom in view of marked rectangular section where input signal range is from 20kHz to 105kHz

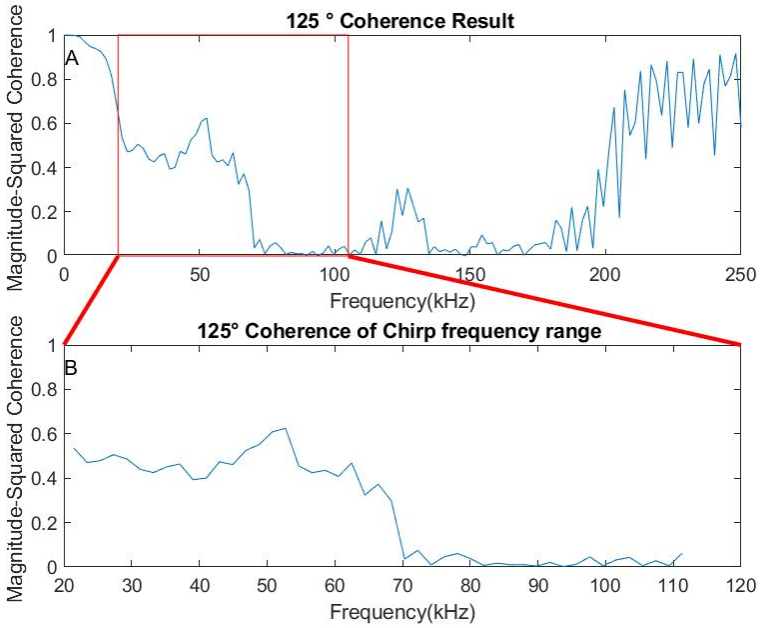

Figure A.96: Reflected top edge of signal echo Coherence between N time and N+1 times from three layers bush wall surface with grazing angle 125°,0.5 meter from bush wall at position 16.a) Entire reflected signal echo coherence.b)Zoom in view of marked rectangular section where input signal range is from 20kHz to 105kHz

A.1.4 0.8 Meter Coherence Result

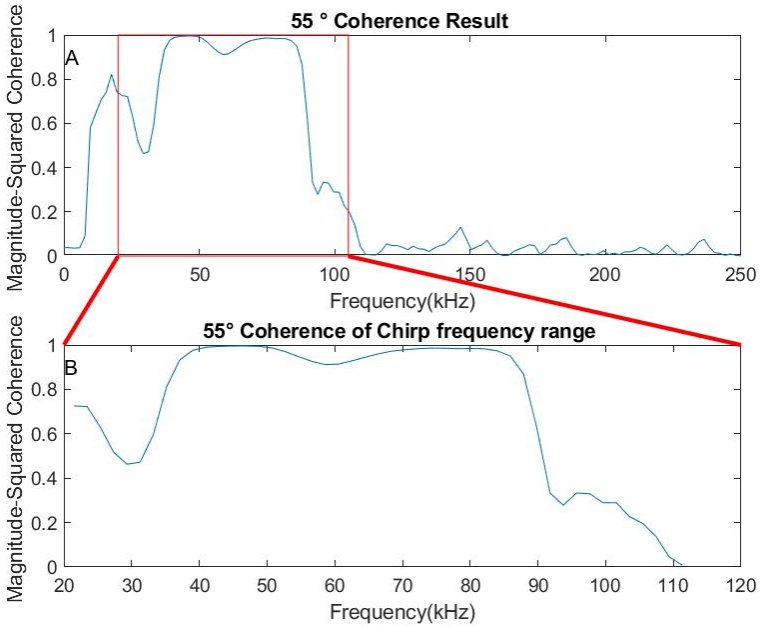

Figure A.97: Reflected signal Coherence between N time and N+1 times from three layers bush wall surface with grazing angle 55°,0.5 meter from bush wall at position 2.a) Entire reflected signal echo coherence.b)Zoom in view of marked rectangular section where input signal range is from 20kHz to 105kHz

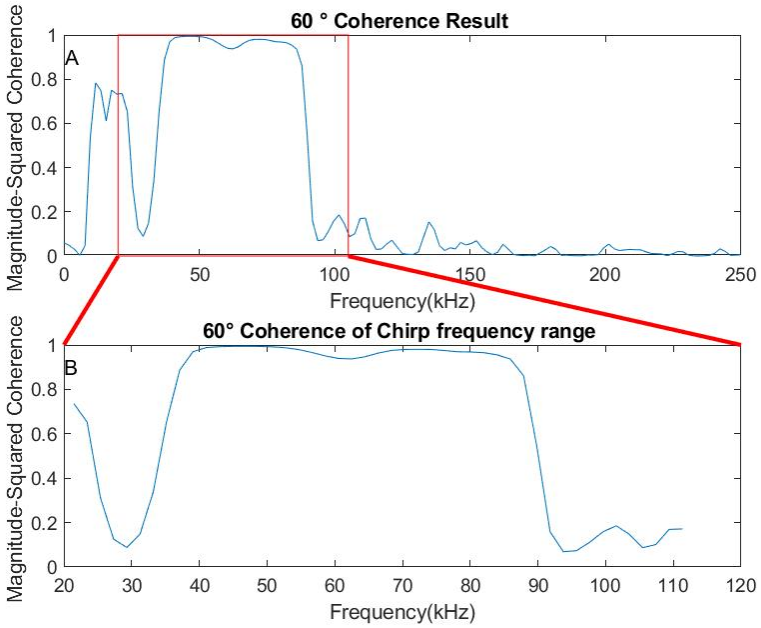

Figure A.98: Reflected signal Coherence between N time and N+1 times from three layers bush wall surface with grazing angle 60°,0.5 meter from bush wall at position 3.a) Entire reflected signal echo coherence.b)Zoom in view of marked rectangular section where input signal range is from 20kHz to 105kHz

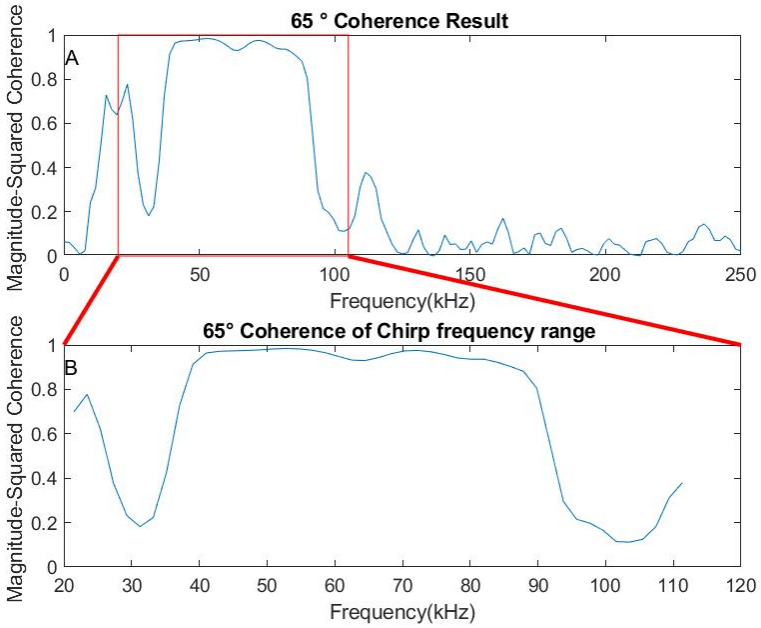

Figure A.99: Reflected signal Coherence between N time and N+1 times from three layers bush wall surface with grazing angle 65°,0.5 meter from bush wall at position 4.a) Entire reflected signal echo coherence.b)Zoom in view of marked rectangular section where input signal range is from 20kHz to 105kHz

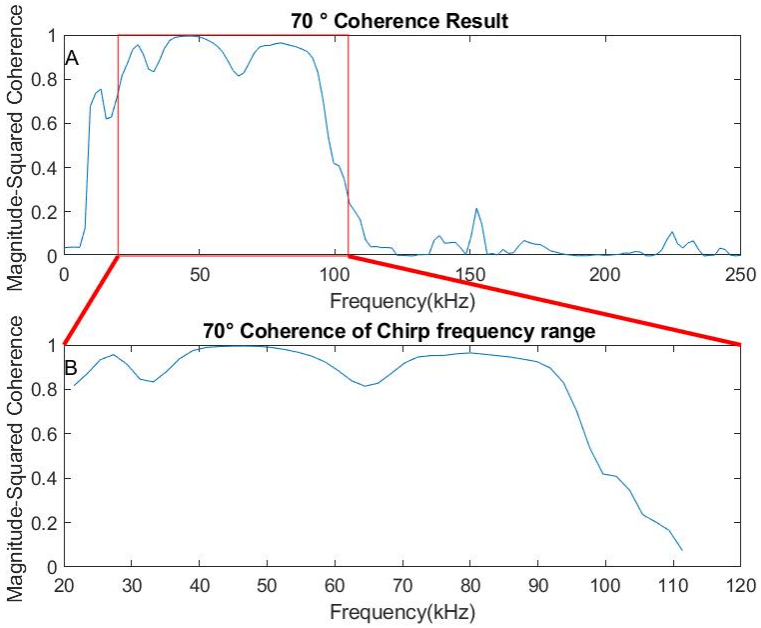

Figure A.100: Reflected signal Coherence between N time and N+1 times from three layers bush wall surface with grazing angle 70°,0.5 meter from bush wall at position 5.a) Entire reflected signal echo coherence.b)Zoom in view of marked rectangular section where input signal range is from 20kHz to 105kHz

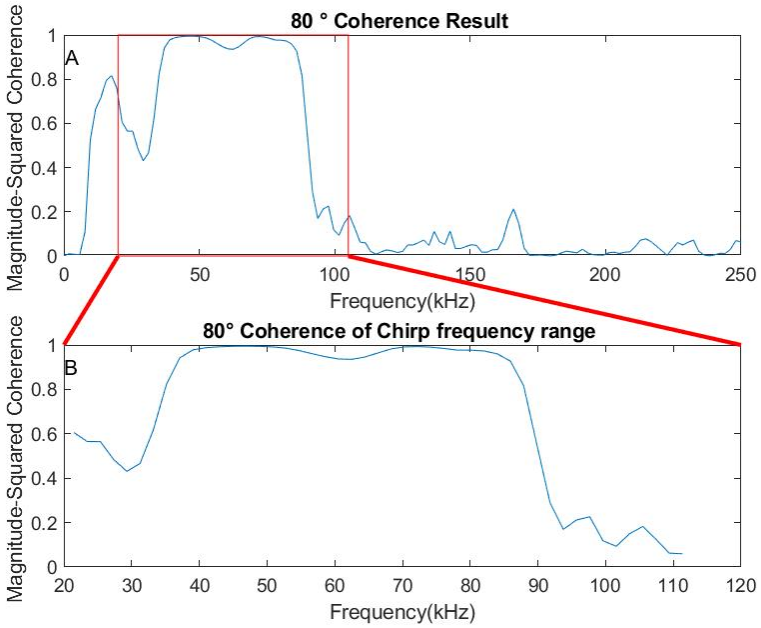

Figure A.101: Reflected signal Coherence between N time and N+1 times from three layers bush wall surface with grazing angle 80°,0.5 meter from bush wall at position 7.a) Entire reflected signal echo coherence.b)Zoom in view of marked rectangular section where input signal range is from 20kHz to 105kHz

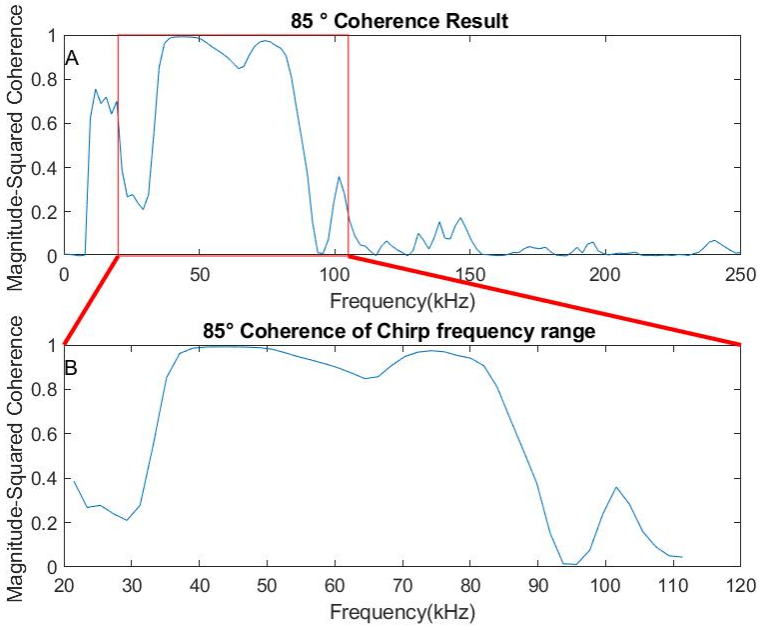

Figure A.102: Reflected signal Coherence between N time and N+1 times from three layers bush wall surface with grazing angle 85°,0.5 meter from bush wall at position 8.a) Entire reflected signal echo coherence.b)Zoom in view of marked rectangular section where input signal range is from 20kHz to 105kHz

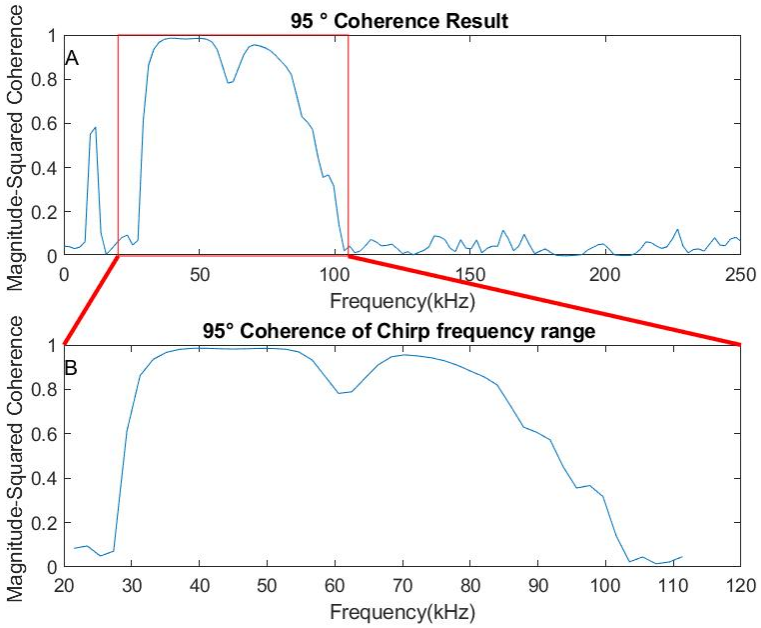

Figure A.103: Reflected signal Coherence between N time and N+1 times from three layers bush wall surface with grazing angle 95°,0.5 meter from bush wall at position 10.a) Entire reflected signal echo coherence.b)Zoom in view of marked rectangular section where input signal range is from 20kHz to 105kHz

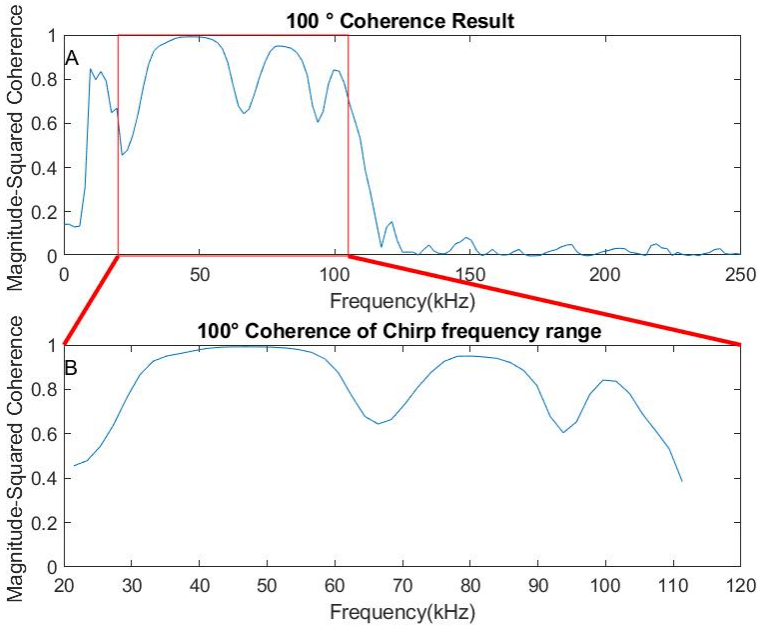

Figure A.104: Reflected signal Coherence between N time and N+1 times from three layers bush wall surface with grazing angle 100°,0.5 meter from bush wall at position 11.a) Entire reflected signal echo coherence.b)Zoom in view of marked rectangular section where input signal range is from 20kHz to 105kHz

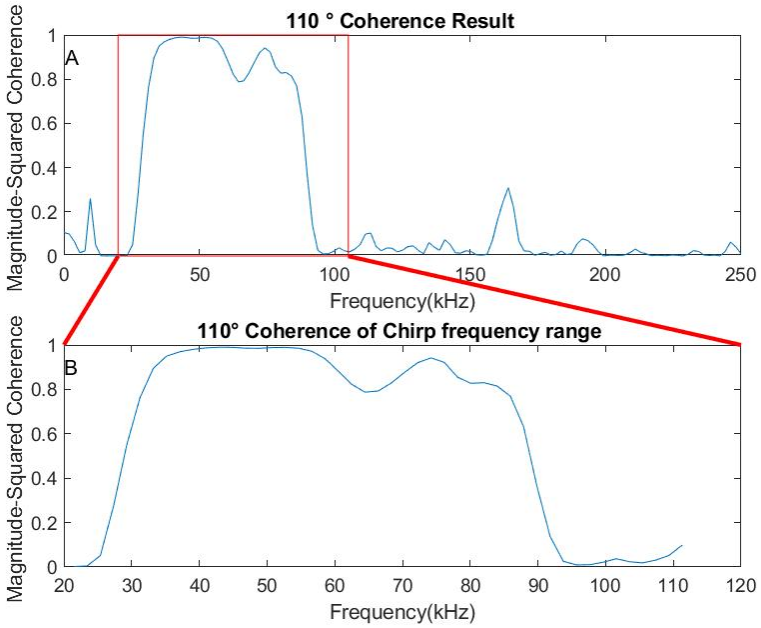

Figure A.105: Reflected signal Coherence between N time and N+1 times from three layers bush wall surface with grazing angle 110°,0.5 meter from bush wall at position 13.a) Entire reflected signal echo coherence.b)Zoom in view of marked rectangular section where input signal range is from 20kHz to 105kHz

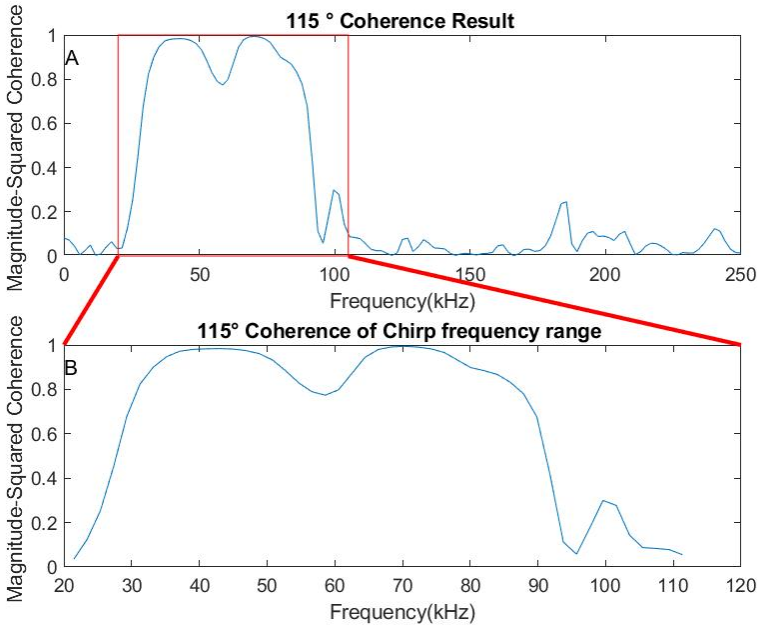

Figure A.106: Reflected signal Coherence between N time and N+1 times from three layers bush wall surface with grazing angle 115°,0.5 meter from bush wall at position 14.a) Entire reflected signal echo coherence.b)Zoom in view of marked rectangular section where input signal range is from 20kHz to 105kHz

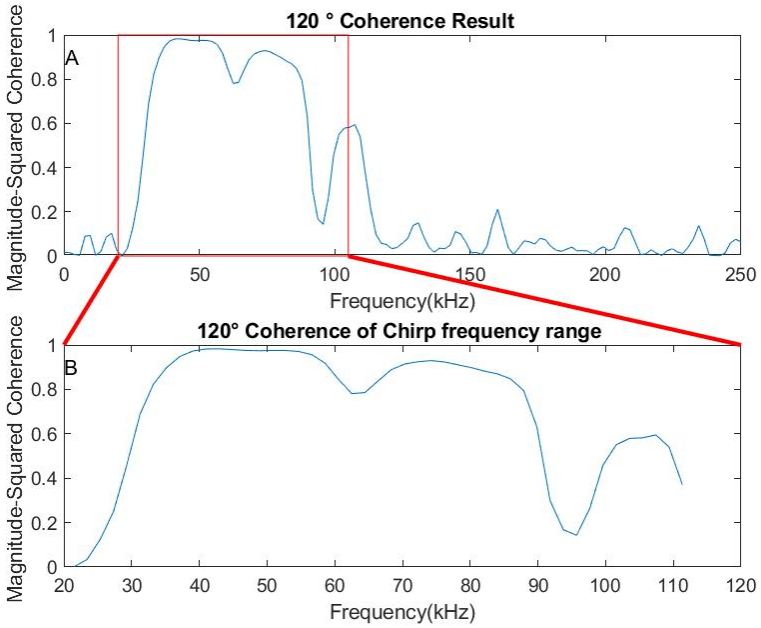

Figure A.107: Reflected signal Coherence between N time and N+1 times from three layers bush wall surface with grazing angle 120°,0.5 meter from bush wall at position 15.a) Entire reflected signal echo coherence.b)Zoom in view of marked rectangular section where input signal range is from 20kHz to 105kHz

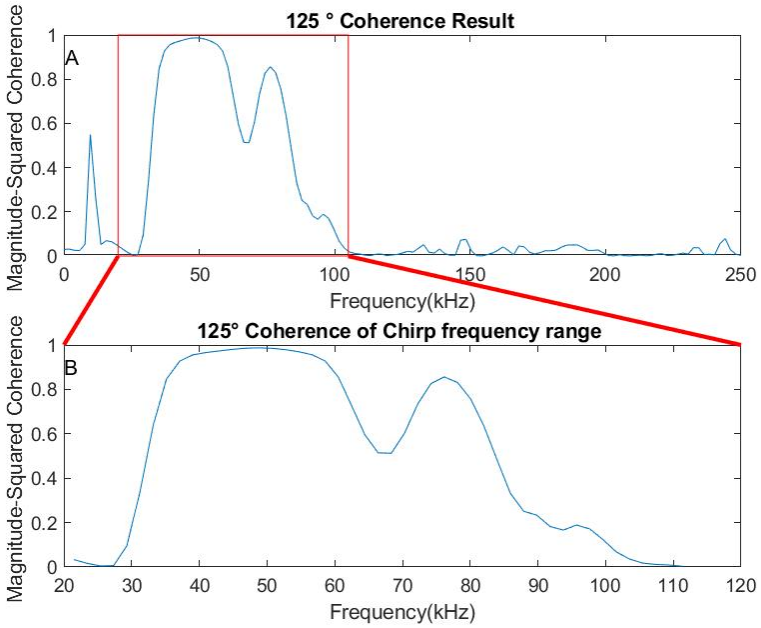

Figure A.108: Reflected signal Coherence between N time and N+1 times from three layers bush wall surface with grazing angle 125°,0.5 meter from bush wall at position 16.a) Entire reflected signal echo coherence.b)Zoom in view of marked rectangular section where input signal range is from 20kHz to 105kHz

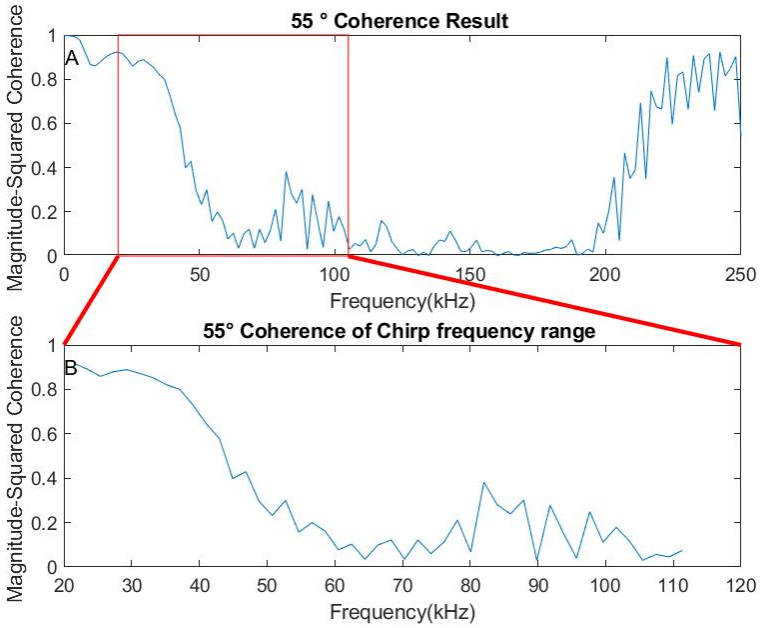

Figure A.109: Reflected top edge of signal echo Coherence between N time and N+1 times from three layers bush wall surface with grazing angle 55°,0.5 meter from bush wall at position 2.a) Entire reflected signal echo coherence.b)Zoom in view of marked rectangular section where input signal range is from 20kHz to 105kHz

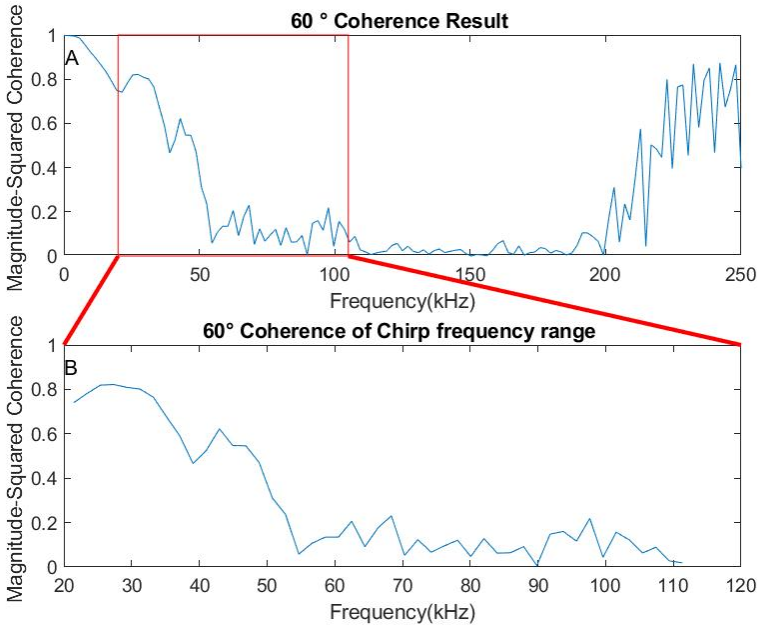

Figure A.110: Reflected top edge of signal echo Coherence between N time and N+1 times from three layers bush wall surface with grazing angle 60°,0.5 meter from bush wall at position 3.a) Entire reflected signal echo coherence.b)Zoom in view of marked rectangular section where input signal range is from 20kHz to 105kHz

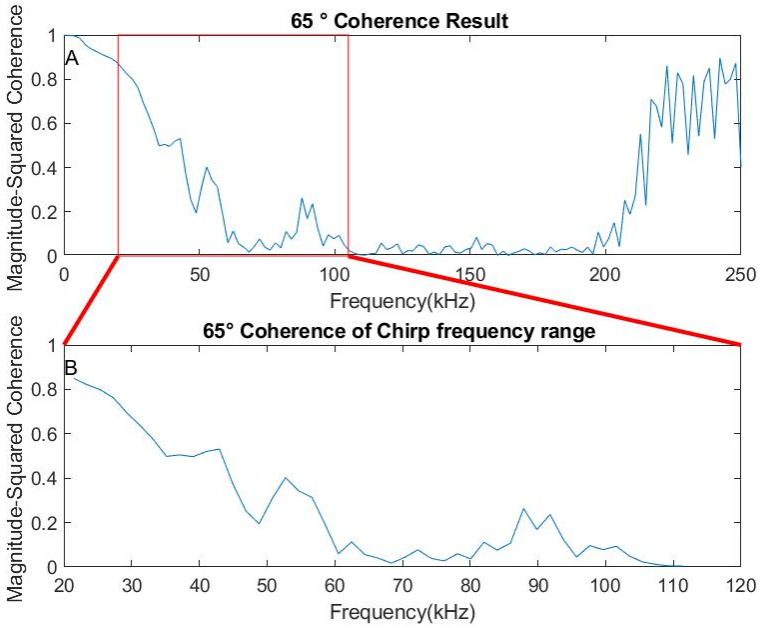

Figure A.111: Reflected top edge of signal echo Coherence between N time and N+1 times from three layers bush wall surface with grazing angle 65°,0.5 meter from bush wall at position 4.a) Entire reflected signal echo coherence.b)Zoom in view of marked rectangular section where input signal range is from 20kHz to 105kHz

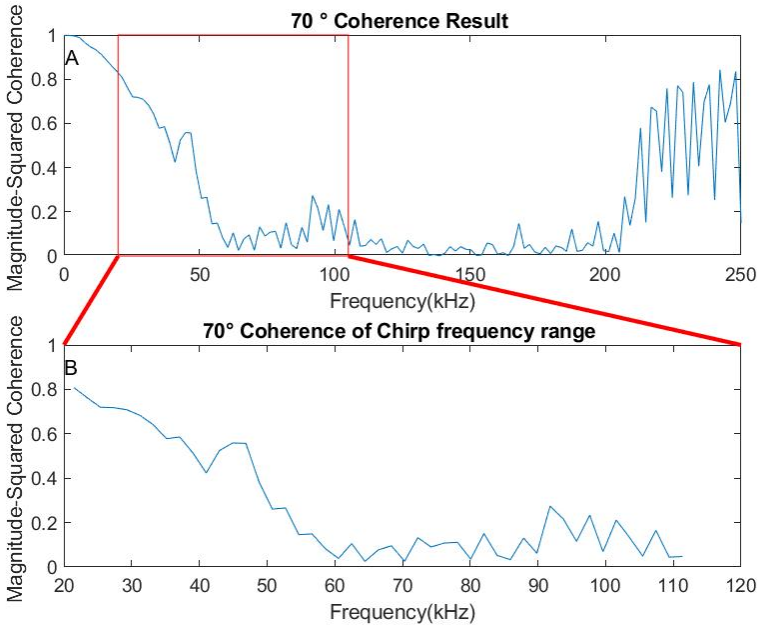

Figure A.112: Reflected top edge of signal echo Coherence between N time and N+1 times from three layers bush wall surface with grazing angle 70°,0.5 meter from bush wall at position 5.a) Entire reflected signal echo coherence.b)Zoom in view of marked rectangular section where input signal range is from 20kHz to 105kHz

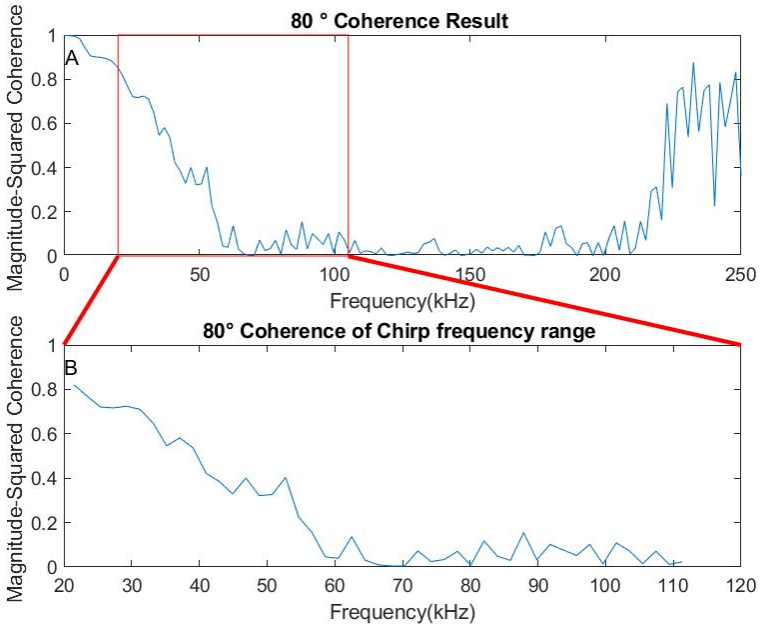

Figure A.113: Reflected top edge of signal echo Coherence between N time and N+1 times from three layers bush wall surface with grazing angle 80°,0.5 meter from bush wall at position 7.a) Entire reflected signal echo coherence.b)Zoom in view of marked rectangular section where input signal range is from 20kHz to 105kHz

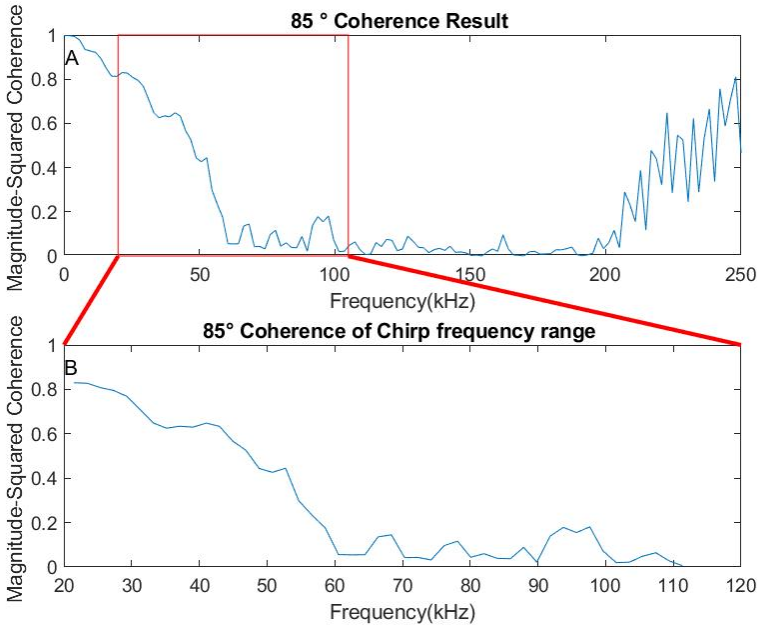

Figure A.114: Reflected top edge of signal echo Coherence between N time and N+1 times from three layers bush wall surface with grazing angle 85°,0.5 meter from bush wall at position 8.a) Entire reflected signal echo coherence.b)Zoom in view of marked rectangular section where input signal range is from 20kHz to 105kHz

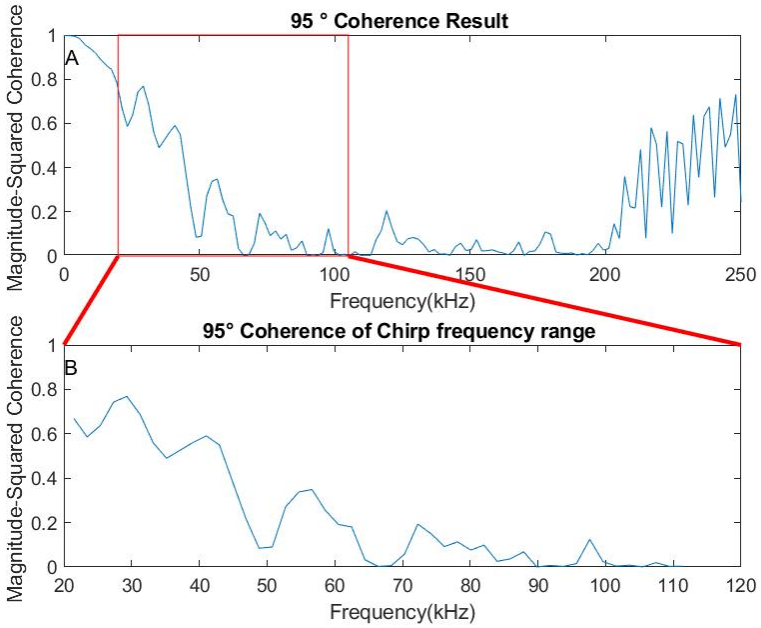

Figure A.115: Reflected top edge of signal echo Coherence between N time and N+1 times from three layers bush wall surface with grazing angle 95°,0.5 meter from bush wall at position 10.a) Entire reflected signal echo coherence.b)Zoom in view of marked rectangular section where input signal range is from 20kHz to 105kHz

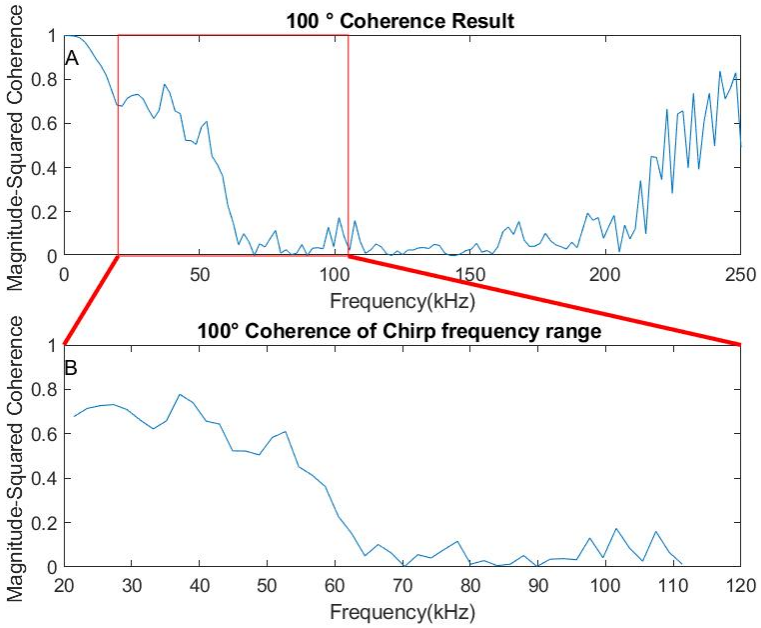

Figure A.116: Reflected top edge of signal echo Coherence between N time and N+1 times from three layers bush wall surface with grazing angle 100°,0.5 meter from bush wall at position 11.a) Entire reflected signal echo coherence.b)Zoom in view of marked rectangular section where input signal range is from 20kHz to 105kHz

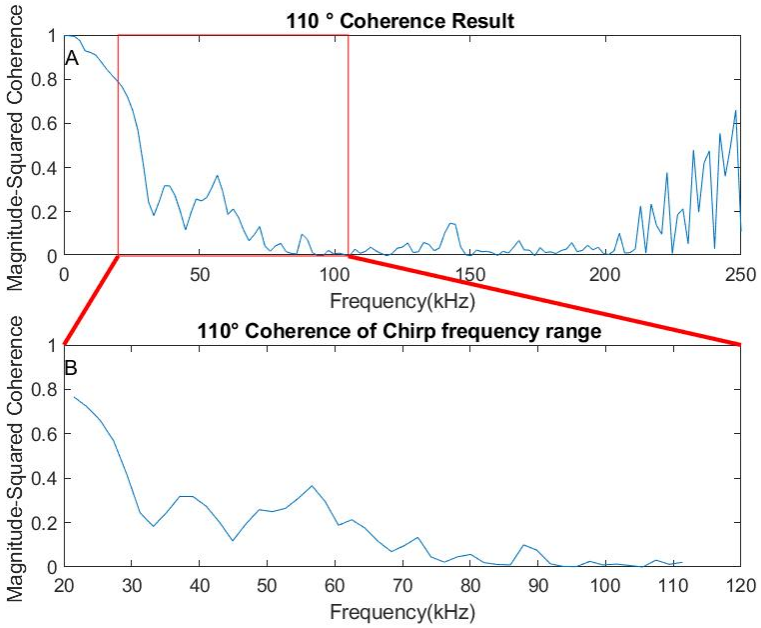

Figure A.117: Reflected top edge of signal echo Coherence between N time and N+1 times from three layers bush wall surface with grazing angle 110°,0.5 meter from bush wall at position 13.a) Entire reflected signal echo coherence.b)Zoom in view of marked rectangular section where input signal range is from 20kHz to 105kHz

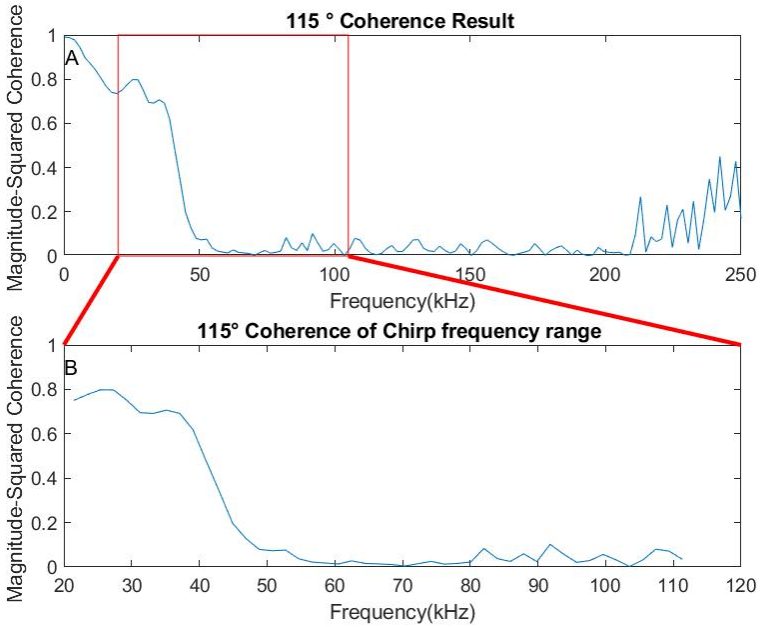

Figure A.118: Reflected top edge of signal echo Coherence between N time and N+1 times from three layers bush wall surface with grazing angle 115°,0.5 meter from bush wall at position 14.a) Entire reflected signal echo coherence.b)Zoom in view of marked rectangular section where input signal range is from 20kHz to 105kHz

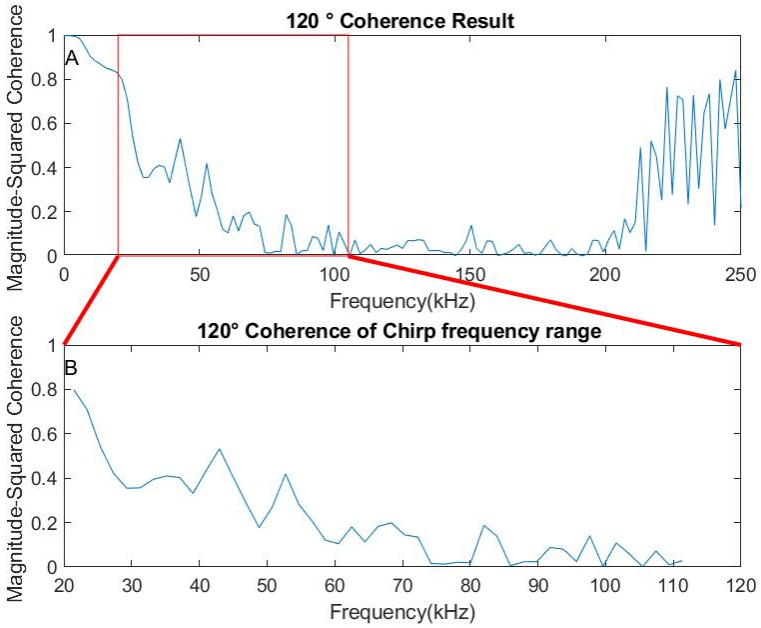

Figure A.119: Reflected top edge of signal echo Coherence between N time and N+1 times from three layers bush wall surface with grazing angle 120°,0.5 meter from bush wall at position 15.a) Entire reflected signal echo coherence.b)Zoom in view of marked rectangular section where input signal range is from 20kHz to 105kHz

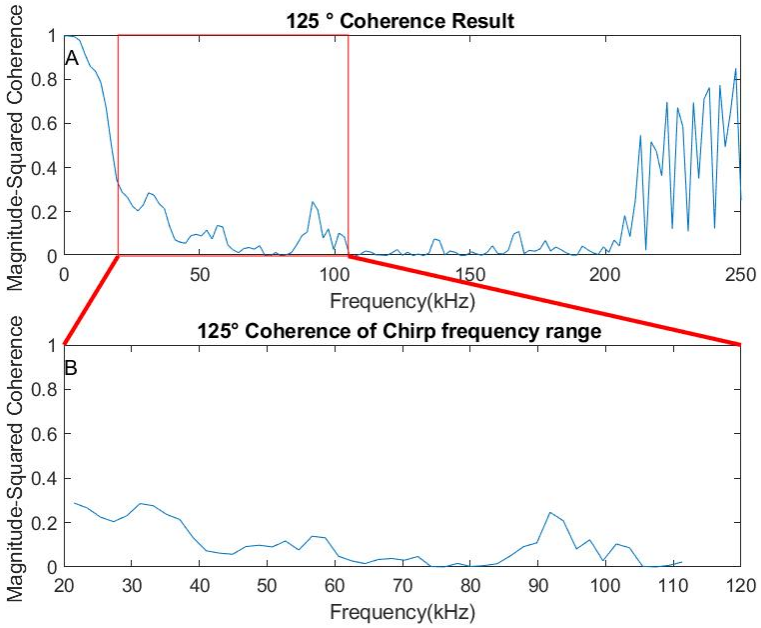

Figure A.120: Reflected top edge of signal echo Coherence between N time and N+1 times from three layers bush wall surface with grazing angle 125°,0.5 meter from bush wall at position 16.a) Entire reflected signal echo coherence.b)Zoom in view of marked rectangular section where input signal range is from 20kHz to 105kHz

0.5 meter with two layers bush wall

For two layers bush wall, the echo share same regularity as one layer bush wall echo does, but with stronger amplitude and intensity.When the angle equal to 90 °, the echo has the most concentrate shape, and at 50 or 130 °,echoes has the most dispersed shape.

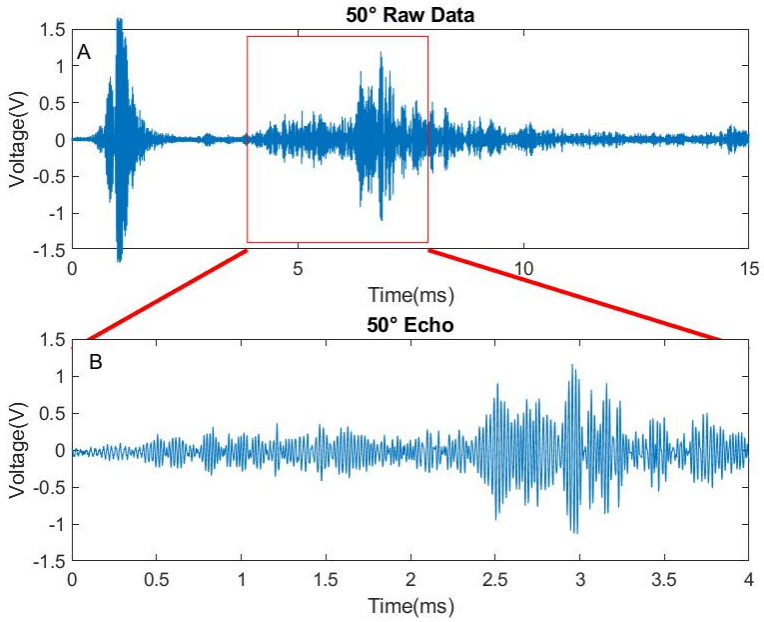

Figure A.121: Reflected signal from two layers bush wall surface with grazing angle 50°,0.5 meter from bush wall at position 1.a) Entire reflected signal.b)Zoom in view of marked rectangular section

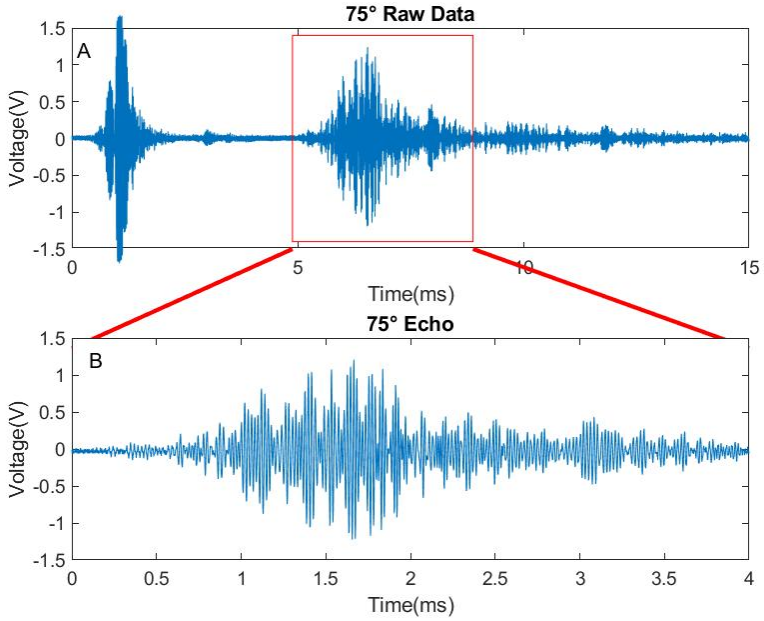

Figure A.122: Reflected signal from two layers bush wall surface with grazing angle 75°,0.5 meter from bush wall at position 6.a) Entire reflected signal.b)Zoom in view of marked rectangular section

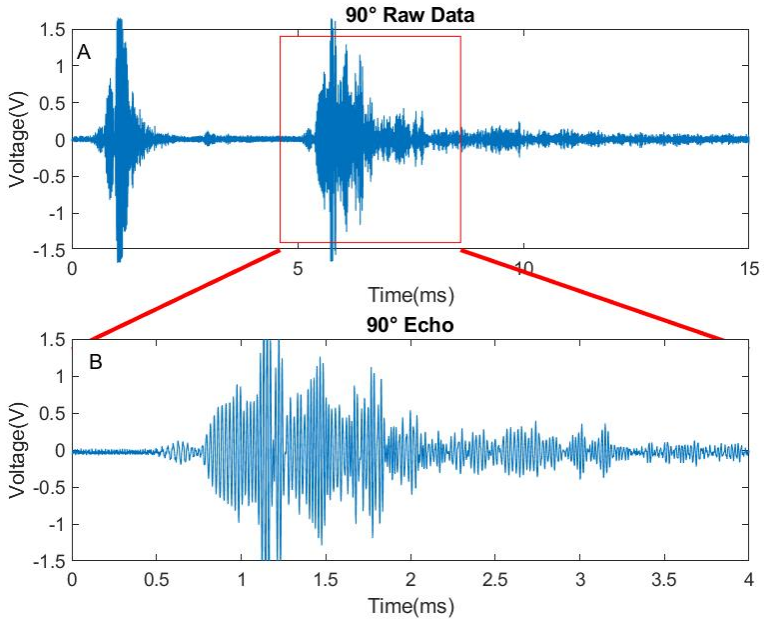

Figure A.123: Reflected signal from two layers bush wall surface with grazing angle 90°,0.5 meter from bush wall at position 9.a) Entire reflected signal.b)Zoom in view of marked rectangular section

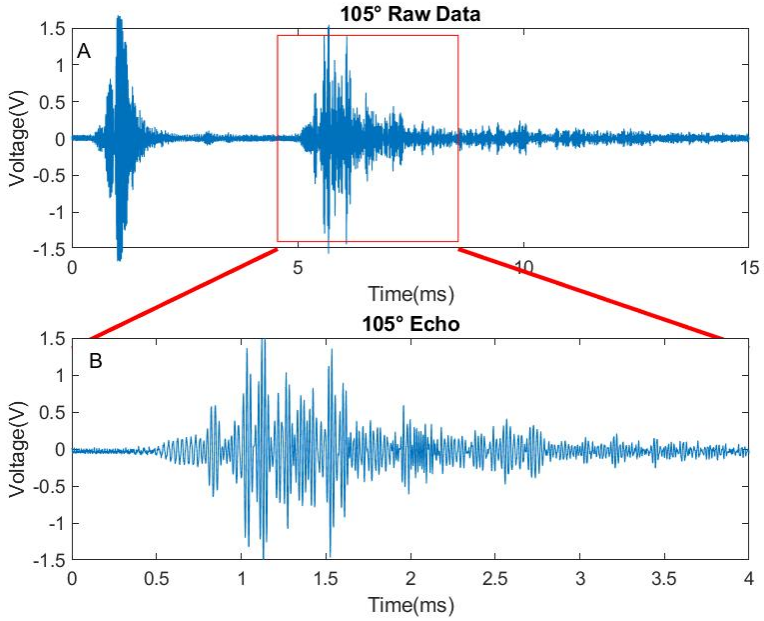

Figure A.124: Reflected signal from two layers bush wall surface with grazing angle 105°,0.5 meter from bush wall at position 12.a) Entire reflected signal.b)Zoom in view of marked rectangular section

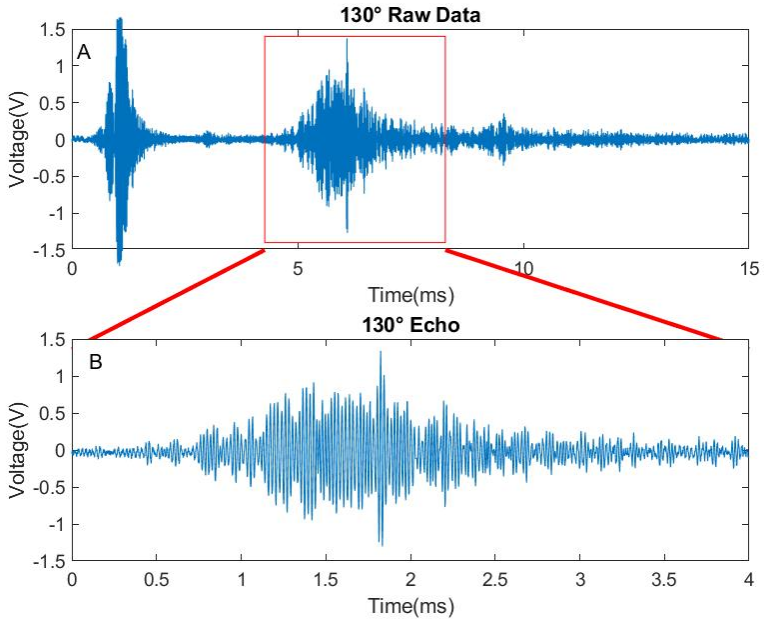

Figure A.125: Reflected signal from two layers bush wall surface with grazing angle 130°,0.5 meter from bush wall at position 17.a) Entire reflected signal.b)Zoom in view of marked rectangular section

A.1.5 1.2 meter echo result

For the 1.2 meter detection, all position's result are very minor, there was a high possibility that our sonar head might out of range or the gain value is not high enough. The 0.8 meter detection is the best experiment result, no matter in echo intensity or in echo range.

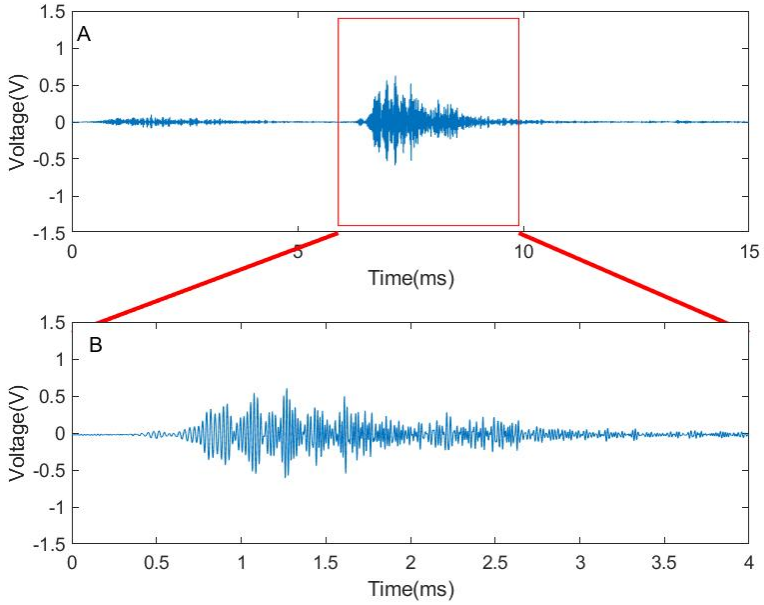

Figure A.126: Reflected signal from three layers bush wall surface with grazing angle 50°,1.2 meter at position 1.a) Entire reflected signal.b)Zoom in view of marked rectangular section

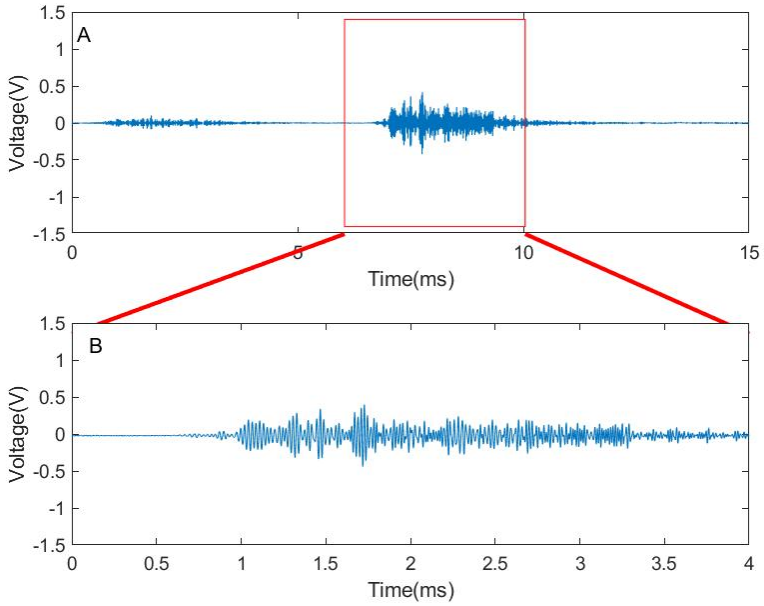

Figure A.127: Reflected signal from three layers bush wall surface with grazing angle 75°,1.2 meter at position 6.a) Entire reflected signal.b)Zoom in view of marked rectangular section

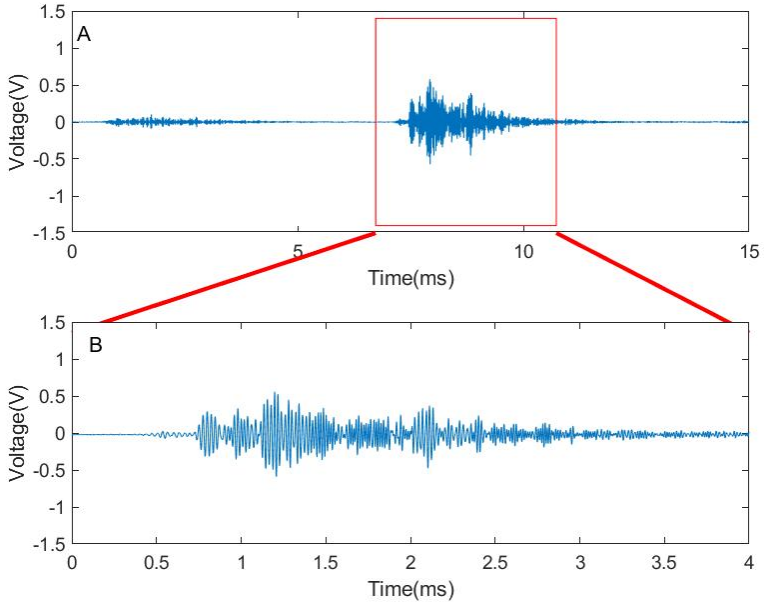

Figure A.128: Reflected signal from three layers bush wall surface with grazing angle 90°,1.2 meter at position 9.a) Entire reflected signal.b)Zoom in view of marked rectangular section

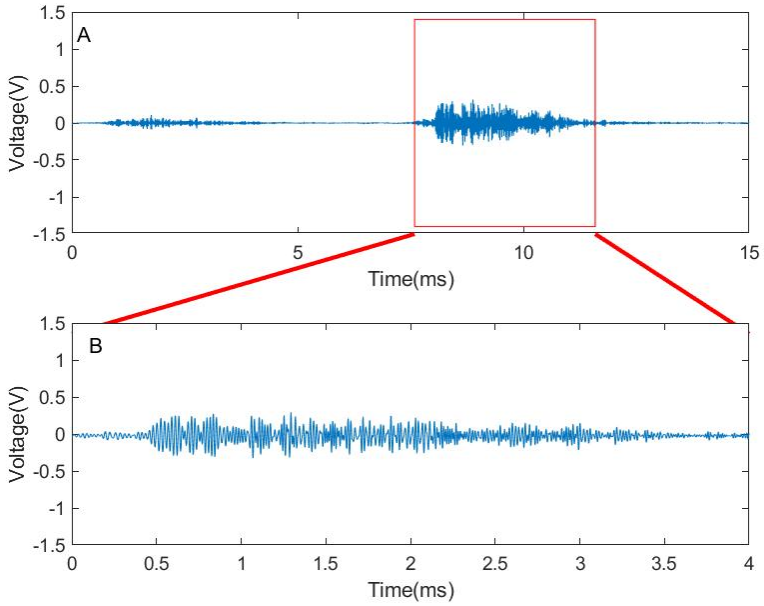

Figure A.129: Reflected signal from three layers bush wall surface with grazing angle 105°,1.2 meter at position 12.a) Entire reflected signal.b)Zoom in view of marked rectangular section

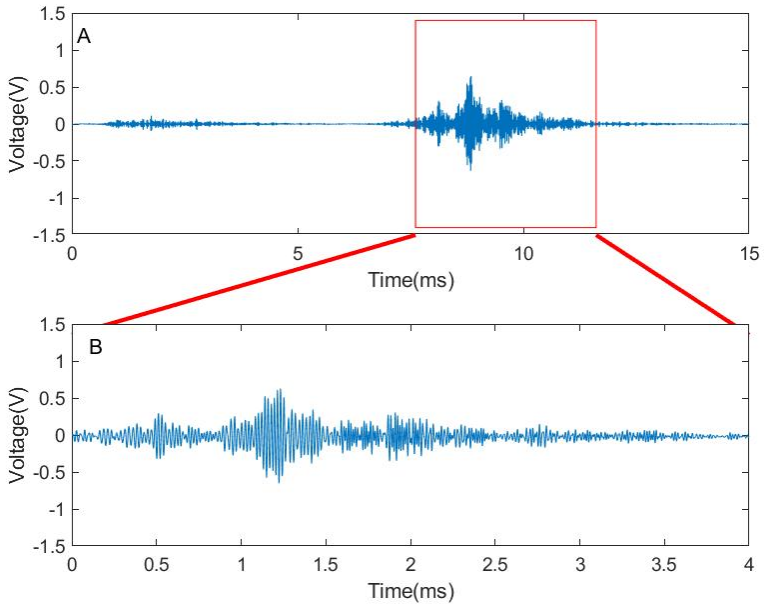

Figure A.130: Reflected signal from three layers bush wall surface with grazing angle 130°,1.2 meter at position 17.a) Entire reflected signal.b)Zoom in view of marked rectangular section

A.2 Section two

Appendix B

Second Appendix: Matlab Code

```
close all;
clc;
clear all;
load('11172017HShalfgain1mcalibrationIndoor_2.mat');
load('11172017HShalfgain1mcalibrationIndoor.mat')
Fs=500000;
fre=2000;
data = sonarTest.data.xdata ;
prp = sonarTest.prps;
t2= (0:15/7500:4);
t3= (0:15/7500:15);
t4= (1.5:15/7500:15);
 for f= 1:17;

data1=data(:,:,f);
     noisepostion=data1(:,1);
     noisedata=noisepostion(1300:1500);
     standnoise= std(noisedata);
     udata1= data1 - standnoise;
     nudata1=udata1(1500:7500);

   loc=find(nudata1>0.25,1,'first');
```

```
23
24      gdata1=udata1(loc+1100:loc+3100,1:20);
25
26  k0 = 1 ; % reference column
27  add some columns for demo purposes
28  gdata1(:,end+1) = 2*gdata1(:,k0)   ; % perfect correlation with
29  find the correlations among columns
30  N = size(gdata1,2) ;
31  CC = zeros(1,N) ; % pre-allocation to store the coefficients
32  for k = 1:N,% loop over all columns
33    tmp = corrcoef(gdata1(:,k0),gdata1(:,k)) ;
34    CC(k) = tmp(1,2) ;
35  end
36   t=(-1.5:1/1000:0-1/1000);
37
38  for n=1:20
39       rawposin=data1(:,n);
40       posin=gdata1(:,n);
41        fposin=gdata1(:,1)-mean(posin);
42        posi=posin-mean(posin);
43       au(:,n)=xcorr(fposin,posin);
44        aun=mean(au,2);
45
46   aupn=mean(au,2);
47  [Cxy,fre]= mscohere(fposin,posin,hamming(100),[],[],Fs);
48  paupnx(:,f)=aupn(1:2001);
49
50  paunx=aun(1:2000);
51     paupn=posin/max(posin);
52          [aup(:,n),alo(:,n)]=envelope(paupn,100,'analytic');
53  aaup=aup(:,1);
```

```
54          ass(:,f)=aun(1200:2000);
55  aaaxxx=abs(paunx);
56  aaxxxx=abs(ass);
57    [Cxy,fre]= mscohere(aaup,aup,hamming(100),[],[],Fs);
58    [Cxy,fre]= mscohere(aaup,aup,hamming(100),[],[],Fs);
59
60        paun=paunx/max(paunx);
61        aFt=fft(paunx);
62        P2=abs(aFt/2000);
63        P1=P2(1:(2000/2+1));
64        P1(2:end-1) = 2*P1(2:end-1);
65        fs=Fs*(0:(2000/2))/2000000;
66        [aup,alo]=envelope(posi,100,'analytic');
67  Area= trapz(t2,aup);
68  aupnor=aup./Area;
69   Area2= trapz(t2,posi);
70  aupnor2=aup2./Area2;
71
72  MM=moment(posi,2);
73  MMM(:,f)=sqrt(moment(posi,2));
74    fun=@(time) (time.^2)*MM;
75  q = integral(fun,0,4);
76  qf(n,f)=sqrt(integral(fun,0,4));
77  %%%%%% moment_2 (n,f)= mean((aupnor - mean(aupnor)).^2);
78  %%%%%% moment_23=sqrt(moment_2);
79  %%%%%% moment_22(n,f)= mean((posi - mean(posi)).^2);
80  %%%%%% moment_223=sqrt(moment_22);
81  %%%%%%
82  %%%%%% km= kurtosis(aupnor);
83  %%%%%% kmm(:,f)=kurtosis(aupnor);
84  %%%%%%   fun = fit(t2(:),aup,'gauss1');
```

```
85 %%%%%%%
86 %%%%%%   ener=sum(abs(posi(1:1500)).^2);
87 %%%%%%   energy(n,f)=sum(aupnor.^2);
88 %%%%%% eener(n,f)=ener;
89  fun = fit(t2(:),aup,'gauss1');
90    stdddd(:,f)=std(aup);
91
92   disp(fun);
93     hold on
94
95 end
96 [Ccxy(:,f),fre]= mscohere(aaup,aup,hamming(100),[],[],Fs);
97  Ccxyn=Ccxy(12:58,f);
98   frecxy=fre(12:58)/1000;
99 [Ccxy(:,f),fre]= mscohere(fposin,posin,hamming(100),[],[],Fs);
100
101 paund(:,f)=paun;
102 rng 'default'
103 h=figure
104  subplot(2,1,1)
105       plot(t3,rawposin)
106
107        txta={'A'};
108       text(0.1,1.2,txta)
109
110       ylabel('Voltage(V)');
111   xlabel('Time(ms)');
112   title([ num2str(45+5*f) '° Echo' ])
113
114   ylim([-1.5 1.5]);
115    subplot(2,1,2)
```

```
116         plot(t2,posin)
117         txtb={'B'};
118         text(0.1,1.2,txtb)
119          ylabel('Voltage(V)');
120    xlabel('Time(ms)');
121    ylim([-1.5 1.5]);
122    title([ num2str(45+5*f) '° Echo Teop Edge After Hilbert Transform ' ])
123       set(gca,'Clipping','Off')
124 hh1 = line([20 28],[1 1.4]);
125 hh2 = line([120 62],[1 1.4]);
126
127 set(hh1,'LineWidth',2,'color','r')
128 hold on
129 set (hh2,'LineWidth',2,'color','r')
130
131  subplot(2,1,1)
132         plot(fre/1000,Ccxy(:,f))
133
134            rectangular('Position',[20 0 85 1],'EdgeColor','r')
135
136         txtb={'A'};
137
138         text(0.5,0.9,txtb)
139         ylabel('Magnitude-Squared Coherence ');
140    xlabel('Frequency(kHz)');
141    title([ num2str(45+5*f) ' ° Coherence Result ' ])
142
143    ylim([0 1]);
144  subplot(2,1,2)
145
146         plot(frecxy,Ccxyn)
```

```
147     txta={'B'};
148    text(20,0.9,txta)
149         ylabel('Magnitude-Squared Coherence ');
150    xlabel('Frequency(kHz)');
151    title([ num2str(45+5*f) '° Coherence of Chirp frequency range ' ])
152
153    ylim([0  1]);
154
155   subplot(2,1,1)
156         plot(t3,rawposin)
157          rectangular('Position',[(loc+1100)/500 -1.4  4  2.8],'EdgeColor','r')
158          txta={'A'};
159         text(0.1,1.2,txta)
160         ylim([-1.5  1.5]);
161         ylabel('Voltage(V)');
162    xlabel('Time(ms)');
163    title([ num2str(45+5*f) '° Raw Data' ])
164     ylim([-1.5  1.5]);
165     set(gca,'Clipping','Off')
166 hh1 = line([(loc+1100)/500  0],[-1.5  -2.85]);
167 hh2 = line([(loc+1100)/500+4  15],[-1.5  -2.85]);
168
169 set(hh1,'LineWidth',2,'color','r')
170 hold on
171 set (hh2,'LineWidth',2,'color','r')
172
173     subplot(2,1,2)
174         plot(t2,posin)
175         txtb={'B'};
176         text(0.1,1.2,txtb)
177          ylabel('Voltage(V)');
```

```
178     xlabel('Time(ms)');
179     ylim([-1.5 1.5]);
180     title([ num2str(45+5*f) '° Echo' ])
181
182         plot(t3,rawposin)
183  fut=fft(uudata1);
184  P2=abs(fut/7500);
185  P1 = P2(1:7500/2+1);
186  f = Fs*(0:(7500/2))/7500;
187  plot(f,P1)
188  title('Single-Sided Amplitude Spectrum of 20k to 105k chrip')
189  xlabel('f (Hz)')
190  ylabel('|P1(f)|')
191  plot(t2,aupnor)
192  hold on
193  plot(t2,aup)
194
195    subplot(2,1,1)
196   figure(h)
197   plot(fun,t2,aup)
198    subplot(311),plot(t3,udata1)
199   subplot(312),plot(t2,posi)
200   subplot(313),plot(t2,aup)
201       plot(t,aup,'-',t,paun,t,alo,'black')
202
203        a3=gca;
204       a3.XTick=sort([-1.5:2000:0]
205     ylabel('Voltage ');
206     xlabel('time(ms)');
207     title([num2str(65+5*f) ' Degree Raw Data' ])
208     ylim([-1.5 1.5]);
```

```
209     grid on
210  legend('Original','Normalized')
211     subplot(2,1,2)b
212      plot(fre,Cxy)
213      grid on
214
215  xlabel('Frequency (kHz)')
216  ylabel('P')
217
218  saveas(h,sprintf('1mfigure1%d.jpg',f));
219  saveas(h,sprintf('sanfigure%d.jpg',f));
220      end
221  as=sum(au);
222  abs=sum(abs(au));
223  end
224   avgdata= mean(data,2);
225  for  j= 1:23
226       positionx(:,j)=avgdata(:,:,j);
227       noisedata = positionx(1:2500);
228       standnoise= std(noisedata);
229       gdata= positionx - 3*standnoise;
230  loc(:,j)=find(abs(gdata(:,j)-0.08)<0.01,1,'first');
231      figure(j)
232   plot(gdata(:,j))
233  end
234
235     for k=1:23
236          udata=gdata(loc(k):loc(k)+2000,1:23);
237          pdata=udata;
238          figure(k)
239          plot(pdata(:,k))
```

```
240     end
241
242  position12= udata(:,12);
243  for i=1:23
244   cxy= mscohere(udata,position12);
245   mag= sum(cxy);
246   nmag=mag/257;
247
248  figure(i)
249
250   plot(udata(:,i))
251
252   plot(F,cxy(:,i));
253  end
254  for w=1:23
255  posi=udata(:,w);
256  au(:,w)=xcorr(posi);
257  figure()
258  plot(au(:,w))
259  end
```

```
1  close all
2  clear all
3  clc
4  angle=50:5:130;
5  filename='PSDdata.xlsx';
6  function fun = gauss_distribution(x, mu, s)
7  p1 = -.5 * ((x - mu)/s) .^ 2;
8  p2 = (s * sqrt(2*pi));
```

```
fun = exp(p1) ./ p2;
end
for j=[12];
sheet=j;
posin1='b2:b211:r2:r211';

    avej='b270:r270';
maxj='b271:r271';
minj='b272:r272';
sttdj='b275:r275';
 ave=xlsread(filename,sheet,avej);
  maxjj=xlsread(filename,sheet,maxj);
   minjj=xlsread(filename,sheet,minj);
sttd=xlsread(filename,sheet,sttdj);
 posi1=xlsread(filename,sheet,posin1);
 t=1:size(posi1,1);
 for i=1:17;
     maxi=maxjj(:,i);
     mini=minjj(:,i);

avei= ave(:,i);
stdi=sttd(:,i);
      posii=posi1(:,i);
      Edge=[mini:((maxi-mini)/210):maxi];
      n=histcounts(posii,Edge);
      [n,edge]= histcounts(posii);
      Edge=edge((1:size(edge,2)-1));
  fun = fit(t(:),posii,'gauss1')\
edge=Edge(1:210);

fun=gaussmf(edge,[stdi avei]);
```

```
40
41 polfit=polyfit(angle,ave,4);
42 y1=polyval(polfit,angle);
43 fi=polfit(:,1);
44 se=polfit(:,2);
45 th=polfit(:,3);
46 fo=polfit(:,4);
47 fif=polfit(:,5);
48 x=angle;
49  yfun=(fi*x.^4+se*x.^3+th*x.^2+fo*x+fif);
50 p = pchip(x,ave,angle);
51 pl=csapi(angle,ave);
52 s = spline(x,ave,angle);
53  xc=[0,50,130];
54 cc=[eye(2),eye(2)];
55 con=struct('xc',xc,'cc',cc);
56 ppl=splinefit(x,ave,5);
57 y2 = ppval(ppl,x);
58 ymax=maxi;
59 ymin=mini;
60  xmax(:,i)=interp1(yfun,x,ymax);
61  xmin(:,i)=interp1(yfun,x,ymin);
62    fun = fit(edge(:),n','gauss1')
63 posi3=xlsread(filename,sheet,posin3);
64 posi4=xlsread(filename,sheet,posin4);
65 posi5=xlsread(filename,sheet,posin5);
66 posi6=xlsread(filename,sheet,posin6);
67 posi7=xlsread(filename,sheet,posin7);
68 posi8=xlsread(filename,sheet,posin8);
69 posi9=xlsread(filename,sheet,posin9);
70 posi10=xlsread(filename,sheet,posin10);
```

```
71  posi11=xlsread(filename,sheet,posin11);
72  posi12=xlsread(filename,sheet,posin12);
73  posi13=xlsread(filename,sheet,posin13);
74  posi14=xlsread(filename,sheet,posin14);
75  posi15=xlsread(filename,sheet,posin15);
76  posi16=xlsread(filename,sheet,posin16);
77  posi17=xlsread(filename,sheet,posin17);
78  x=posii;
79  mu=avei;
80  s=stdi;
81  fun=gauss_distribution(x, mu, s);
82    [f,x]=hist(posii);
83  M=max(N);
84  www=1:1:size(x,2);
85
86  MMAX=max(f);
87  figure()
88  plot(angle,y2)
89  fnplt(pl,'r',3)
90  hold on
91  plot(angle,ave,'o')
92  ylabel('time variance(ms)')
93  xlabel('degree')
94
95  figure()
96  plot(edge,fun)
97  hold on
98  bar(x,1/max(f)*f);
99   end
100
101   errorbar(t,ave,neg,pos);
```

```
102
103 xlabel('position(degree)')
104 ylabel('time(ms)')
105 %  title(['1 meter last ' num2str(1450-50*i) ' points and first ' ...
        num2str(50+50*i) ' by envelope'])
106 % legend([' ' num2str(1450-50*i) 'data / ' num2str(50+50*i) 'data'])
107  saveas(h,sprintf('0.5liangceng%d.jpg',i));
108 close all;
109 clear all;
110 sigmaS=2*10^-3;
111 theta=90;
112 lamdac=1*10^-3;
113 c=340;
114 roo=0.5;
115 thetaz=11.8/180*pi;
116 sigmap=lamdac/c;
117 R=1;
118 Ts=2.8*10^-3;
119 durationR=sqrt(((4*sigmaS^2*cosd(theta)^2)/c^2)+((thetaz^2*roo^2*tand(theta)^2)/4*c^2)+
120
121 % ...
        energyR=(R*2*thetaz^2*sqrt(pi))/(256*sigmap*roo^2*cosd(theta)^5)*((Ts^2/sigmaS^2)*ex
122 % eee=mag2db(energyR);
123 end
```